



Doctoral Thesis

**CONTROL OF SEISMICALLY FORCED VIBRATIONS OF
ASYMMETRIC BUILDINGS BY MEANS OF A NOVEL BASE
ISOLATION SYSTEM**

submitted in satisfaction of the requirements for the degree of
Doctor of Science in Civil Engineering
of the Vienna University of Technology, Faculty of Civil Engineering

Dissertation

**REGELUNG SEISMISCH ERREGTER SCHWINGUNGEN
ASYMMETRISCHER GEBÄUDE DURCH EIN NEUARTIGES
ISOLIERSYSTEM IM FUNDAMENT**

ausgeführt zum Zwecke der Erlangung des akademischen Grades eines
Doktors der technischen Wissenschaften
eingereicht an der Technischen Universität Wien, Fakultät für Bauingenieurwesen
von

Basit Khalid, M.S.
Matrikelnummer 0628013
Karlsplatz 13/E2063, 1040 Wien

Gutachter: Em. O. Univ.Prof. Dipl.-Ing. Dr.techn. Dr.h.c. Franz Ziegler
Institut für Hochbau und Technologie, TU Wien
Karlsplatz 13/E2063, 1040 Wien

Gutachter: Univ.Prof. Dipl.-Ing. Dr.techn. Christoph Adam
Institut für Grundlagen der Bauingenieurwissenschaften
Leopold-Franzens-Universität Innsbruck
Technikerstr. 13, 6020 Innsbruck

Wien, November 2010

Acknowledgement

This work was developed and finally written in a standard format during my research as a doctoral student at the Institute of Building Construction and Technology at the Vienna University of Technology (TU Wien). My special thanks go to respected Em.O.Univ.Prof. Dip.-Ing. Dr.techn. Dr. h.c Franz Ziegler, the former Chairman of the Institute of Applied Mechanics of TU Wien, for his excellent research supervision, continuous guidance, valuable advices and devotion of his precious time for technical discussions during the development of this novel research work. The author would like to express his gratitude to honorable Univ.Prof. Dipl.-Ing. Dr.techn. Christoph Adam, Head of Institut für Grundlagen der Bauingenieurwissenschaften at Leopold-Franzens-Universität Innsbruck for his second opinion on my thesis.

The author is grateful to Univ.Prof. Dipl.-Ing. Dr.techn. Rudolf Heuer, Head of the well-equipped Laboratory of the institute for the provision of laboratory equipments and his guidance whenever needed. The author also pays his thanks to Univ.Prof. Dipl.-Ing. Dr.techn. Christian Bucher, Head of the Institute of Building Construction and Technology, for the provision of work-place, and his soft & co-operative attitude deepen his respect into the heart. The author would also like to acknowledge the Higher Education Commission (HEC) of Pakistan, for their financial support without which this research would have not been possible. I personally honor Prof. Dr. Atta-ur-Rahman, the former Chairman of HEC, for his valuable contributions for the higher education in Pakistan.

The author also appreciates personally his wife who managed her PhD work in parallel with the fulfilment of all the responsibilities of our child and home in an excellent way. The author feels that all of his achievements are the result of untiring efforts and prayers of his parent especially his mother who has no parallel in this world.

The author acknowledges the Austrian Association of Earthquake Engineering (OGE), especially the General Secretary, Univ.Prof. DI Dr.techn. Rainer Flesch for the travel grant for presenting my research work at International Conferences. Finally, the author likes to thank to all of his friends and acquaintances especially Mr. Zafar Zarif, Dr. Markus Hochrainer and Mr. Maximilian Billmaier who remained cooperative and supportive during this time.

Abstract

The vulnerability of multi-purpose buildings with fundamental frequency say above 1 Hz when exposed to the strong motion phase of an earthquake is considerably reduced by means of base isolation. A novel base isolation system, a combination of spring-pendulum (SP) units with compatible sliding elements and tuned liquid column-gas dampers (TLCGDs), is presented to overcome some of the disadvantages of the conventional ones. The SP unit is an assembly of innovatively designed SP elements acting as a low pass filter for isolating horizontal vibrations. The SP elements consist of pre-stressed helical steel springs with pivoted columns along vertical axes carrying part of the dead weight of the building and guiding the horizontal motion. The static-stability of the SP elements and stability criterion even in post-buckling regime and with vertical seismic forcing taken into account, reveals that the ratio of axial to shear stiffness of helical spring should be maximized within proper design limits. To resist loads by wind gusts and small seismic disturbances, say of traffic origin, compatible “sliding elements” consisting of two circular plates contacting in static dry friction and controlled by a prestressed conical spring are designed without having continuous energy dissipation resulting in less wear and tear of the interface surfaces due to abrasive action. Thus, a limited horizontal force can be transmitted analogously to the rigid-plastic lead core of the standard steel reinforced rubber isolation element. However, in case of horizontal motion of the building, a lever system releases this frictional contact. A single-storey asymmetric building, considered as 3-DOF main system, is exemplary base-isolated by putting a number of properly designed SP units in-between the rigid foundations of the building to produce a basic natural period of about 2 sec. In its vibration modes, the isolated building is considered to be rigid and low cost TLCGDs, in optimal arrangement in the plan of the basement of the building, supply the effective damping of the remaining horizontal vibrations. Modal tuning of each TLCGD is performed for a modally isolated coupled TLCGD-main system by properly transforming the classical Den Hartog formulas; an analogy to an equivalent TMD (tuned mass damper) exists. Fine-tuning of three TLCGDs in the state-space domain in favorable generalized modal coordinates is performed using MATLAB and renders optimal natural frequencies (slightly changed) and the damping ratios of fluid flow (considerably reduced). The dynamic response of the base-isolated asymmetric building equipped with TLCGDs subjected to base excitation (e.g., El Centro seismogram scaled to a maximum acceleration of 0.32g) is numerically investigated when the equations of motion for the coupled system are solved by using the state-space approach when favorably expressed in the generalized modal coordinates. However, early peaks in the response may still require active control for their proper reduction. Numerical simulations approve the novel SP units as a replacement of the classical elastomeric bearings and illustrate the effectiveness of these liquid absorbers to mitigate the seismically forced vibrations of base-isolated asymmetric buildings with fairly small mass ratio assigned. A laboratory model of a single-storey 3-DOF space-frame under variable oblique base excitation when equipped with an indigenously developed TLCGD, tuned and optimally placed with respect to the fundamental mode, is considered to experimentally verify its effectiveness in a general horizontal motion and the measured results are found to be in good agreement when compared to the analytical solutions derived by simulating the experimental setup.

Kurzfassung

Die Gefährdung von Mehrzweckgebäuden mit einer Grundfrequenz von mehr als 1 Hz durch die Starkbebenphase eines Erdbebens wird durch die Isolierung des Fundaments stark reduziert. Ein neuartiges Isolierelement, bestehend aus der Kombination einer Schraubenfeder mit einer koaxialen Pendelstütze, wurde entwickelt, das zusammen mit der Dämpfungswirkung des Flüssigkeits-Gas-Kombitilgers einige der wesentlichen Nachteile des „klassischen“ Gummifederelementes eliminiert. Um Schwingungen des Gebäudes sowohl unter Windböenbelastung wie auch schwachen seismischen Einwirkungen z.B. aus Verkehrsbelastung zu vermeiden, sind zusätzlich „Festhalteelemente“ einzusetzen. Solche „verträglichen“ Elemente basierend auf der Haftung kontaktierender Platten (ohne kontinuierlicher Energiedissipation durch Reibung) werden ebenfalls vorgeschlagen. Mehrere Isolierelemente werden zu einer Isoliereinheit zusammengefasst und bilden in ihrer Gesamtheit ein Tiefpassfilter. Das Gewicht des Gebäudes wird teilweise über die axial vorgespannten Schraubenfedern und über die Pendelstützen in das Fundament übertragen. Letztere übernehmen die kinematische Führung der Gebäudeschwingungen. Die statische Stabilität der Elemente, auch im Nachbeulbereich untersucht und quasistatisch auch unter lotrechter Bebenerrregung, erfordert ein möglichst hohes Verhältnis der axialen Steifigkeit zur Schubsteifigkeit der Schraubenfedern. Das Festhalteelement besteht aus je zwei kontaktierenden Kreisplatten die über die Vorspannung einer konischen Feder regelbar zusammengepresst werden. Damit kann dann eine begrenzte horizontale Kraft übertragen werden, analog zum starr-plastischen Bleikern des Standard Gummielementes. Allerdings wird bei horizontaler Bewegung des Gebäudes der Kontakt zwischen den Kreisplatten über eine Hebelwirkung mit Vergrößerungsfunktion der vertikalen Gebäudebewegung aufgehoben. Ein asymmetrisches ebenerdiges Haus wird beispielhaft gegen Erdbeben isoliert, wobei die Schraubenfedern so ausgelegt werden, dass sich eine Grundperiode von ca. 2 Sekunden ergibt. In den drei resultierenden Schwingungsformen des Starrkörpermodells wird die Dämpfung effektiv durch die optimale Anordnung und Abstimmung von drei Flüssigkeits-Gas-Kombitilgern in Tieflage im Gebäude erreicht. Die Abstimmung dieser Tilger erfolgt zuerst im modal isolierten System unter Verwendung der für mechanische Tilger entwickelten Formeln von Den Hartog. Die Feinabstimmung des Gesamtsystems erfolgt dann im Zustandsraum, wo vorteilhaft die modalen generalisierten Koordinaten weiter verwendet werden, unter Verwendung des Programms MATLAB. Das auf 0.32g maximaler Beschleunigung skalierte El Centro Erdbeben wird dann zu Testzwecken für die Simulationen eingesetzt. Die Einfallrichtung der Erdbebenwelle wird stufenweise variiert und der kritische Einfallwinkel (auch aus den verallgemeinerten Partizipationsfaktoren ersichtlich) wird durch die Simulationen bestätigt. Die numerischen Simulationen bestätigen die hervorragende Wirkung der neuartigen Schwingungsisolierung. Stoßartige Anfangsbeschleunigungen erfordern allerdings u.U. den Einsatz einer aktiven Regelung (des Gasdruckes) der Flüssigkeits-Gas-Kombitilger. Als Labormodell für experimentelle Untersuchungen diente ein räumlicher Stockwerksrahmen unter richtungsabhängiger Anregung mit einem auf die Grundschiwingung optimal ausgelegten und angeordneten Flüssigkeits-Gas-Kombitilger. Die gemessenen Daten ergaben gute Übereinstimmung mit den über analytische Lösungen erzielten Simulationsergebnissen des Labormodells.

1	Introduction	1
1.1	Evolution of base isolation technology	1
1.2	Literature review	2
1.2.1	Applications of base isolation systems	2
1.3	Base isolation with external passive damper	5
1.3.1	Overview of passive dampers	5
1.3.1.1	The tuned mechanical damper, TMD	6
1.3.1.2	The tuned liquid column damper and its extension by gas-spring	6
1.4	Motivation of the research	7
1.5	Overview of the dissertation	8
	References	10
2	Single-storey Asymmetric Space Frame with TLCGDs: Laboratory Model	12
2.1	Introduction	12
2.2	Equation of motion for single-storey asymmetric space frame	13
2.2.1	Effective mass and stiffness of the column	15
2.2.2	Geometric stiffness correction: P- Δ effect	16
2.2.3	Natural frequencies and modal centers of velocity	16
2.3	The equation of relative fluid flow in a TLCGD	19
2.4	Control forces of TLCGD	26
2.5	Approximate substructure synthesis of the space frame with TLCGD	31
2.6	Modal tuning of TLCGD, Den Hartog optimization	34
2.6.1	Analogy between equivalent TMD and TLCGD	35
2.6.2	Parameters of the gas-spring	36
2.6.3	Steps of modal tuning of TLCGD in the design stage	37
2.7	Steady state response and modal dynamic magnification factor	38

2.7.1	Steady state vibrations of space frame without TLCGD	38
2.7.2	Steady state vibrations of modally isolated 2-DOF system	39
References		41
3	Experimental Verification of TLCGD Damping	43
3.1	Introduction	43
3.2	Design and development of the asymmetric structural model in view of base isolation	43
3.2.1	Properties of the columns	46
3.2.2	Properties of the structural model	47
3.2.3	Corrected properties of structural model after TLCGD installation	49
3.3	Optimal positioning of TLCGD	50
3.4	Design and development of TLCGD	51
3.5	Experimental measurements	53
3.6	Experimental results	56
3.7	Numerical Simulations	60
3.8	Comparison of experimental and simulated results	63
References		64
4	Novel Base Isolation System	66
4.1	Introduction	66
4.1.1	Key concept of base isolation	67
4.1.2	Classical base isolation systems	68
4.2	Novel base isolation system	71
4.2.1	Design of novel base isolation element	72
4.2.1.1	Design details of the novel base isolation element	74
4.2.2	Static stability of base isolation element	75

4.2.2.1	Quasi-static consideration for vertical ground motion _____	76
4.2.2.2	Contact stability under vertical ground motion _____	77
4.2.2.3	Static stability even including the post-buckling regime _____	78
4.2.3	Base isolation unit for asymmetric building _____	81
4.2.4	Base isolation unit for skeletal structure _____	83
4.3	Equation of motion for the base-isolated building _____	85
4.3.1	Modal analysis of base-isolated building _____	89
4.4	Equations of motion for coupled system in state-space domain _____	90
4.4.1	Modally isolated 2-DOF coupled system in state space _____	90
4.4.2	Modally coupled system in state-space _____	92
4.5	Application with numerical examples _____	96
4.5.1	Base-isolated plane frame _____	97
4.5.1.1	Modal analysis and installation of TLCGD _____	98
4.5.1.2	TLCGD design parameters _____	99
4.5.1.3	Simulation results _____	100
4.5.2	Base-isolated single-storey asymmetric building _____	106
4.5.2.1	Modal analysis and installation of TLCGDs _____	107
4.5.2.2	Design steps of base isolation element for asymmetric building _____	109
4.5.2.3	Design of novel sliding element for asymmetric building _____	110
4.5.2.4	TLCGD design parameters _____	114
4.5.2.5	Dimensioning of TLCGD piping _____	116
4.5.2.6	Simulated results _____	119
References	_____	132
5	Conclusions _____	134
References	_____	136

1 Introduction

In this section an overall view of the dissertation is presented to establish the basics of the research work by connecting the sequential flow among various aspects of base isolation. A brief review of the literature covering the recent scientific developments in the area of base isolation, an essential approach to earthquake-resistant design, is highlighted. The motivation towards this research is also presented to convincingly establish the importance of the objectives achieved and the organisation of the dissertation is finally laid out in detail.

1.1 Evolution of base isolation technology

Earthquakes are among such natural hazards that have primarily motivated the development of earthquake engineering through much of its evolution over the past century. The level of knowledge and technology in earthquake engineering is rising to meet this demand for buildings, bridges, and other constructions that can withstand strong earthquakes without structural failure, costly retrofit of damage, significant chance of injuries, or major functional interruption.

The basic dilemma facing a structural engineer charged with providing superior seismic resistance of a building is how to minimize interstory drift and floor accelerations. Large interstory drifts cause damage to nonstructural components and to equipment that interconnects stories. Interstory drifts can be minimized by stiffening the structure, but this leads to high floor accelerations, which can damage sensitive internal equipment. Floor accelerations can be reduced by making the system more flexible, but this leads to large interstory drifts. Thus, the only practical way of reducing simultaneously interstory drift and floor accelerations is to use base isolation, see Naeim-Kelly^[1-1]; the isolation system provides the necessary flexibility, with the displacements concentrated at the isolation (basement) level. Seismic isolation is an approach to earthquake-resistant design

that is based on the concept of reducing the seismic demand rather than increasing the earthquake resistance capacity of the structure.

In conventional fixed-base design, efforts to strengthen the structural system to provide superior seismic performance lead to a stiffer structure, and thus will attract more force to the structure and its contents. However, this solution revealed considerable disadvantages because of construction expenditures for conventional strengthening of the structure and its foundation, Bachmann^[1-2]. Therefore, the idea that a building can be uncoupled from the damaging effects of the ground movement produced by a strong earthquake has appealed to inventors and engineers for more than a century. Among the structural control schemes developed, seismic base isolation is one of the most promising strategies and thus became an increasingly applied structural design technique for buildings.

1.2 Literature review

The history of development of the base isolation has been covered in several review articles, for example, Kelly^[1-3] and Buckle-Mayes^[1-4]. Prof. James Kelly provides a survey of the early history of isolation inventions; approximately 100 schemes have been published or patented to 1960, though almost all remained only ideas on paper, Reitherman^[1-5]. But eventually, the practical application of this concept in real world has come into being followed by the series of the developments by various researchers and engineers.

1.2.1 Applications of base isolation systems

One of the earliest concepts that were actually built was the room that John Milne, Professor of Geology and Mining at the Imperial College of Engineering in Tokyo, erected next to his house in Japan in 1880s. It rested on pillar foundations but had a layer of cast-iron shot placed between the iron plates. Milne carried out pioneering research on seismology, so much so that he is often referred to as the “Father of Modern Seismology”, Reitherman^[1-5]. The first use of a rubber isolation system to protect a structure from earthquake was in 1969 for an elementary Pestalozzi School in Skopje, Macedonia. The

1. Introduction

world first seismically isolated building by means of lead-rubber bearings (rubber sheets reinforced between steel plates with the energy dissipating lead core) is the William Clayton Building, designed in 1970 and constructed in 1982, in Wellington, New Zealand. The Union House, Auckland, and Wellington Central Police Station are isolated using sleeved-pile approach. The National Museum of New Zealand in Wellington is isolated with 142 lead-rubber bearings and 36 Teflon pads under the shear walls. New Zealand Parliament House is recently retrofitted using more than 514 lead-rubber bearings.

The first base-isolated building in the United States was the Foothill Communities Law and Justice Center (FCLJC) in California by means of 98 high-damping natural rubber bearings, Kelly^[1-6]. The Fire Command and Control Facility (FCCF), Emergency Operation Center (EOC) in Los Angeles and Traffic Management Center for Caltrans (TMCC) in California are other base-isolated buildings by using high-damping rubber. The C. R. Drew Diagnostic Trauma Center in California is supported on 70 high-damping natural rubber bearings and 12 sliding bearings with lead bronze plates that slide on stainless steel surface. The newly constructed Flight Simulator Manufacturing Facility (FSMF) in Salt Lake City completed in 1988 in Utah is isolated by 98 lead-rubber bearings.

In process of seismic retrofit, some of the most prominent U.S. monuments like, e.g., Pasadena City Hall, San Francisco City Hall, Salt Lake City and County Building and Los Angeles City Hall were mounted on base isolation systems. The Los Angeles City Hall is the tallest base-isolated structure in the world, having undergone a seismic retrofit by means of 475 high-damping rubber isolators in combination with 60 sliders. Earthquake-resistant design has always been a high priority in Japan, and many mechanisms for the seismic protection of structures, including forms of seismic isolation, have been developed there. Japanese structural engineers generally design buildings with more seismic resistance than do U.S. or European because of frequent earthquakes in their region. There are many base-isolated buildings in Japan e.g., West Japan Postal Center and Matsumura-Gumi Technical Research Institute are famous one. There are now

427 isolated buildings constructed or under construction just in Japan, with 225 building permits issued in 1996 alone, Reitherman^[1-5]. There are some applications in New Zealand, Dowrick, Cousins, Robinson and Babor^[1-7]; several in Italy, Giuliani^[1-8], including one project of five large buildings; large number of applications in France, including two nuclear power plants, Jolivet and Richli^[1-9] and few buildings in China, Lee^[1-10].

It seems clear that the increasing acceptance of base isolation throughout the world will lead to many more applications of this technology. But as a matter of fact, the lifetime problems associated with conventional base isolation systems e.g., lead-rubber bearings (LRB), mainly caused by the increase of temperature, like reduction in yield stress with repeated cycling and plastic deformation of the lead core within the first occurrence of the earthquake or during the aftershocks are encountered.

Therefore, it was strongly desired either some-how to improve the design philosophy of such bearings or to replace them by an advanced mechanism that could withstand the said problems so that the isolation mechanism remain effective and durable throughout the life of the structure. For all systems, the most important area of future research is that of long-term stability of the mechanical characteristics of the isolators and its constituent materials, Naeim-Kelly^[1-1].

Recently an advancement has been practically implemented by Bachmann^[1-2] for the seismic upgrading of a Fire-brigade building in Basel, Switzerland, where he preferred to use elastomeric bearings made of reinforced rubber without having lead core, placed in the peripheral basement walls under the columns. Whereas, the sliding bearings situated under the column-less partition walls provide damping and static friction. When following the current trends and Bachmann^[1-2] as recent example of separating the damping from isolation bearings, a novel base isolation system, a combination of spring-pendulum (SP) units along with sliding elements and tuned liquid column-gas dampers (TLCGDs), is proposed with a step ahead. For design details, see Khalid-Ziegler^[1-11], and detailed description in sub-section 4.2. In connection to

Bachmann's strategy, novel SP units substitute the reinforced rubber bearings while low-cost TLCGDs substitute the sliding bearings with the added advantage of no moving mechanical parts resulting in maintenance-free long life of the whole base isolation system. However, to resist loads by wind gusts and small seismic disturbances, say of traffic origin, compatible sliding elements are designed without having continuous energy dissipation. Thus, a limited horizontal force can be transmitted analogously to the rigid-plastic lead core of the standard steel reinforced rubber isolation element. However, in case of horizontal motion of the building, a lever system releases this frictional contact.

1.3 Base isolation with external passive damper

Seismic isolation has helped plant the seeds for other response control devices (e.g., active and passive control technologies), which, like isolation are based on strategy of reducing demand than increasing capacity. Because the natural damping of such a base isolation system is low, additional damping is provided by some form of damper. The idea of separately supplying the damping by means of external dampers for a base-isolated building is not new but the combination of innovatively developed base isolation units with low-cost TLCGD as mentioned above, possibly first time with best of the author's knowledge, makes the design novel and superior because of its advantageous features e.g., maintenance-free long-life etc. Before touching the functionality and importance of the novel base isolation system, a brief overview of the passive damping devices is also presented.

1.3.1 Overview of passive dampers

Passive devices protect a structure by increasing its energy dissipation capacity. A supplemental damping system works by absorbing a portion of the input energy to a structure thereby reducing structural energy dissipation demands and preventing damage to the primary structure. This effect is achieved either by conversion of kinetic energy to heat or through the transfer of energy among vibration modes. The first method utilizes devices that operate on principles such as frictional sliding, yielding of metals, phase

transformation in metals, and deformation of viscoelastic solids or fluids, examples include metallic yield dampers, friction dampers, viscoelastic dampers, viscous fluid dampers, etc. The second method of energy dissipation incorporates dynamic vibration absorbers, such as tuned mechanical damper (TMD), tuned liquid damper (TLD) and tuned liquid column damper (TLCD). The following sub-sections are conceptually concerned with TMD, and TLCD along with its modified forms.

1.3.1.1 The tuned mechanical damper, TMD

The most commonly used passive device is tuned mechanical damper consisting of a mass attached to the building through a spring and a dashpot. Alternatively, a pendulum-type mechanical damper is used in high-rise buildings, e.g. in the Taipei 101 tower. In order to be effective, its parameters need to be optimally tuned to the building dynamic characteristics, thus imparting indirect damping through modification of the combined structural system.

Den Hartog^[1-12] derived expressions for the optimum damping coefficient and the tuning ratio (i.e., ratio of the absorber frequency to the natural frequency of the undamped single-degree-of-freedom (SDOF)-primary system) for the coupled generalized SDOF-TMD system subjected to harmonic excitation. The optimum absorber parameters that minimize the displacement response of the primary system were found to be simple functions of the mass ratio (ratio of mass of SDOF-structure and damper).

1.3.1.2 The tuned liquid column damper and its extension by gas-spring

TLCD is an effective passive energy absorbing device that has been proposed for controlling vibrations of structures under different dynamic loading conditions; see e.g. Balendra^[1-13]. Such a TLCD consists of a rigid U or V-shaped tube smoothly integrated into a building and partially filled with a liquid (preferably water) allowing water column to oscillate. Finally, the energy is dissipated by viscous and turbulent fluid damping. TLCDs provide many advantages, when compared to TMD, such as low cost, no moving mechanical parts, relatively easy installation in new buildings or in retrofitting existing structures, simple maintenance requirements. Indeed, a TLCD may not cause additional

cost or weight if a water tank used for water supply and fire fighting is incorporated into design of a TLCD, see Fu-Ziegler^[1-14]. Furthermore, they can be combined with active control mechanisms to function as hybrid absorbers, see Hochrainer-Ziegler^[1-15].

In recent years, there has been an increasing interest in the application of TLCDs to the problem of vibration suppression in civil engineering structures. Since Sakai and his co-authors^[1-16] developed the idea of TLCD in 1989 for the purpose of structural vibration suppression, many successors had employed it in many civil engineering applications to verify its control effectiveness see e.g., Hitchcock, Kwok, Watkins and Samali^[1-17]. Hochrainer^[1-18] invented the gas-spring effect to achieve tuning conveniently just by changing the equilibrium gas-pressure in the sealed piping system. Applications of such tuned liquid column-gas damper (TLCGD) to tall buildings or slender bridges, see Hochrainer-Ziegler^[1-15], Ziegler^[1-19] or Reiterer-Ziegler^[1-20], effectively reduce steady state vibrations, equally well as a direct increase of the modal structural damping.

Recently, Fu^[1-21] presented that the TLCGD instead of the TMD are used to mitigate bending and torsional vibrations of tall multipurpose buildings. In her study, the passive action of TLCGD is considered and the coupled torsional response of plan-asymmetric structures was investigated. She also investigated the torsional tuned liquid column-gas dampers (TTLCGD; including the gas-spring effect) to effectively control the torsional response of structures, for details see again Fu^[1-21]. The plane TLCGDs and TTLCGDs were applied in numerical studies in a total of eight different small-scale building models and to a 30-storey high-rise eccentric structure, see Huo^[1-22].

1.4 Motivation of the research

The loss of lives and collapse of infrastructure in the history and a few in my self-experience in Pakistan due to earthquake has motivated to play my role as a researcher in this field. I was always inspired by the majesty of high-rise buildings but being a civil engineer, I remained focus to find ways enabling a structure to withstand under dynamic loads e.g., earthquakes and wind excitations. Through literature review

and basic research, I would be able to find a slot to step-in and therefore present research work as my PhD thesis is a contribution in the sea of knowledge that would lead towards the strengthening of seismically safer world.

The increasing acceptance of base isolation itself, throughout the world as a successful earthquake-resistant technique is evidence by rapidly increasing number of applications both for new construction and retrofit, see Kelly^[1-3]. Similarly the effectiveness of TLCD (or more advanced form TLCDG) as passive damper to mitigate the structural vibrations is exceeded by far the capabilities of other vibration reducing devices due to its salient features, see Hitchcock^[1-17]. But the idea of incorporating the TLCDG to the base-isolated building is unique of its own nature and thus, subjected to investigation to take the advantage of both recently matured technologies in their combined action. In addition, the lifetime problems, mainly caused by increase of temperature, related to the conventional isolation systems give way to the emergence of such a solution that remains effective and durable throughout the life of the structure. Consequently, in this dissertation, a novel base isolation system, see details in sub-section 4.2, is proposed and numerical studies are worked out in state-space for the coupled system (TLCDGs installed on the base-isolated building). Although this new and radical approach to seismic design will be able to provide safer buildings at little additional cost as compared to the conventional design but on the other hand, this method also limits some requirements to meet; base isolation is not suitable for high-rise buildings and for other types of loads e.g., for strong wind excitations.

1.5 Overview of the dissertation

This dissertation consists of five main Sections, the thematic taken from base isolation of the buildings. The control of seismically forced vibrations of multipurpose and consequently asymmetric buildings is achieved by means of novel base isolation system innovatively developed by the author in course of his PhD research work.

Section 2 forms the mathematical basis for the implementation of TLCDGs. More

precisely, it provides a theoretical foundation on the performance of TLCGDs for mitigating the coupled lateral vibrations of single-storey asymmetric space frames which can be modeled as a three degree-of-freedom (3-DOF) structure. Such a 3-DOF asymmetric space frame is considered because it is an economical main structural model in the laboratory when equipped with TLCGD to confirm the effectiveness of the gas-spring effect for frequency tuning. And most importantly, it serves as an easily manufactured model of a base-isolated main structure. The coupled equations of motion of the TLCGD-space frame considering the rigid-floor and damper interaction lead towards the approximate substructure synthesis of the 2-DOF modally isolated coupled TLCGD-space frame system. The directional dependency of the modal dynamic magnification factor, somehow hidden previously, on varying angle of incidence of seismic excitation is pointed out with due justification.

In Section 3, the effectiveness of the TLCGD is confirmed through experimentation by installing an indigenously designed and developed TLCGD, tuned to fundamental mode of vibrations of the single-storey space frame lab-model. However, due to financial and laboratory constraints, the incorporation of novel base isolation units for such a light weight 3-DOF structural lab-model was not possible. A series of experiments is performed for different cases, i.e., empty TLCGD-piping system, open TLCGD and tuned TLCGD installed in optimal position and direction on the floor of the asymmetric structural lab-model, to verify the tuning of TLCGD achieved by means of gas-spring effect. The experimental results are found to be in good agreement when compared with analytical solutions by simulating the experimental setup.

Section 4 deals with the core concern of the subject starting with the design equations of the novel base isolation element referred to as spring-pendulum (SP) element. The static-stability of the SP element and stability criterion extended in post-buckling regime is determined along with contact-stability considerations under vertical ground acceleration. The details of the SP unit designed for a single-storey asymmetric building (e.g., four SP elements in parallel action to form an assembly) and a description of an

analogous skeletal structure is also presented. To resist loads by wind gusts and small seismic disturbances, say of traffic origin, compatible sliding elements with lever system are designed without having continuous energy dissipation. The equation of motion for base-isolated 3-DOF asymmetric building is formulated rendering modal analysis. In its fundamental modes, the base-isolated building is considered to be rigid and low cost TLCGDs, in optimal arrangement in the plan of the basement of the building, supply the effective damping of the remaining horizontal vibrations. A benchmark five-storey plane frame and a single-storey 3-DOF asymmetric building are subjected to base-isolation and numerical investigations are performed in state-space for the coupled system when the TLCGDs are incorporated. Numerical simulations approve the novel SP system as a replacement of classical elastomeric bearings, and illustrate the effectiveness of these liquid absorbers (i.e., TLCGDs) to mitigate the seismically forced vibrations of the base-isolated buildings with fairly small mass ratio assigned.

Finally, Section 5 summarizes the results drawn from the research presented in this dissertation. This work is expected to convince the professionals in this field for the implementation of the proposed novel base isolation system due to its low cost, effective performance and maintenance-free long life probably could substitute the problematic conventional isolation systems.

References

- [1-1] Naeim F., Kelly J. M., Design of Seismic Isolated Structures, John Wiley & Sons, New York, 1999.
- [1-2] Bachmann H., Seismic upgrading of a fire-brigade building by base isolation in Basel, Switzerland, Structural Engineering International, 2010; **20/7**, 268-274.
- [1-3] Kelly J. M., Seismic base isolation: review and bibliography, Soil Dynamics and Earthquake Engineering, 1986; **5**, 202-216.
- [1-4] Buckle I. G., Mayes R. L., Seismic isolation history: application and performance- a world review, Earthquake Spectra, 1990; **6**, 161-201.
- [1-5] Reitherman R., Historic development in the evolution of earthquake engineering, Consortium of Universities for Research in Earthquake Engineering (CUREE), California, USA, 1997.
- [1-6] Kelly J. M., Implementation of base isolation in United States, Proc. of 10th World

- Conf. on Earthquake Engineering (10 WCEE), Madrid, Spain, 1992, Balkema, Rotterdam; **11**, 6507-6517, ISBN 9054100710.
- [1-7] Dowrick D.J., Cousins W.J., Robinson W.H. & J. Barbor, Recent developments in seismic isolation in New Zealand, Proc. of 10th World Conf. on Earthquake Engineering (10 WCEE), Madrid, Spain, 1992, Balkema, Rotterdam; **4**, 2305-2310, ISBN 9054100648.
- [1-8] Giuliani G.C., Design experience on seismically isolated buildings, Nuclear Engineering and Design, 1991; **127/3**, 349-366.
- [1-9] Jolivet J., Richli M.H., Aseismic foundation system for nuclear power stations, Proc. of SMiRT-4, San Francisco, CA, 1977; Paper K.9/2.
- [1-10] Lee L., A base isolation measure for aseismic building in China, Proc. of 8th World Conf. on Earthquake Engineering (8 WCEE), San Francisco, CA, 1984; **VI**, 791-798.
- [1-11] Khalid B., Ziegler F., A novel base isolation system for asymmetric buildings effectively damped by tuned liquid column-gas dampers. Proc. of 14th European Conf. on Earthquake Engineering (14 ECEE), Ohrid, Macedonia, 2010; CD-ROM paper, 8 pages.
- [1-12] Den Hartog J.P., Mechanical Vibrations, 4th ed., McGraw-Hill, New York, 1956.
- [1-13] Balendra T., Wang C. M., Cheong H.F, Effectiveness of tuned liquid column dampers for vibration control of towers, Engineering Structures, 1995; **17/9**, 668-675.
- [1-14] Fu Chuan, Ziegler F., Vibration prone multi-purpose buildings and towers effectively damped by tuned liquid column gas dampers. Asian J. Civil Engineering, 2009; **10/1**, 21-56.
- [1-15] Hochrainer M.J., Ziegler F., Control of tall building vibrations by sealed tuned liquid column dampers, Structural Control and Health Monitoring, 2006; **6/13**, 980-1002.
- [1-16] Sakai F., Takaeda S., Tamaki T., Tuned liquid column damper-new type device for suppression of building vibration. Proc. of Int. Conf. on High-rise Buildings, Nanjing, China, 1989; 926-931.
- [1-17] Hitchcock P. A., Kwok K. C. S., Watkins R. D. and Samali B., Characteristics of liquid column vibration absorbers (LCVA)-I, Engineering Structures, 1997; **19/2**, 126-134.
- [1-18] Hochrainer M.J., Control of vibrations of civil engineering structures with special emphasis on tall buildings, Dissertation (in English), Vienna University of Technology, Vienna, Austria, 2001; <http://www.tuwien.ac.at/>.
- [1-19] Ziegler F., Special design of tuned liquid column-gas dampers for the control of spatial structural vibrations, Acta Mechanica, 2008; **201**, 249-267.
- [1-20] Reiterer M., Ziegler F., Control of pedestrian-induced vibrations of long-span bridges, Structural Control and Health Monitoring, 2006; **13/6**, 1003-1027.
- [1-21] Fu Chuan, Effective damping of vibrations of plan-asymmetric buildings, Dissertation (in English), Vienna University of Technology, Vienna, Austria, 2008; <http://www.tuwien.ac.at/>.
- [1-22] Huo L.S., Li H. N., Sun L., Parameter study of TLCD control system excited by multi-dimensional ground motions, Earthquake Engineering and Engineering Vibration, 2001; **21/4**, 147-153.

2 Single-storey Asymmetric Space Frame with TLCGDs: Laboratory Model

2.1 Introduction

A real building possesses a large number of degrees of freedom and is actually asymmetric to some extent even with a nominally symmetric plan. Hence, the asymmetric buildings are prone to coupled lateral vibrations under even purely translational excitations which may cause occupant discomfort, structural damage, or even collapse. Therefore, the idealization of asymmetric buildings makes its way for the proper investigation of their response under dynamic loads like earthquakes and wind excitations. Thus, a rigid floor supported by the columns, for which center of mass and center of stiffness do not coincide, is considered here as a single-storey asymmetric space frame. Three degree of freedom (3-DOF) are assigned in horizontal motion of the single-storey space frame when its floor is considered as a rigid-plate. Such a 3-DOF asymmetric space frame is focused because it is considered as an economical main structural model in the laboratory when equipped with TLCGD to confirm the effectiveness of the gas-spring effect for the frequency tuning. And most importantly, it serves as a conveniently manufactured model of a base-isolated asymmetric building. A novel base isolation system is developed with its design details presented in Section 4 taking into account the damping properties of the TLCGD based on this model.

The formulation of the equation of motion of asymmetric space frame and the derivation of the equation of relative fluid flow in TLCGD are given by Hochrainer^[2-1] and repeated in this Section with a more result-oriented approach in regard to their practical implementation. The coupled equations of motion of the TLCGD-space frame considering the rigid-floor and damper interaction lead towards the approximate substructure synthesis of the 2-DOF modally isolated coupled TLCGD-space frame

system that forms the theoretical basis required for the implementation of TLCGD in its design stage. The analogy between TMD and TLCGD when attached to main SDOF-structure under the horizontal base excitation established by Hochrainer^[2-1], see also Hochrainer-Ziegler^[2-2] was extended for more general 3DOF-space frame by Fu^[2-3], see also Fu-Ziegler^[2-4] and hence, the modal tuning of TLCGD is conveniently performed. The modal dynamic magnification factor is also formulated when the linearized approximate coupled equations are subsequently transformed to their respective time-reduced linear equations for the 2-DOF modally isolated system.

It is also pointed out that the directional dependency of such an approximate modal dynamic magnification factor on varying angle of incidence of base excitation is because of the fact that the position of the center of mass of the main system is no longer exact as the small fraction of the dead fluid-mass is not considered in the dynamics of the main system.

2.2 Equation of motion for single-storey asymmetric space frame

A simple single-storey space frame consisting of a “rigid” rectangular floor of size $a \times b$ having an arbitrarily distributed floor-mass m_S supported on clamped-clamped elastic columns with anisotropic stiffness k_y and k_z in y - and z -directions, respectively is sketched in Fig. 2.1.

The centre of mass C_M and center of stiffness C_S of the asymmetric space frame, two distinct points, are not coincident with the geometric centre O of the floor because of the non-uniform distribution of the floor-mass and non-symmetric distribution of the supporting columns respectively, rendering the mass- and stiffness-asymmetric space frame.

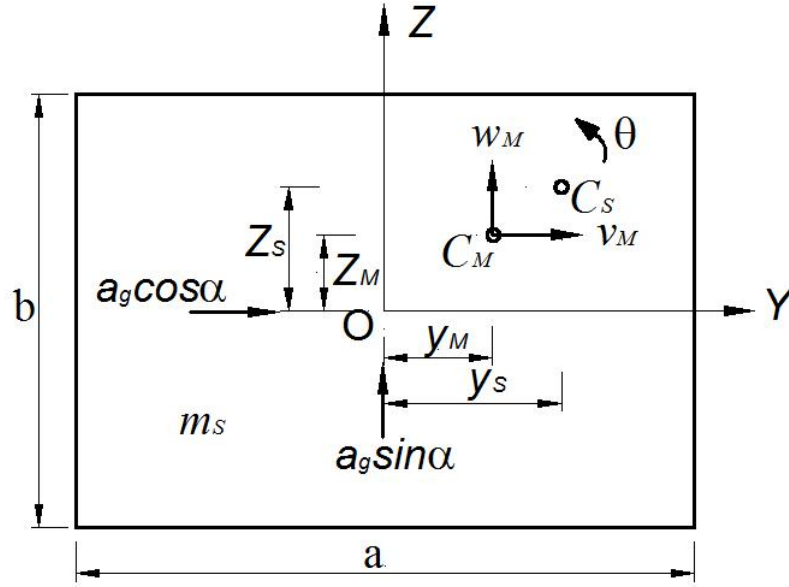


Fig. 2.1: Plan of single-storey asymmetric space frame.

Let $\vec{r}_M^T = [y_M \ z_M]$ and $\vec{r}_S^T = [y_S \ z_S]$ denote the position vectors of C_M and C_S respectively, as shown in Fig. 2.1. The asymmetric space frame is considered under single point horizontal base excitation (e.g., seismic ground acceleration $a_g(t)$) with angle of incidence α to y -direction, thus $a_g \cos \alpha$ and $a_g \sin \alpha$ are the horizontal components of the seismic ground acceleration in y - and z -directions, whereas the vertical component $\lambda_g a_g$ in x -direction causing the parametric excitation, see sub-section 2.4, is not considered in this Section. Since the centre of mass C_M and the centre of stiffness C_S do not coincide, even a uni-directional seismic horizontal (ground) excitation, in general, causes a three dimensional in-plane motion of the floor. The lateral displacements of C_M denoted by v_M and w_M along y - and z -axes, respectively and the rotational angle θ about the vertical x -axis define three degree of freedom (3-DOF) in horizontal motion of the single-storey space frame when its floor is considered as a rigid-plate.

The mass moment of inertia about the vertical x -axis of the rectangular floor is $I_x = m_s r_x^2$, where r_x denotes the radius of inertia with respect to the center of mass C_M .

The summation of the lumped columns' stiffness in y - and z -directions render the first two diagonal elements of the stiffness matrix respectively, whereas third diagonal and remaining off-diagonal elements depend upon arrangement of the columns of the asymmetric space frame. The direct stiffness method renders the elements of stiffness matrix when applied later on, for the similar asymmetric space frame (i.e., laboratory scaled structural model); by considering the lumped columns' stiffness with respect to center of mass to avoid the inertial coupling of the conservation equations.

The equation of undamped motion of the asymmetric space frame subjected to single point horizontal base excitation, considering the conservation of momentum and conservation of angular momentum, in matrix form,

$$\underline{M}\ddot{\underline{x}} + \underline{K}\underline{x} = -\underline{M}\underline{\ddot{a}}_g, \quad \underline{\bar{x}}^T = [v_M \quad w_M \quad u_T], \quad \underline{\bar{a}}_g^T = a_g [\cos \alpha \quad \sin \alpha \quad 0], \quad u_T = \theta r_x, \quad (2.1)$$

where, \underline{M} and \underline{K} are the diagonal mass and the symmetric stiffness matrix of the 3-DOF asymmetric space frame, respectively and $\underline{\bar{x}}$ is referred to the displacement vector of the center of mass; $\underline{\bar{a}}_g$ denotes the single point horizontal seismic ground acceleration vector.

2.2.1 Effective mass and stiffness of the column

The mass of the column is commonly lumped as a single equivalent mass and hence its static stiffness is calculated for the proper idealization of the space frame. If the mass per unit of length ρA , as well as the stiffness EI of the column both considered to be constant (for convenience of integration), an approximation of the equation of motion of the flexural vibration in the first natural mode can be determined. An admissible Ritz approximation can always be given affined to a proper static deformation. Hence, see Ziegler^[2-5], page 611,

$$w(\xi, t) = q(t)\varphi(\xi), \quad (2.2)$$

where $\varphi(\xi)$ suffices to choose the Hermite shape function for the cc-beam, unit displacement at $x = l$ is 1,

$$H_3(\xi) = -2\xi^3 + 3\xi^2, \quad 0 \leq \xi = x/l \leq 1 \quad (2.3)$$

The kinetic energy becomes,

$$T = \frac{1}{2} \int_0^1 \dot{w}^2 \rho A l d\xi = \frac{\dot{q}^2}{2} \rho A l \int_0^1 H_3^2(\xi) d\xi = \frac{\dot{q}^2 m_e}{2}. \quad (2.4)$$

Thus, the kinetic energy is equivalent to that of a single equivalent mass m_e

$$m_e = \rho A l \int_0^1 H_3^2(\xi) d\xi = \frac{13}{35} m_c, \quad m_c = \rho A l \quad \text{is the mass of the column.} \quad (2.5)$$

The potential energy of the slender column (rigid in shear) is approximated by

$$V = U = \frac{1}{2} \int_0^1 \frac{EI}{l^3} \left(\frac{\partial^2 w}{\partial \xi^2} \right)^2 d\xi = \frac{EI}{2l^3} q^2 \int_0^1 \left(\frac{d^2 H_3}{d\xi^2} \right)^2 d\xi = \frac{kq^2}{2} \quad (2.6)$$

The effective static stiffness of the cc-column becomes

$$k = \frac{EI}{l^3} \int_0^1 \left(\frac{d^2 H_3}{d\xi^2} \right)^2 d\xi = \frac{12EI}{l^3}. \quad (2.7)$$

The effective lumped mass and the static stiffness of the columns of the laboratory scaled structural model (lab-model) are calculated by using Eqs. (2.5) and (2.7), see sub-section 3.2.

2.2.2 Geometric stiffness correction: P - Δ effect

If a slender column is subjected to a large compressive force, its lateral stiffness is significantly reduced, termed as P - Δ effect. The geometric correction of stiffness of c-c beam is $k_G = 6F_c/5l$, where $F_c < 0$ is the compressive axial force, l is the length of the beam. If the lateral load is less than 30% of the critical buckling load, the linear geometric stiffness correction is applicable, see e.g. Clough-Penzien^[2-6], page 167 and Ziegler^[2-5], page 604. The geometric stiffness correction is applied for the columns of the lab-model and the corresponding corrected stiffness matrix is also presented in sub-section 3.2.

2.2.3 Natural frequencies and modal centers of velocity

The solution of the eigen-value problem associated with the homogenous equation (2.1)

2. Single-storey Asymmetric Space Frame with TLCDs: Laboratory Model

when considering the diagonal mass and symmetric corrected stiffness matrix, renders the natural circular frequencies ω_j and modal vector $\vec{\phi}_j$, $j=1,2,3$ of the undamped main system (i.e., asymmetric space frame). Consequently, the undamped free vibration is time-harmonic, see e.g., Chopra^[2-7], page 404,

$$\vec{x}(t) = \vec{\phi}_j A_j \cos \omega_j t, \quad (2.8)$$

After substituting Eq. (2.8) in the homogenous equation (2.1), the time-reduced equation results, $\left[\bar{K} - \omega_j^2 \bar{M} \right] \vec{\phi}_j = \vec{0}$ and hence the characteristic equation becomes $\det \left[\bar{K} - \omega_j^2 \bar{M} \right] = 0$. The solution by calling the function *eig* in MATLAB^[2-8], renders the first three natural frequencies and ortho-normalized modal vectors $\vec{\phi}_j$ of the undamped asymmetric space frame by requiring modal mass $m_j = \vec{\phi}_j^T \bar{M} \vec{\phi}_j = 1$.

The point of a rigid body in-plane motion that instantly has zero velocity is called the modal center of velocity C_{Vj} , the acceleration of C_{Vj} is generally non-zero. The velocity of any point P of the rigid body is calculated by using rigid body kinematics, see e.g., Ziegler^[2-5], page19,

$$\vec{v}_P = \vec{v}_M + \dot{\theta} \hat{r}_{PM} \quad (2.9)$$

where, $\hat{r}_{PM} = \vec{e}_x \times \vec{r}_{PM}$ is the positively rotated orthogonal vector to \vec{r}_{PM} . If $P = C_V$, its material position with respect to C_M is thus defined, $\dot{\theta} \neq 0$,

$$\vec{v}_V = \vec{v}_M + \dot{\theta} \hat{r}_{VM} = 0. \quad (2.10)$$

With respect to small displacements and small rotation, Eq. (2.10) is multiplied by the time differential to render,

$$\delta \vec{r}_M + \delta \theta \hat{r}_{VM} = 0. \quad (2.11)$$

The modal displacements and rotation combine kinematically to a sufficiently small rotation about the floor's modal center of velocity. Consequently, the mode shapes are defined by rotations of the floor about the modally resulting centers of velocity, a general displaced position (exaggerated) of the floor, is sketched in Fig. 2.2.

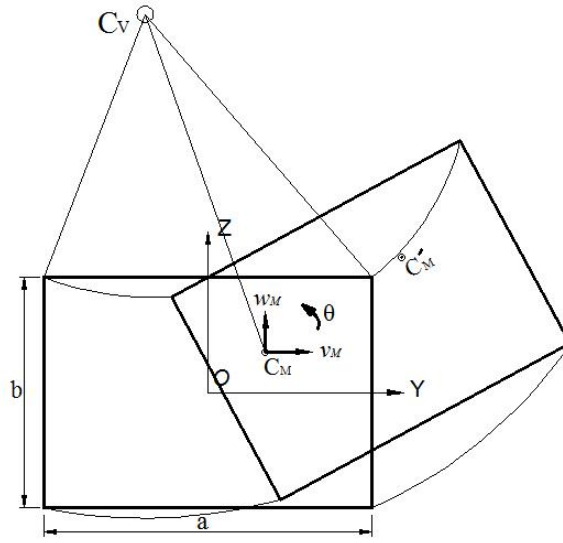


Fig. 2.2: General mode shape (exaggerated) for asymmetric space frame; small displacement and small rotation $|\theta| \ll 1$ of the floor are understood.

The position vector of the center of velocity C_V is $\vec{r}_V^T = [y_V \quad z_V]$ and the displacement of C_V for sufficiently small motion is zero. The material vector $\vec{r}_{VM}^T = [y_V - y_M \quad z_V - z_M]$ becomes when rotated, $\hat{r}_{VM}^T = [-(z_V - z_M) \quad (y_V - y_M)]$. The coordinates of the center of velocity can be derived by Eq. (2.11) under such conditions, $\delta\theta \doteq \theta$, $\delta v_M \doteq v_M$, $\delta w_M \doteq w_M$,

$$y_V = y_M - \frac{1}{\theta} w_M, z_V = z_M + \frac{1}{\theta} v_M \quad (2.12)$$

In terms of the components of the modal vector $\vec{\phi}_j$, the co-ordinates of modal center of velocity become,

$$y_{Vj} = y_M - \frac{\phi_{j2}}{\phi_{j3}} r_x, z_{Vj} = z_M + \frac{\phi_{j1}}{\phi_{j3}} r_x, \phi_{j3} \neq 0, \quad j = 1, 2, 3. \quad (2.13)$$

The position of the modal center of velocity plays a key role in determining the effective location of the respective TLCD to be installed on the floor of the main system, for practical implementation for lab-model, see sub-section 3.4.

2.3 The equation of relative fluid flow in a TLCGD

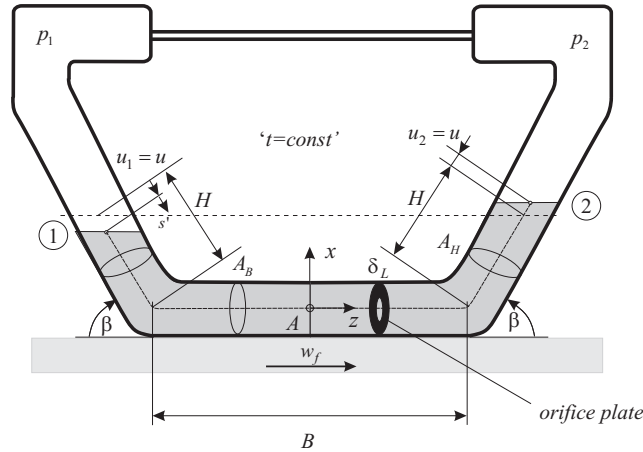


Fig. 2.3: Tuned liquid column-gas damper (TLCGD).

A TLCGD with geometry shown in Fig. 2.3 is a symmetric, U- or V-shaped rigid piping system consisting of one horizontal and two inclined ($\pi/4 \leq \beta \leq \pi/2$), partially water-filled pipe sections. Let B and H denote the horizontal and inclined lengths of the liquid columns in their associated pipe sections at rest, whose cross-sectional areas A_B , A_H assumed to be constant, respectively. The relative motion of the liquid column is described by the displacement $u_1 = u_2 = u(t)$ of the interface with emphasis that $u(s', t)$ is a relative displacement of the liquid with respect to the moving frame. In a sealed design of TLCGD, the ends of the piping system are closed and the gas (e.g. air) pressure denoted by p_1 and p_2 is build up in the gas contained on either end of the piping system above the liquid with respect to the reference equilibrium gas-pressure p_0 , see Hochrainer^[2-1] and Hochrainer-Ziegler^[2-2].

A model of the single-storey asymmetric space frame equipped with a TLCGD with its trace under the general angle γ to the y -direction is illustrated in Fig. 2.4. The position coordinate of the reference point A of the TLCGD is $(y_A, z_A, 0)$.

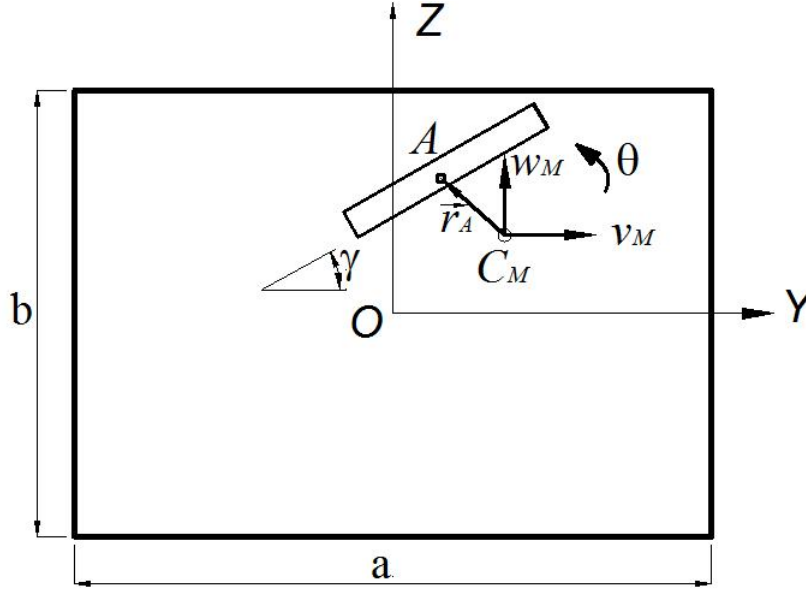


Fig. 2.4: Asymmetric space frame with a TLCGD oriented at angle γ reference configuration.

The liquid motion in TLCGD can be classified as two types: i) the global motion of the liquid with respect to the main structure; and ii) its relative flow, assuming the piping system to be rigid. The generalized non-stationary Bernoulli equation can be used to derive the equation of relative fluid flow, see e.g. Ziegler^[2-5], page 483. The generalized Bernoulli equation of the ideal fluid-flow takes on the form,

$$\int_{1'}^{2'} \vec{a} \cdot \vec{e}_t' ds' = -g(x_2 - x_1) - \frac{1}{\rho}(p_2 - p_1) \quad (2.14)$$

where, x_1, x_2 denote the geodesic height of the displaced free surfaces 1' and 2' respectively; \vec{a} and g denote the absolute acceleration of the fluid particle (i.e., water in TLCGD) and the constant of gravity $g = 9.81 m/s^2$, and \vec{e}_t' is the relative streamline's tangential direction.

The motion of TLCGD during lateral and torsional vibrations is illustrated in Fig. 2.5 and Fig. 2.6, where v_g and w_g used to describe the instant position of C_M due to the horizontal seismic ground acceleration in y - and z - directions, respectively.

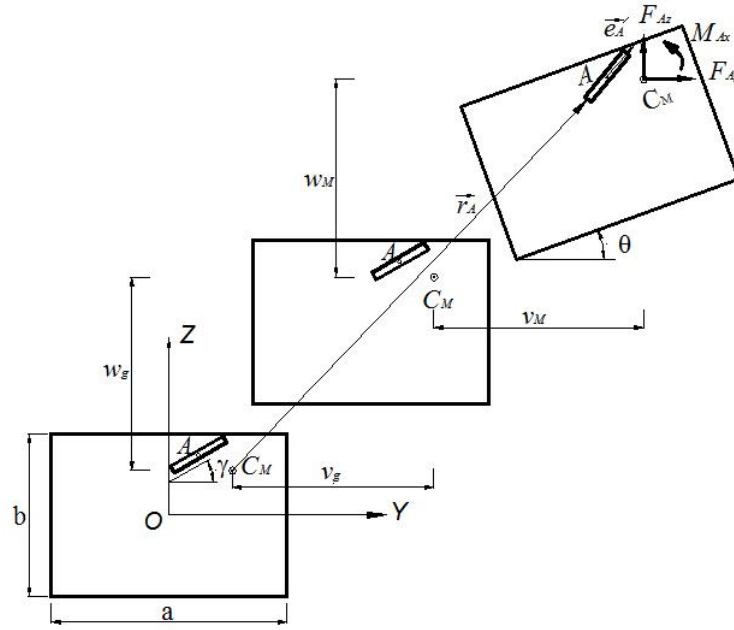


Fig. 2.5: TLCGD under general in-plane acceleration of the floor: $a_g \cos \alpha + \ddot{v}_M$, $a_g \sin \alpha + \ddot{w}_M$ and $\ddot{\theta}$. Resulting force components F_{Ay} , F_{Az} and moment M_{Ax} are indicated in the instant configuration.

The position of the fluid particle against the center of mass C_M of the asymmetric space frame is described by $\vec{r} = \vec{r}_A + \vec{r}'$, where \vec{r}' denotes the relative position of the fluid particle with respect to reference point A of the TLCGD. The relative position vector \vec{r}' is decomposed into its horizontal and vertical components, $\vec{r}' = \vec{r}'_{y'z'} + \vec{r}'_x$. \vec{r}_A is the in-plane position vector of point A against C_M , see e.g. Ziegler^[2-5], page 497. The velocity of fluid particle \vec{v} can be derived straightforwardly by differentiating \vec{r} with respect to time,

$$\vec{v} = \frac{d\vec{r}_A}{dt} + \frac{d\vec{r}'}{dt} = \vec{v}_A + \frac{d\vec{r}'}{dt} \quad (2.15)$$

$$\frac{d\vec{r}'}{dt} = \dot{\theta} \vec{e}_x \times \vec{r}' + \frac{d\vec{r}'}{dt} = \dot{\theta} \hat{r}'_{y'z'} + \dot{\vec{u}}.$$

Here, we define $\dot{\vec{u}} = \dot{u}(s', t) \vec{e}'_t$, see Fig. 2.6, as the relative velocity of the fluid particle with respect to the moving reference frame. $\vec{v}_{gu} = \vec{v}_A + \dot{\theta} \hat{r}'_{y'z'}$ denotes the guiding

2. Single-storey Asymmetric Space Frame with TLCGDs: Laboratory Model

velocity, where $\vec{v}_A = \vec{v}_M + \hat{\theta} \hat{r}_{AM}$. A second differentiation with respect to time renders an expression for the acceleration,

$$\vec{a} = \vec{a}_A + \hat{\theta} \hat{r}'_{y'z'} - \dot{\theta}^2 \vec{r}'_{y'z'} + 2\dot{\theta} \vec{e}_x \times \dot{\vec{u}} + \frac{d'\dot{\vec{u}}}{dt} = \vec{a}_{gu} + \vec{a}_c + \vec{a}', \quad (2.16)$$

with the guiding acceleration $\vec{a}_{gu} = \vec{a}_A + \hat{\theta} \hat{r}'_{y'z'} - \dot{\theta}^2 \vec{r}'_{y'z'}$ and the Coriolis acceleration

$\vec{a}_c = 2\dot{\theta} \vec{e}_x \times \dot{\vec{u}}$, the latter is perpendicular to the relative velocity $\dot{\vec{u}}$. The relative

acceleration $\vec{a}' = \frac{d'\dot{\vec{u}}}{dt}$ is the relative rate of the relative velocity and with respect to the

moving frame can be expressed as $\vec{a}' \cdot \vec{e}'_t = \frac{\partial \dot{u}}{\partial t} + \frac{\partial}{\partial s'} \left(\frac{\dot{u}^2}{2} \right)$, see again Ziegler^[2-5], page

498. Projecting absolute acceleration, Eq. (2.16) along the relative streamline's tangent

\vec{e}'_t yields,

$$\vec{a} \cdot \vec{e}'_t = \vec{a}_{gu} \cdot \vec{e}'_t + \underbrace{\vec{a}_c \cdot \vec{e}'_t}_0 + \vec{a}' \cdot \vec{e}'_t = \vec{a}_A \cdot \vec{e}'_t - \dot{\theta}^2 \vec{r}'_{y'z'} \cdot \vec{e}'_t + \frac{\partial \dot{u}}{\partial t} + \frac{\partial}{\partial s'} \left(\frac{\dot{u}^2}{2} \right). \quad (2.17)$$

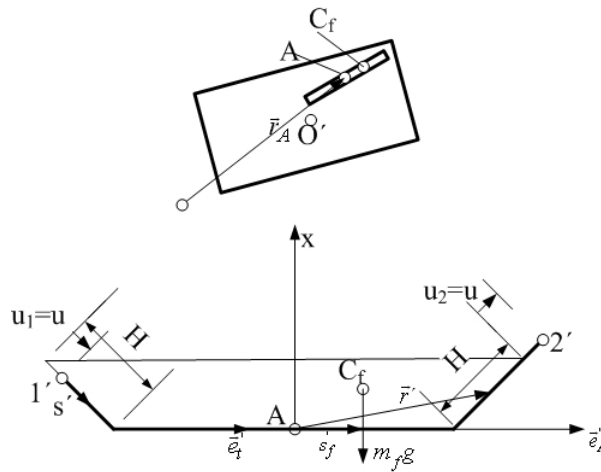


Fig. 2.6: TLCGD in general horizontal motion; C_f is instant position of the fluid's center of mass.

The absolute acceleration of the reference point A is given, Fig. 2.5,

2. Single-storey Asymmetric Space Frame with TLCDs: Laboratory Model

$$\vec{a}_A = a_y \vec{e}_y + a_z \vec{e}_z = \vec{a}_M + \ddot{\theta} \hat{r}_{AM} - \dot{\theta}^2 \vec{r}_{AM}, \quad (2.18)$$

where, $\vec{r}_{AM} = (y_A - y_M) \vec{e}_y + (z_A - z_M) \vec{e}_z$, $\hat{r}_{AM} = -(z_A - z_M) \vec{e}_y + (y_A - y_M) \vec{e}_z$.

Thus, the components of acceleration become,

$$\begin{aligned} a_y &= a_g \cos \alpha + \ddot{v}_M - (z_A - z_M) \ddot{\theta} - (y_A - y_M) \dot{\theta}^2, \\ a_z &= a_g \sin \alpha + \ddot{w}_M + (y_A - y_M) \ddot{\theta} - (z_A - z_M) \dot{\theta}^2, \end{aligned} \quad (2.19)$$

where \ddot{v}_M , \ddot{w}_M and $\ddot{\theta}$ are the acceleration of the floor's center of mass in y -, z -directions and the angular acceleration of the rigid floor of the space frame, respectively.

\vec{a}_A projected in \vec{e}'_A -direction is

$$\vec{a}_A \cdot \vec{e}'_A = a_y \cos(\gamma + \theta) + a_z \sin(\gamma + \theta) \quad (2.20)$$

For the inclined segments: Fig. 2.6,

$$0 \leq s' \leq H - u_1 : \vec{e}'_A \cdot \vec{e}'_t = \cos \beta ; \quad 0 \leq s' \leq H + u_2 : \vec{e}'_A \cdot \vec{e}'_t = \cos \beta ,$$

For the horizontal segment: Fig. 2.6; $0 \leq s' \leq B : \vec{e}'_A \cdot \vec{e}'_t = 1$.

Using $u_1 = u_2 = u(t)$ and the continuity equation $\dot{u}(s', t) A(s') = \text{const}$, the integral term, see Eq. (2.14), becomes,

$$\int_1^2 \vec{a}_A \cdot \vec{e}'_t ds' = \{(H - u) \cos \beta + B + (H + u) \cos \beta\} (\vec{a}_A \cdot \vec{e}'_A) = (B + 2H \cos \beta) (\vec{a}_A \cdot \vec{e}'_A). \quad (2.21)$$

For the inclined segments: $0 \leq s' \leq H - u_1 : \vec{r}'_{y'z'} = -\{B/2 + (H - u_1) \cos \beta - s' \cos \beta\} \vec{e}'_A$,

$$\vec{r}'_{y'z'} \cdot \vec{e}'_t = -\{B/2 + (H - u_1) \cos \beta - s' \cos \beta\} \cos \beta, \quad (2.22)$$

$$0 \leq s' \leq H + u_2 : \vec{r}'_{y'z'} = (B/2 + s' \cos \beta) \vec{e}'_A, \quad \vec{r}'_{y'z'} \cdot \vec{e}'_t = (B/2 + s' \cos \beta) \cos \beta. \quad (2.23)$$

For the horizontal segment: $0 \leq s' \leq B : \vec{r}'_{y'z'} = -(B/2 - s') \vec{e}'_A, \vec{r}'_{y'z'} \cdot \vec{e}'_t = -(B/2 - s')$.

Substituting $u_1 = u_2 = u(t)$, the integral terms become,

$$-\dot{\theta}^2 \int_1^2 \vec{r}'_{y'z'} \cdot \vec{e}'_t ds' = -\dot{\theta}^2 u (B \cos \beta + 2H \cos^2 \beta), \quad (2.24)$$

$$\int_1^{2'} \frac{\partial}{\partial s'} \left(\frac{\dot{u}^2}{2} \right) ds' = \frac{1}{2} (\dot{u}_2^2 - \dot{u}_1^2) = 0 \quad (\text{symmetry}), \quad (2.25)$$

$$\int_1^{2'} \frac{\partial \dot{u}}{\partial t} ds' = \ddot{u} (H - u_1) + \ddot{u} B \frac{A_H}{A_B} + \ddot{u} (H + u_2) = \left(2H + B \frac{A_H}{A_B} \right) \ddot{u}, \quad (2.26)$$

and the difference between geodesic heights of fluid-gas interfaces in the TLCGD is

$$x_2 - x_1 = (H + u_2) \sin \beta - (H - u_1) \sin \beta = 2u \sin \beta. \quad (2.27)$$

If the ends of piping system are open to the environmental atmosphere (not sealed) then the air pressure at the free surface is approximately equal to the ambient pressure, $p_1 = p_2 = p_0$ and hence, pressure difference vanishes; the same holds true in case of free flow of the gas through a connecting pipe. If the piping system is sealed on both sides, the gas inside the sealed volume $V_0 = A_H H_a$ is quasi-statically compressed, see Ziegler^[2-5], page 88 by the liquid surface in a sufficiently slow motion (piston theory applies). H_a denotes the effective height of the gas-volume at rest $V_0 = A_H H_a$. Hence, the pressure difference $p_2 - p_1$ in Eq. (2.14) in the range of linearized gas compression, i.e. if the maximum fluid-stroke is limited by $\max |u| \leq H_a/3$, changes the undamped natural frequency of the TLCGD defined in Eq. (2.30), see Hochrainer^[2-1] and Hochrainer-Ziegler^[2-2]. Thus, $p_2 - p_1 \approx 2np_0 u / H_a$, where $1 \leq n \leq 1.4$ is the polytropic index determined by the type of quasi-static change of state of the gas. For an adiabatic process of any diatomic gas $n=1.4$, whereas for the isothermal (slow) process $n=1.0$, Ziegler^[2-5], page 88. Any other polytropic process is in-between these two extreme situations. In the application of TLCGD in base isolation, we expect rather low frequencies around 0.5 Hz. Consequently, the gas compression might be close to isothermal conditions and thus becomes linear for the strokes to be considered, we put $n=1$ in Eqs. (2.30). Whereas for the laboratory testing, we had to consider polytropic gas compression, $n=1.2$.

Finally, the experimentally observed averaged turbulent damping $\delta_L |u| \dot{u}$ must be added,

2. Single-storey Asymmetric Space Frame with TLCGDs: Laboratory Model

see Hochrainer^[2-1], where, $\delta_L = \lambda_L/2L_{eff}$ is the head-loss coefficient. Substituting equations (2.21)-(2.27) in Eq. (2.14) and considering the linearized gas compression yield the nonlinear and parametrically forced ($\beta < \pi/2$) equation of the relative fluid flow in the TLCGD, any vertical motion is not considered here,

$$\ddot{u} + \delta_L |\dot{u}| \dot{u} + \omega_A^2 \left(1 - \kappa_\beta \frac{\dot{\theta}^2}{\omega_A^2} \right) u = -\kappa (\vec{a}_A \cdot \vec{e}'_A), \quad (2.28)$$

$$\kappa = \frac{B + 2H \cos \beta}{L_{eff}}, \quad \kappa_\beta = \kappa \cos \beta, \quad L_{eff} = 2H + \frac{A_H}{A_B} B$$

$$\omega_A = \sqrt{\frac{g}{L_{eff}/2} \sin \beta} \quad (\text{“open TLCD”, no gas-spring}), \quad (2.29)$$

$$\omega_A = \sqrt{\frac{g}{L_{eff}/2} \left(\sin \beta + \frac{h_0}{H_a} \right)}, \quad h_0 = np_0/\rho g \quad (\text{linearized gas-spring}), \quad 1 \leq n \leq 1.4 \quad (2.30)$$

where, L_{eff} can be considered as the length of an equivalent uniform liquid column of constant cross sectional area A_H rendering the same natural circular frequency ω_A of the TLCD; κ and κ_β are geometry dependent coupling factors linking the floor acceleration and the TLCGD excitation, respectively.

The ratio h_0/H_a in Eq. (2.30) accounts for the gas-spring effect enabling the TLCGD not only a self-controlling device, as large liquid strokes produce a weakly nonlinear compression of the gas, but also the tuning of the TLCGD is controlled conveniently just by changing the equilibrium gas-pressure. Hence, the TLCGD is ideally suited to extend the frequency range of civil engineering applications by properly adjusting the equilibrium gas-pressure p_0 .

The vertical floor acceleration, expected to be present in seismic excitation and commonly equal to the vertical component of the ground acceleration $\lambda_g a_g$, commonly $0 \leq \lambda_g \leq 1$, adds parametric forcing in Eq. (2.28) $\omega_A^2 u (\lambda_g a_g / g)$ in addition to the

rotational excitation. In the course of the tuning procedure, an equivalent linearized damping coefficient $C_A = 2m_f \zeta_A \omega_A$ might be used to replace the nonlinear turbulent damping term in Eq. (2.28), $\zeta_A = (4/3\pi) \delta_L \max|u|$, see Hochrainer^[2-1]. If this linear damping coefficient of relative fluid flow ζ_A exceeds the cut-off value of parametric resonance, the influence of parametric excitation becomes fully negligible, for detailed experimental and numerical investigations see Reiterer^[2-9], page 77 and Reiterer-Ziegler^[2-10],

$$\zeta_A > \zeta_{A,0} = \frac{\lambda_g a_g / g}{4(1 + h_0 / H_a \sin \beta)}. \quad (2.31)$$

Ziegler^[2-11] pointed out the speed limitation of the fluid-gas interface to keep the interface intact and thus to allow the application of the piston theory, based on Lindner-Silvester and Schneider^[2-12],

$$\max|\dot{u}| = \omega_A \max|u| < 10 \text{ m/s}. \quad (2.32)$$

Substituting the acceleration components, Eq. (2.19) in Eq. (2.28), and further linearizing the forcing terms yield the simplified and linearized equation for the relative fluid flow in the TLCD in proper form for tuning and to be compared to the equivalent TMD-equation,

$$\ddot{u} + 2\zeta_A \omega_A \dot{u} + \omega_A^2 u = -\kappa \left\{ \begin{array}{l} (\ddot{v}_M - (z_A - z_M) \ddot{\theta}) \cos \gamma + (\ddot{w}_M + (y_A - y_M) \ddot{\theta}) \sin \gamma + \\ a_g \cos(\alpha - \gamma) \end{array} \right\}. \quad (2.33)$$

Left-hand terms in Eq. (2.33) are corresponding to the vibration-terms of the relative liquid motion and right-hand terms can be regarded as the linearized portions of the generalized external forces causing the motion of the liquid.

2.4 Control forces of TLCD

To couple the TLCD with the main structure (i.e., asymmetric space frame) it becomes important to know the interface reactions. Assuming that the dead weight of a rigid piping system has been added to the corresponding floor-mass (dead fluid-mass is

neglected at this stage), only the interaction forces between the massless, rigid, liquid filled piping system and the supporting floor are considered. The control forces F_{Ay} , F_{Az} and M_{Ax} in y , z and θ directions are derived by conservation of momentum and angular momentum of the moving fluid.

(i) Instant coordinates of center of fluid-mass C_f , conservation of momentum $\vec{R} = m_f \vec{a}_f$.

The instant position of C_f with respect to reference point A is given by $\vec{r}'_f + x_f \vec{e}_x$,

$$\vec{r}'_f = s'_f \vec{e}'_A, \text{ see again Fig. 2.6. Hence, } \vec{r}_f = \vec{r}_A + \vec{r}'_f + x_f \vec{e}_x,$$

$$\frac{d\vec{r}'_f}{dt} = s'_f \dot{\vec{e}}'_A + s'_f \dot{\theta} \hat{\vec{e}}'_A, \vec{v}_f = \frac{d\vec{r}_f}{dt} = \vec{v}_A + s'_f \dot{\vec{e}}'_A + s'_f \dot{\theta} \hat{\vec{e}}'_A + \dot{x}_f \vec{e}_x, \quad (2.34)$$

$$\vec{a}_f = \frac{d\vec{v}_f}{dt} = \vec{a}_A + (s''_f - s'_f \dot{\theta}^2) \vec{e}'_A + (2s'_f \dot{\theta} + s'_f \ddot{\theta}) \hat{\vec{e}}'_A + \ddot{x}_f \vec{e}_x, \quad (2.35)$$

and by means of the static fluid-mass-moments

$$\begin{aligned} m_f s'_f &= \rho A_H (H+u) \left(\frac{B}{2} + \frac{H+u}{2} \cos \beta \right) - \rho A_H (H-u) \left(\frac{B}{2} + \frac{H-u}{2} \cos \beta \right) \\ &= \rho A_H u (B + 2H \cos \beta) \end{aligned} \quad (2.36)$$

$$m_f x_f = \rho A_H (H+u) \frac{H+u}{2} \sin \beta + \rho A_H (H-u) \frac{H-u}{2} \sin \beta = \rho A_H (H^2 + u^2) \sin \beta \quad (2.37)$$

Hence, we define,

$$\begin{aligned} s'_f &= \frac{B + 2H \cos \beta}{L_1} u = \bar{\kappa} u, \dot{s}'_f = \bar{\kappa} \dot{u}, \ddot{s}'_f = \bar{\kappa} \ddot{u}, \\ x_f &= \frac{(H^2 + u^2) \sin \beta}{L_1} = \bar{\kappa}_{T\beta} \frac{1}{2H} (H^2 + u^2), \dot{x}_f = \bar{\kappa}_{T\beta} \frac{1}{H} u \dot{u}, \ddot{x}_f = \bar{\kappa}_{T\beta} \frac{1}{H} (\dot{u}^2 + u \ddot{u}) \end{aligned} \quad (2.38)$$

with the following geometry coefficients and the total fluid-mass,

$$\bar{\kappa} = \kappa L_{eff} / L_1, \quad \bar{\kappa}_{T\beta} = \bar{\kappa}_{T0} \sin \beta, \quad \bar{\kappa}_{T0} = 2H / L_1,$$

$$m_f = \rho \int_1^{2'} A(s') ds' = \rho A_H L_1, \quad L_1 = 2H + \frac{A_B}{A_H} B. \quad (2.39)$$

L_1 equals L_{eff} in the case of $A_H = A_B$ and thus $\kappa = \bar{\kappa}$.

Substituting Eq. (2.38) into Eq. (2.35) after multiplication with m_f , Eq. (2.40) results,

$$\vec{R} = m_f \vec{a}_A + m_f \bar{\kappa}_{T\beta} \frac{1}{H} (\dot{u}^2 + u\ddot{u}) \vec{e}_x + m_f \bar{\kappa} (\ddot{u} - u\dot{\theta}^2) \vec{e}'_A + m_f \bar{\kappa} (2\dot{u}\dot{\theta} + u\ddot{\theta}) \hat{\vec{e}}'_A, \quad (2.40)$$

where,

$$\vec{a}_A = \{a_y \cos(\gamma + \theta) + a_z \sin(\gamma + \theta)\} \vec{e}'_A + \{-a_y \sin(\gamma + \theta) + a_z \cos(\gamma + \theta)\} \hat{\vec{e}}'_A. \quad (2.41)$$

It must be mentioned, that fluid-mass is not included in the unwanted vertical reaction force component F_{Ax} . However, when working with framed structures, this vertical force is generally negligible. Equation (2.40) renders the components of the control forces in-plane acting on the piping system, Fig. 2.5,

$$F_A \vec{e}'_A = m_f \{a_y \cos(\gamma + \theta) + a_z \sin(\gamma + \theta)\} + m_f (\bar{\kappa} \ddot{u} - \bar{\kappa} u \dot{\theta}^2), \quad (2.42)$$

$$F_A \hat{\vec{e}}'_A = m_f \{-a_y \sin(\gamma + \theta) + a_z \cos(\gamma + \theta)\} + m_f (2\bar{\kappa} \dot{u} \dot{\theta} + \bar{\kappa} u \ddot{\theta}), \quad (2.43)$$

and become when rotated,

$$F_{Ay} = m_f \{a_y + (\bar{\kappa} \ddot{u} - \bar{\kappa} u \dot{\theta}^2) \cos(\gamma + \theta) - (2\bar{\kappa} \dot{u} \dot{\theta} + \bar{\kappa} u \ddot{\theta}) \sin(\gamma + \theta)\}, \quad (2.44)$$

$$F_{Az} = m_f \{a_z + (\bar{\kappa} \ddot{u} - \bar{\kappa} u \dot{\theta}^2) \sin(\gamma + \theta) + (2\bar{\kappa} \dot{u} \dot{\theta} + \bar{\kappa} u \ddot{\theta}) \cos(\gamma + \theta)\}. \quad (2.45)$$

Equations (2.44) and (2.45) are simplified under the condition $|\theta| \ll 1$ and the essential linear parts become

$$F_{Ay} = m_f \{a_g \cos \alpha + \ddot{v}_M - (z_A - z_M) \ddot{\theta}\} + \bar{\kappa} m_f \ddot{u} \cos \gamma, \quad (2.46)$$

$$F_{Az} = m_f \{a_g \sin \alpha + \ddot{w}_M + (y_A - y_M) \ddot{\theta}\} + \bar{\kappa} m_f \ddot{u} \sin \gamma. \quad (2.47)$$

(ii) Conservation of the angular momentum of the fluid particle, see again Ziegler^[2-5] page 405, yields the resultant of the acting moment with respect to the accelerated point of reference A ,

$$\frac{d\vec{D}_A}{dt} + m_f (\vec{r}'_f + x_f \vec{e}_x) \times \vec{a}_A = \vec{M}_A, \quad \frac{d\vec{D}_A}{dt} = \frac{d'\vec{D}_A}{dt} + \dot{\theta} (\vec{e}_x \times \vec{D}_A) \quad (2.48)$$

with the relative angular momentum

$$\begin{aligned}\bar{D}_A &= \int_{m_f} (\bar{r}' \times \bar{v}') dm_f = \int_{m_f} \left\{ \bar{r}' \times (\dot{\theta} \hat{r}'_{y'z'} + \dot{u}) \right\} dm_f \\ &= \rho \left\{ \dot{\theta} \int_{1'}^{2'} A(s') (\bar{r}' \times \hat{r}'_{y'z'}) ds' + \int_{1'}^{2'} A(s') \dot{u}(s', t) (\bar{r}' \times \bar{e}'_t(s')) ds' \right\}\end{aligned}\quad (2.49)$$

For inclined and horizontal segments,

$$0 \leq s' \leq H - u_1 : \bar{r}' \times \bar{e}'_t = -\frac{B}{2} \sin \beta \hat{e}'_A, \quad 0 \leq s' \leq H + u_2 : \bar{r}' \times \bar{e}'_t = -\frac{B}{2} \sin \beta \hat{e}'_A,$$

$$0 \leq s' \leq B : \bar{r}' \times \bar{e}'_t = 0,$$

$$\rho \int_{1'}^{2'} A(s') \dot{u}(s', t) (\bar{r}' \times \bar{e}'_t(s')) ds' = -\bar{\kappa}_T \beta m_f \frac{B}{2} \dot{u} \hat{e}'_A \quad (2.50)$$

$$\begin{aligned}\rho \dot{\theta} \int_{1'}^{2'} A(s') |\hat{r}'_{y'z'}|^2 ds' &= \rho \dot{\theta} A_H \int_0^{H-u} \left\{ -\left(\frac{B}{2} + (H - u_1) \cos \beta - s' \cos \beta \right) \right\}^2 ds' \\ &\quad + \rho \dot{\theta} A_B \int_0^B \left(-\left(\frac{B}{2} - s' \right) \right)^2 ds' + \rho \dot{\theta} A_H \int_0^{H+u} \left(\frac{B}{2} + s' \cos \beta \right)^2 ds' \\ &= \rho \dot{\theta} A_H \left\{ \frac{A_B}{A_H} \frac{B^3}{12} + \frac{B^2}{2} H + B(H^2 + u^2) \cos \beta + \left(\frac{2}{3} H^3 + 2Hu^2 \right) \cos^2 \beta \right\}\end{aligned}\quad (2.51)$$

$$0 \leq s' \leq H - u_1 : \bar{r}'_x \times \hat{r}'_{y'z'} = -\left\{ ((H - u_1) - s') \sin \beta \right\} \left\{ -\left(\frac{B}{2} + (H - u_1) - s' \right) \cos \beta \right\} \bar{e}'_A,$$

$$0 \leq s' \leq H + u_2 : \bar{r}'_x \times \hat{r}'_{y'z'} = -(s' \sin \beta) (B/2 + s' \cos \beta) \bar{e}'_A,$$

$$\rho \dot{\theta} \int_{1'}^{2'} A(s') (\bar{r}'_x \times \hat{r}'_{y'z'}) ds' = -\rho \dot{\theta} A_H \left\{ HBu \sin \beta + \left(\frac{2}{3} u^3 + 2H^2 u \right) \sin \beta \cos \beta \right\} \bar{e}'_A, \quad (2.52)$$

$$\begin{aligned}\bar{D}_A &= m_f \left\{ -\left(\frac{HB}{L_1} + \left(\frac{2}{3} \frac{u^2}{L_1} + 2 \frac{H^2}{L_1} \right) \cos \beta \right) u \dot{\theta} \sin \beta \bar{e}'_A - \bar{\kappa}_T \beta \frac{B}{2} \dot{u} \hat{e}'_A \right. \\ &\quad \left. + \left(\frac{A_B}{A_H} \frac{B^3}{12L_1} + \frac{B^2}{2L_1} H + B \left(\frac{H^2}{L_1} + \frac{u^2}{L_1} \right) \cos \beta + \left(\frac{2}{3} \frac{H^3}{L_1} + 2 \frac{Hu^2}{L_1} \right) \cos^2 \beta \right) \dot{\theta} \bar{e}_x \right\},\end{aligned}\quad (2.53)$$

$$D_{Ax} = m_f \left(\bar{\kappa}_T H^2 + \bar{\kappa}_\beta u^2 \right) \dot{\theta}, \quad (2.54)$$

with the following additional geometry coefficients,

$$\bar{\kappa}_T = \bar{\kappa}_{T0} \left\{ \left(\frac{B}{2H} \right)^2 + \frac{A_B}{3A_H} \left(\frac{B}{2H} \right)^3 + \frac{B}{2H} \cos \beta + \frac{1}{3} \cos^2 \beta \right\}, \quad \bar{\kappa}_\beta = \kappa_\beta \frac{L_{eff}}{L_1}, \quad \bar{\kappa}_{T0} = \frac{2H}{L_1},$$

$$\frac{dD_{Ax}}{dt} = m_f \left\{ \bar{\kappa}_T H^2 \ddot{\theta} + \bar{\kappa}_\beta (u^2 \ddot{\theta} + 2ui\dot{\theta}) \right\}. \quad (2.55)$$

Substituting equations (2.38) and (2.41) in Eq. (2.48) yields,

$$\begin{aligned} m_f (\vec{r}'_f + x_f \vec{e}_x) \times \vec{a}_A = m_f \left\{ -\bar{\kappa}_{T\beta} \frac{H^2 + u^2}{2H} (-a_y \sin(\gamma + \theta) + a_z \cos(\gamma + \theta)) \vec{e}'_A \right. \\ \left. + \bar{\kappa}_{T\beta} \frac{H^2 + u^2}{2H} (a_y \cos(\gamma + \theta) + a_z \sin(\gamma + \theta)) \hat{e}'_A + \bar{\kappa}u (-a_y \sin(\gamma + \theta) + a_z \cos(\gamma + \theta)) \vec{e}_x \right\} \end{aligned} \quad (2.56)$$

The undesired additional moment \vec{M}_p from gravity force with respect to the reference point A is

$$\vec{M}_p = -m_f g (\vec{r}'_f + x_f \vec{e}_x) \times \vec{e}_x = m_f g \bar{\kappa} u \hat{e}'_A. \quad (2.57)$$

The undesired axial moment M_A about lateral \hat{e}'_A direction is the sum of the TLCGD-floor interaction, Eq. (2.53) and a second contribution resulting from gravity force acting at the (displaced) center of fluid-mass $m_f g \bar{\kappa} u$, Eq. (2.57). The latter is similar to that of a TMD with displaced mass. The axial moments M_A about \hat{e}'_A and \vec{e}'_A directions are generally both found negligible in their action on the structure. The nonlinear resultant control moment M_{Ax} (acting on the piping system) becomes finally, adding Eq. (2.55) and the proper component of Eq. (2.56), see again Fig. 2.5,

$$M_{Ax} = m_f \left\{ \bar{\kappa}u (-a_y \sin(\gamma + \theta) + a_z \cos(\gamma + \theta)) + \bar{\kappa}_T H^2 \ddot{\theta} + \bar{\kappa}_\beta (u^2 \ddot{\theta} + 2ui\dot{\theta}) \right\}. \quad (2.58)$$

Equation (2.58) is simplified under the condition $|\theta| \ll 1$ and when properly linearized, becomes,

$$M_{Ax} = m_f \bar{\kappa}_T H^2 \ddot{\theta}, \quad \bar{\kappa}_T = \bar{\kappa}_{T0} \left\{ \left(\frac{B}{2H} \right)^2 + \frac{A_B}{3A_H} \left(\frac{B}{2H} \right)^3 + \frac{B}{2H} \cos \beta + \frac{1}{3} \cos^2 \beta \right\}, \quad (2.59)$$

and the linearized moment at C_M is determined by

$$M_x = M_{Ax} - F_{Ay} (z_A - z_M) + F_{Az} (y_A - y_M). \quad (2.60)$$

The interaction forces and the moment of TLCGD, equations (2.46), (2.47) and (2.60) derived by considering the conservation of momentum and angular momentum

respectively, refer to the center of mass C_M whose position is no longer exact, because the dead fluid-mass of TLCGD is not considered in the main system and thus introduces an approximation.

2.5 Approximate substructure synthesis of the space frame with TLCGD

The equation of motion for the coupled system considering the undamped single-storey asymmetric space frame under horizontal ground excitation, Eq. (2.1), and the TLCGD, Fig. 2.5, in substructure synthesis when Eqs. (2.46), (2.47) and (2.60) are combined,

$$\underline{M} \ddot{\bar{x}} + \underline{K} \bar{x} = -\underline{M} \bar{a}_g + \bar{F}, \quad \bar{a}_g^T = a_g [\cos \alpha \quad \sin \alpha \quad 0] \quad (2.61)$$

where, $\bar{F}^T = -[F_{Ay} \quad F_{Az} \quad M_x/r_x]$ is the linearized control force vector.

If the floor displacements \bar{x} are expanded into modal series, $\bar{x} = \sum_{i=1}^3 \bar{\phi}_i q_i$ and substituted on left-hand side of Eq. (2.61), it decouples by pre-multiplication with the transposed ortho-normalized modal vector $\bar{\phi}_j^T$,

$$\bar{\phi}_j^T \underline{M} \bar{\phi}_j \ddot{q}_j + \bar{\phi}_j^T \underline{K} \bar{\phi}_j q_j = -\bar{\phi}_j^T \underline{M} \bar{a}_g + \bar{\phi}_j^T \bar{F}. \quad (2.62)$$

Equation (2.62) divided by modal mass m_j with light modal structural damping added, becomes,

$$\ddot{q}_j + 2\zeta_{Sj} \omega_{Sj} \dot{q}_j + \omega_{Sj}^2 q_j = -\frac{1}{m_j} \bar{\phi}_j^T \underline{M} \bar{a}_g + \frac{1}{m_j} \bar{\phi}_j^T \bar{F}, \quad (2.63)$$

where, $\omega_{Sj}^2 = \bar{\phi}_j^T \underline{K} \bar{\phi}_j / m_j$, $m_j = \bar{\phi}_j^T \underline{M} \bar{\phi}_j$, for ortho-normalized modal vector, $m_j = 1$.

The control force term,

$$\frac{1}{m_j} \bar{\phi}_j^T \bar{F} = \frac{-1}{m_j} [\phi_{j1} F_{Ayj} + \phi_{j2} F_{Azj} + \phi_{j3} M_{xj}/r_x], \quad (2.64)$$

renders modal coupling when the linearized control forces, Eqs. (2.46), (2.47) and (2.60), are substituted in Eq. (2.64) by using modal expansion,

$$\ddot{v}_M = \sum_{i=1}^3 \ddot{q}_i \phi_{i1}, \quad \ddot{w}_M = \sum_{i=1}^3 \ddot{q}_i \phi_{i2}, \quad \ddot{u}_T = \sum_{i=1}^3 \ddot{q}_i \phi_{i3}, \quad (2.65)$$

$$\frac{1}{m_j} \bar{\phi}_j^T \bar{F}_j = -\mu_{ff} \left\{ v_{A,j} \sum_{i=1}^3 \ddot{q}_i \phi_{i1} + w_{A,j} \sum_{i=1}^3 \ddot{q}_i \phi_{i2} + a_g V_{\alpha j} + \bar{\kappa}_j V_{\gamma j} \ddot{u}_j + \frac{1}{r_x} \left\{ \bar{\kappa}_{Tj} H_j^2 \phi_{j3} / r_x - v_{A,j} (z_{Aj} - z_M) + w_{A,j} (y_{Aj} - y_M) \right\} \sum_{i=1}^3 \ddot{q}_i \phi_{i3} \right\}, \quad (2.66)$$

$$\mu_{ff} = m_{ff} / m_j, \quad v_{A,j} = \phi_{j1} - \phi_{j3} (z_{Aj} - z_M) / r_x, \quad w_{A,j} = \phi_{j2} + \phi_{j3} (y_{Aj} - y_M) / r_x,$$

$$V_{\gamma j} = v_{A,j} \cos \gamma_j + w_{A,j} \sin \gamma_j, \quad V_{\alpha j} = v_{A,j} \cos \alpha + w_{A,j} \sin \alpha.$$

Equation (2.66) can be rearranged,

$$\frac{1}{m_j} \bar{\phi}_j^T \bar{F}_j = -\mu_{ff} \left\{ \begin{aligned} & \ddot{q}_1 \left\{ (\phi_{11} - \phi_{13} (z_{A1} - z_M) / r_x) v_{A,1} + (\phi_{12} + \phi_{13} (y_{A1} - y_M) / r_x) w_{A,1} + \bar{\kappa}_{T1} (H_1 \phi_{13} / r_x)^2 \right\} \\ & + \ddot{q}_2 \left\{ (\phi_{21} - \phi_{23} (z_{A2} - z_M) / r_x) v_{A,2} + (\phi_{22} + \phi_{23} (y_{A2} - y_M) / r_x) w_{A,2} + \bar{\kappa}_{T2} (H_2 \phi_{23} / r_x)^2 \right\} \\ & + \ddot{q}_3 \left\{ (\phi_{31} - \phi_{33} (z_{A3} - z_M) / r_x) v_{A,3} + (\phi_{32} + \phi_{33} (y_{A3} - y_M) / r_x) w_{A,3} + \bar{\kappa}_{T3} (H_3 \phi_{33} / r_x)^2 \right\} \\ & + a_g V_{\alpha j} + \bar{\kappa}_j V_{\gamma j} \ddot{u}_j \end{aligned} \right\} \quad (2.67)$$

Equation (2.67), depicts more clearly the modal coupling, and it is approximated for the selected mode number j for the sake of modal tuning of the TLCD in a first step in the design stage, and hence reduces to,

$$\begin{aligned} \frac{1}{m_j} \bar{\phi}_j^T \bar{F}_j &= -\mu_{ff} \left\{ \ddot{q}_j \left\{ \begin{aligned} & (\phi_{j1} - \phi_{j3} (z_{Aj} - z_M) / r_x) v_{A,j} + (\phi_{j2} + \phi_{j3} (y_{Aj} - y_M) / r_x) w_{A,j} \\ & + \bar{\kappa}_{Tj} (H_j \phi_{j3} / r_x)^2 \end{aligned} \right\} \right. \\ & \left. + a_g V_{\alpha j} + \bar{\kappa}_j V_{\gamma j} \ddot{u}_j \right\} \\ &= -\mu_{ff} \left\{ \ddot{q}_j \left(v_{A,j}^2 + w_{A,j}^2 + \bar{\kappa}_{Tj} (H_j \phi_{j3} / r_x)^2 \right) + a_g V_{\alpha j} + \bar{\kappa}_j V_{\gamma j} \ddot{u}_j \right\} \end{aligned}$$

Thus, the control force term results in the modally isolated form,

$$\frac{1}{m_j} \bar{\phi}_j^T \bar{F}_j = -\mu_j \ddot{q}_j - \mu_{ff} V_{\alpha j} a_g - \mu_{ff} V_{\gamma j} \bar{\kappa}_j \ddot{u}_j \quad (2.68)$$

where, $\mu_j = \mu_{ff} V_j^2$, $V_j^2 = V_j^{*2} + \bar{\kappa}_{Tj} (H_j \phi_{j3} / r_x)^2$, $V_j^{*2} = v_{A,j}^2 + w_{A,j}^2$.

The term $\frac{1}{m_j} \vec{\phi}_j^T \underline{M} \vec{a}_g$ in Eq. (2.63) can also be expanded to identify the classical modal participation factor,

$$\frac{1}{m_j} \vec{\phi}_j^T \underline{M} \vec{a}_g = \mu_{Sj} (\phi_{j1} \cos \alpha + \phi_{j2} \sin \alpha) a_g = L_{Sj} a_g, \quad (2.69)$$

where, $\mu_{Sj} = m_S / m_j$, and $L_{Sj} = \mu_{Sj} (\phi_{j1} \cos \alpha + \phi_{j2} \sin \alpha)$ denotes the classical modal participation factor without considering TLCGD.

Hence, Eq. (2.63) becomes,

$$(1 + \mu_j) \ddot{q}_j + 2\zeta_{Sj} \omega_{Sj} \dot{q}_j + \omega_{Sj}^2 q_j + \mu_{ff} \bar{\kappa}_j V_{\gamma j} \ddot{u}_j = -(L_{Sj} + \mu_{ff} V_{\alpha j}) a_g. \quad (2.70)$$

Right-hand side of the above equation (2.70) can also be expressed as

$$-(L_{Sj} + \mu_{ff} V_{\alpha j}) a_g = -\mu_{Sj} (\phi_{j1} \cos \alpha + \phi_{j2} \sin \alpha) a_g - \mu_{ff} (v_{A,j} \cos \alpha + w_{A,j} \sin \alpha) a_g,$$

and simplified as,

$$-(L_{Sj} + \mu_{ff} V_{\alpha j}) a_g = -(L_{yj} \cos \alpha + L_{zj} \sin \alpha) a_g = -L_j a_g, \quad (2.71)$$

where L_j is the generalized modal participation factor, the fluid-mass in TLCGD is considered,

$$L_j = L_{yj} \cos \alpha + L_{zj} \sin \alpha, \quad L_{yj} = \mu_{Sj} \phi_{j1} + \mu_{ff} v_{A,j}, \quad L_{zj} = \mu_{Sj} \phi_{j2} + \mu_{ff} w_{A,j}. \quad (2.72)$$

Thus, the following approximate equation in the selected mode is derived,

$$(1 + \mu_j) \ddot{q}_j + 2\zeta_{Sj} \omega_{Sj} \dot{q}_j + \omega_{Sj}^2 q_j + \bar{\kappa}_j \mu_{ff} V_{\gamma j} \ddot{u}_j = -L_j a_g. \quad (2.73)$$

Now, the equation of relative fluid flow in TLCGD, Eq. (2.33), takes the form when right-hand side is modally expanded,

$$\begin{aligned}
 & \ddot{u} + 2\zeta_A \omega_A \dot{u} + \omega_A^2 u \\
 & = -\kappa \left\{ \begin{array}{l} \left[\begin{array}{l} \ddot{q}_1 (\phi_{11} - \phi_{13} (z_A - z_M)/r_x) + \ddot{q}_2 (\phi_{21} - \phi_{23} (z_A - z_M)/r_x) \\ + \ddot{q}_3 (\phi_{31} - \phi_{33} (z_A - z_M)/r_x) \end{array} \right] \cos \gamma \\ + \left[\begin{array}{l} \ddot{q}_1 (\phi_{12} - \phi_{13} (y_A - y_M)/r_x) + \ddot{q}_2 (\phi_{22} - \phi_{23} (y_A - y_M)/r_x) \\ + \ddot{q}_3 (\phi_{32} - \phi_{33} (y_A - y_M)/r_x) \end{array} \right] \sin \gamma \\ + a_g \cos(\alpha - \gamma) \end{array} \right\} \quad (2.74)
 \end{aligned}$$

Modal isolation for the selected mode number j renders,

$$\begin{aligned}
 & \ddot{u}_j + 2\zeta_{Aj} \omega_{Aj} \dot{u}_j + \omega_{Aj}^2 u_j \\
 & = -\kappa_j \left\{ \begin{array}{l} \ddot{q}_j \left\{ (\phi_{j1} - \phi_{j3} (z_{Aj} - z_M)/r_x) \cos \gamma_j + (\phi_{j2} + \phi_{j3} (y_{Aj} - y_M)/r_x) \sin \gamma_j \right\} \\ + a_g \cos(\alpha - \gamma_j) \end{array} \right\} \\
 & = -\kappa_j \left\{ \ddot{q}_j (v_{A,j} \cos \gamma_j + w_{A,j} \sin \gamma_j) + a_g \cos(\alpha - \gamma_j) \right\} \\
 & = -\kappa_j V_{\gamma_j} \ddot{q}_j - \kappa_j a_g \cos(\alpha - \gamma_j).
 \end{aligned}$$

Thus, the approximate equation of relative fluid flow in TLCGD for the selected mode takes on the final form,

$$\ddot{u}_j + 2\zeta_{Aj} \omega_{Aj} \dot{u}_j + \omega_{Aj}^2 u_j + \kappa_j V_{\gamma_j} \ddot{q}_j = -\kappa_j a_g \cos(\alpha - \gamma_j). \quad (2.75)$$

The linearized coupled system of modal approximated equations (2.73) and (2.75) for the 2-DOF modally isolated space frame with TLCGD attached becomes in matrix form,

$$\begin{aligned}
 & \begin{bmatrix} 1 + \mu_j & \bar{\kappa}_j V_{\gamma_j} \mu_{ff} \\ \kappa_j V_{\gamma_j} & 1 \end{bmatrix} \begin{bmatrix} \ddot{q}_j \\ \ddot{u}_j \end{bmatrix} + \begin{bmatrix} 2\zeta_{Sj} \omega_{Sj} & 0 \\ 0 & 2\zeta_{Aj} \omega_{Aj} \end{bmatrix} \begin{bmatrix} \dot{q}_j \\ \dot{u}_j \end{bmatrix} + \begin{bmatrix} \omega_{Sj}^2 & 0 \\ 0 & \omega_{Aj}^2 \end{bmatrix} \begin{bmatrix} q_j \\ u_j \end{bmatrix} \\
 & = - \begin{bmatrix} L_j \\ \kappa_j \cos(\alpha - \gamma_j) \end{bmatrix} a_g \quad (2.76)
 \end{aligned}$$

2.6 Modal tuning of TLCGD, Den Hartog optimization

If the modes of the main structure are well separated, the fundamental mode is considered isolated (with respect to the laboratory experiment) rendering the two degrees of freedom (2-DOF) modally isolated coupled TLCGD-space frame system that is still approximate

because the dead fluid-mass of TLCGD affecting the main system is not considered in the dynamics of the main system. The modal tuning of TLCGD might be performed by transformation of the classical Den Hartog's formulas, see DenHartog^[1-12], by means of the analogy between equivalent TMD and TLCGD.

2.6.1 Analogy between equivalent TMD and TLCGD

The analogy between TMD and TLCGD attached to SDOF main structure has been explored by Hochrainer^[2-1], which serves as the basic guide line for utilizing the results available from the TMD design. Later on, Fu^[2-3] has extended the subsequent procedure for a more general 3-DOF main structure with TLCGD attached, and the useful results are summarized here, a star refers to the equivalent TMD,

$$\omega_{Aj}^* = \omega_{Aj}, \zeta_{Aj}^* = \zeta_{Aj}. \quad (2.77)$$

The modal mass ratio of the TMD-main system is defined by

$$\mu_j^* = \mu_j \frac{\kappa_j \bar{\kappa}_j (V_j^*/V_j)^2}{1 + \mu_j \left(1 - \kappa_j \bar{\kappa}_j (V_j^*/V_j)^2\right)} < \mu_j, \quad (2.78)$$

and frequency and damping ratio of the altered main system with an equivalent TMD are

$$\omega_{Sj}^* = \frac{\omega_{Sj}}{\sqrt{1 + \mu_j \left(1 - \kappa_j \bar{\kappa}_j (V_j^*/V_j)^2\right)}} < \omega_{Sj}, \zeta_{Sj}^* = \frac{\zeta_{Sj}}{\sqrt{1 + \mu_j \left(1 - \kappa_j \bar{\kappa}_j (V_j^*/V_j)^2\right)}} < \zeta_{Sj}. \quad (2.79)$$

The TMD frequency ratio $\delta_{jopt}^* = \frac{\omega_{Aj,opt}^*}{\omega_{Sj}^*}$ and the TLCGD frequency ratio

$\delta_{jopt} = \frac{\omega_{Aj,opt}}{\omega_{Sj}}$ are thus related by the more general transformation,

$$\delta_{jopt} = \frac{\delta_{jopt}^*}{\sqrt{1 + \mu_j \left(1 - \kappa_j \bar{\kappa}_j (V_j^*/V_j)^2\right)}} < \delta_{jopt}^*. \quad (2.80)$$

The optimal frequency ratio δ_{jopt} of the TLCGD turns out slightly lowered than that of equivalent TMD. The term apparent in the denominator of Eq. (2.78)-(2.80), written as

$$\mu_j \left(1 - \kappa_j \bar{\kappa}_j \left(V_j^* / V_j \right)^2 \right) = m_{ff} \left\{ 1 - \left(\kappa_j V_j^* / V_j \right)^2 \right\} \text{ for } \kappa_j = \bar{\kappa}_j \text{ and } m_j = 1, \quad (2.81)$$

is the dead fluid-mass which changes the main system, therefore the former should be minimized by achieving the higher value of geometry factor κ_j within the limits on liquid column H as given by Eq. (2.88).

Optimal TMD design parameters, frequency ratio and damping ratio, are determined subjected to the time-harmonic excitation. The optimum tuning frequency ratio between the equivalent mechanical absorber and the main structure for minimum total acceleration is, see Den Hartog^[2-13], page 97 and 101,

$$\delta_{opt}^* = \frac{1}{1 + \mu^*}, \quad (2.82)$$

and the corresponding optimum linear viscous damping coefficient is given by

$$\zeta_{opt}^* = \sqrt{\frac{3\mu^*}{8(1 + \mu^*)}}. \quad (2.83)$$

2.6.2 Parameters of the gas-spring

The parameter of gas-spring can be conveniently determined by making use of the linear eigen frequency of the mathematical pendulum (i.e. rigid massless rod with a point-mass, attached at a pivot point). The frequency of such a mathematical pendulum for small angular motion is approximately constant and solely depends on its length L_0 by the

following relation, $f_A = \sqrt{\frac{g / \pi^2}{4L_0}}$ (Hz). Thus, its length is related to frequency by a

hyperbola,

$$L_0 = \frac{g / \pi^2}{4f_A^2}. \quad (2.84)$$

The natural frequency of the open TLCD (i.e. without a gas-spring) is, Eq. (2.29),

$$f_A = \frac{\omega_A}{2\pi} = \sqrt{\frac{(g / \pi^2)}{4(L_{eff} / 2)}} \sin \beta. \quad (2.85)$$

If the TLCD and the pendulum have the same frequency, we can write the relation $L_{eff} = 2L_0 \sin \beta$. Now, the frequency of a TLCGD with linearized gas-spring effect, Eq.

(2.30) is rewritten as

$$f_A = \frac{\omega_A}{2\pi} = \sqrt{\frac{(g/\pi^2)}{4(L_{eff}/2)} \left(\sin \beta + \frac{h_0}{H_a} \right)}. \quad (2.86)$$

If the TLCGD and the mathematical pendulum have the same frequency, we can conveniently determine the parameters of the gas-spring, crucial for frequency tuning, in terms of the effective liquid column length L_{eff} in terms of a simple design formula,

$$h_0/H_a = L_{eff}/2L_0 - \sin \beta. \quad (2.87)$$

2.6.3 Steps of modal tuning of TLCGD in the design stage

The modal mass ratio of the equivalent TMD μ^* calculated by Eq. (2.78), when the TLCGD geometry and fluid-mass (thus κ_j and μ_j) are known, results δ_{jopt}^* and ζ_{jopt}^* by using Den Hartog optimization formulas, Eqs. (2.82) & (2.83). The optimal frequency ratio δ_{jopt}^* of TMD is transformed to that of TLCGD by using transformation Eq. (2.80), whereas the optimal damping ratio of TLCGD is same as that of the equivalent TMD (i.e., $\zeta_{Aj,opt}^* = \zeta_{Aj,opt}$). The optimal frequency $f_{Aj,opt}$ calculated by using δ_{jopt} for TLCGD renders the required length of mathematical pendulum, Eq. (2.84), and thus utilizing simple TLCGD design formula, Eq. (2.87) to calculate the critical parameter of gas-spring effect h_0/H_a . Hence, the gas-volume $A_H H_a$ required for the frequency tuning of TLCGD is determined, if for some reasons the equilibrium pressure p_0 and thus h_0 is assigned. For the experimental verification of TLCGD damping, the atmospheric pressure was maintained as the gas equilibrium pressure, for convenience in handling the sealed TLCGD in the laboratory, see sub-section 3.4, without observing any buckling of piping system due to small liquid strokes in the

TLCGD. However, the atmospheric pressure, in full scale real applications where the large liquid strokes are encountered, is not a practical design choice because the gas-pressure during its expansion phase becomes lower than the environmental pressure, and hence resulting in a compressive state of hoop stress in the piping system associated with the danger of buckling, see details in sub-section 4.5.2.5. The maximum liquid strokes in the TLCGD $\max|u_0|$ must be ensured within following acceptable limits,

$$\max|u_0| \leq 2/3H, \quad \max|u_0| \leq H_a/3, \quad \max|u_0|\omega_A \leq 10 \text{ m/s}. \quad (2.88)$$

2.7 Steady state response and modal dynamic magnification factor

The dynamic magnification factor (DMF), i.e., the ratio of dynamic response to static response can be determined by assuming a time harmonic ground excitation under various oblique angles of incidence α ($0 \leq \alpha \leq \pi$ with respect to the y -axis), thus $a_g(t) = a_g e^{i\omega t}$, where a_g is the amplitude of the ground acceleration, commonly assigned as a fraction of $g = 9.81 \text{ m/s}^2$ and ω is the circular forcing frequency of excitation.

2.7.1 Steady state vibrations of space frame without TLCGD

When TLCGD is not installed, control force term in equation (2.61) is absent, however light modal structural damping of the main system is considered, using result from Eq. (2.69),

$$\ddot{q}_j + 2\zeta_{Sj}\omega_{Sj}\dot{q}_j + \omega_{Sj}^2 q_j = -L_{Sj}a_g. \quad (2.89)$$

Inserting $q_j(t) = q_{j,1}e^{i\omega t}$ and $a_g(t) = a_g e^{i\omega t}$ into Eq. (2.89), the time reduced modal equation results,

$$q_{j,1} \left(-\omega^2 + \omega_{Sj}^2 + 2i\zeta_{Sj}\omega_{Sj}\omega \right) = -L_{Sj}a_g, \quad q_{j,1st} = -\frac{L_{Sj}a_g}{\omega_{Sj}^2} \text{ when } \omega = 0. \quad (2.90)$$

The complex amplitude $q_{j,1}$ for main system alone (i.e. without TLCD) becomes, dividing throughout by ω_{Sj}^2 ,

$$q_{j,1} = \frac{q_{j,1st}}{(1 - \beta_{Sj}^2 + 2i\zeta_{Sj}\beta_{Sj})}, \quad \beta_{Sj} = \frac{\omega}{\omega_{Sj}}, \quad (2.91)$$

where β_{Sj} is the ratio of forcing frequency to natural frequency of the main system vibrating in its j -th mode, distinct natural frequencies understood.

Thus, the modal dynamic magnification factor $DMF_{j,1}$ for the main system alone results,

$$DMF_{j,1} = \frac{|q_{j,1}|}{q_{j,1st}} = \frac{1}{\sqrt{1 - 2(1 - 2\zeta_{Sj}^2)\beta_{Sj}^2 + \beta_{Sj}^4}}. \quad (2.92)$$

Equation (2.92) clearly shows that that modal dynamic magnification factor for the main system alone is independent of the excitation direction α as required.

2.7.2 Steady state vibrations of modally isolated 2-DOF system

When the TLCD is installed on the asymmetric space frame, the steady state response of the resulting modally isolated coupled 2-DOF system, that is still in unavoidable approximation because of the dead fluid-mass of TLCD as discussed in sub-section 2.6, can be determined by inserting $q_j(t) = q_{j,2}e^{i\omega t}$, $u_j(t) = u_{j,2}e^{i\omega t}$ and $a_g(t) = a_g e^{i\omega t}$ into Eq. (2.76), and the time-reduced linearized modally approximated equations result,

$$\begin{bmatrix} \omega_{Sj}^2 - (1 + \mu_j)\omega^2 + 2i\zeta_{Sj}\omega_{Sj}\omega & -\bar{\kappa}_j\mu_{ff}V_{\gamma j}\omega^2 \\ -\kappa_jV_{\gamma j}\omega^2 & \omega_{Aj}^2 - \omega^2 + 2i\zeta_{Aj}\omega_{Aj}\omega \end{bmatrix} \begin{bmatrix} q_{j,2} \\ u_{j,2} \end{bmatrix} = - \begin{bmatrix} L_j \\ \kappa_j \cos(\alpha - \gamma_j) \end{bmatrix} a_g. \quad (2.93)$$

The individual equations from matrix Eq. (2.93) become when divided by ω_{Aj}^2 ,

$$\left(\bar{\delta}_j^2 - (1 + \mu_j)\beta_{Aj}^2 + 2i\zeta_{Sj}\bar{\delta}_j\beta_{Aj} \right) q_{j,2} - \bar{\kappa}_jV_{\gamma j}\mu_{ff}\beta_{Aj}^2 u_{j,2} = -\frac{L_j a_g}{\omega_{Aj}^2}, \quad \beta_{Aj} = \frac{\omega}{\omega_{Aj}}, \quad (2.94)$$

$$-\kappa_jV_{\gamma j}\beta_{Aj}^2 q_{j,2} + \left(1 - \beta_{Aj}^2 + 2i\zeta_{Aj}\beta_{Aj} \right) u_{j,2} = -\frac{\kappa_j \cos(\alpha - \gamma_j) a_g}{\omega_{Aj}^2}, \quad \bar{\delta}_j = \frac{\omega_{Sj}}{\omega_{Aj}}. \quad (2.95)$$

2. Single-storey Asymmetric Space Frame with TLCDs: Laboratory Model

Equations (2.94) and (2.95) render static values of $q_{j,2}$ and $u_{j,2}$ when $\omega = 0$,

$$u_{j,2}\Big|_{\omega=0} = u_{j,2st} = -\frac{\kappa_j \cos(\alpha - \gamma_j) a_g}{\omega_{Aj}^2}, \quad q_{j,2}\Big|_{\omega=0} = q_{j,2st} = -\frac{L_j a_g}{\omega_{Aj}^2 \bar{\delta}_j^2} = -\frac{L_j a_g}{\omega_{Sj}^2}, \quad (2.96)$$

and former can also be abbreviated as,

$$A_{11}q_{j,2} - A_{12}u_{j,2} = \bar{\delta}_j^2 q_{j,2st}, \quad (2.97)$$

$$-A_{21}q_{j,2} + A_{22}u_{j,2} = u_{j,2st}, \quad (2.98)$$

where, $A_{11} = \bar{\delta}_j^2 - (1 + \mu_j) \beta_{Aj}^2 + 2i\zeta_{Sj} \bar{\delta}_j \beta_{Aj}$, $A_{22} = 1 - \beta_{Aj}^2 + 2i\zeta_{Aj} \beta_{Aj}$,

$$A_{12} = \bar{\kappa}_j V_{\gamma j} \mu_{ff} \beta_{Aj}^2, \quad A_{21} = \kappa_j V_{\gamma j} \beta_{Aj}^2. \quad (2.99)$$

Solution of equations (2.97) and (2.98) e.g., by using Cramer's rule, render complex $q_{j,2}$

and $u_{j,2}$,

$$q_{j,2} = \frac{A_{22} \bar{\delta}_j^2 q_{j,2st} + A_{12} u_{j,2st}}{A_{11} A_{22} - A_{12} A_{21}}, \quad u_{j,2} = \frac{A_{11} u_{j,2st} + A_{21} \bar{\delta}_j^2 q_{j,2st}}{A_{11} A_{22} - A_{12} A_{21}}, \quad (2.100)$$

Therefore, the complex amplitude $q_{j,2}$ for the modally isolated coupled 2-DOF system results,

$$q_{j,2} = q_{j,2st} \bar{\delta}_j^2 \frac{1 - a_1 \beta_{Aj}^2 + 2i\zeta_{Aj} \beta_{Aj}}{\bar{\delta}_j^2 - b_1 \beta_{Aj}^2 + b_2 \beta_{Aj}^4 + i(b_3 - b_4 \beta_{Aj}^2) \beta_{Aj}}, \quad (2.101)$$

where, $b_1 = 1 + \mu_j + \bar{\delta}_j^2 + 4\zeta_{Sj} \zeta_{Aj} \bar{\delta}_j$, $b_2 = 1 + \mu_j - \bar{\kappa}_j \kappa_j \mu_{ff} V_{\gamma j}^2$, $b_3 = 2\zeta_{Sj} \bar{\delta}_j + 2\zeta_{Aj} \bar{\delta}_j^2$,

$$b_4 = 2\zeta_{Sj} \bar{\delta}_j + 2\zeta_{Aj} (1 + \mu_j),$$

$$a_1(\alpha, \gamma_j) = 1 - \frac{\bar{\kappa}_j \mu_{ff} V_{\gamma j}}{\bar{\delta}_j^2} \left(\frac{u_{j,2st}}{q_{j,2st}} \right) = \left(1 - \kappa_j \bar{\kappa}_j \mu_{ff} V_{\gamma j} \cos(\alpha - \gamma_j) / L_j \right), \quad (2.102)$$

and Eq. (2.101) can be expanded,

$$q_{j,2} = \frac{q_{j,2st}}{1 + B_1 \beta_{Aj}^2 + B_2 \beta_{Aj}^4 + B_3 \beta_{Aj}^6 + B_4 \beta_{Aj}^8} \left((\text{Re})_{q_{j,2}} + i(\text{Im})_{q_{j,2}} \right) \quad (2.103)$$

where,

$$(\text{Re})_{q_{j,2}} = 1 - \frac{1}{\bar{\delta}_j^2} (a_1 \bar{\delta}_j^2 + b_1 - 2\zeta_{Aj} b_3) \beta_{Aj}^2 + \frac{1}{\bar{\delta}_j^2} (b_2 - 2\zeta_{Aj} b_4 + a_1 b_1) \beta_{Aj}^4 - \frac{a_1 b_2}{\bar{\delta}_j^2} \beta_{Aj}^6,$$

$$\begin{aligned}
 (\text{Im})_{q_{j,2}} &= \frac{2\zeta_{Aj}}{\bar{\delta}_j^2} \left(\bar{\delta}_j^2 - b_3\beta_{Aj} + b_4\beta_{Aj}^3 - b_1\beta_{Aj}^4 \right) \beta_{Aj}, \\
 B_1 &= \left(b_3^2 - 2\bar{\delta}_j^2 b_1 \right) / \bar{\delta}_j^4, \quad B_2 = \left(b_1^2 + 2\bar{\delta}_j^2 b_2 - 2b_3 b_4 \right) / \bar{\delta}_j^4, \quad B_3 = \left(b_4^2 - 2b_1 b_2 \right) / \bar{\delta}_j^4, \\
 B_4 &= b_2^2 / \bar{\delta}_j^4,
 \end{aligned} \tag{2.104}$$

Hence, the modal dynamic magnification factor for such a 2-DOF system becomes,

$$DMF_{j,2} = \sqrt{\frac{1 - 2\left(a_1 - 2\zeta_{Aj}^2\right)\beta_{Aj}^2 + a_1^2\beta_{Aj}^4}{1 + B_1\beta_{Aj}^2 + B_2\beta_{Aj}^4 + B_3\beta_{Aj}^6 + B_4\beta_{Aj}^8}}, \tag{2.105}$$

$$= \sqrt{1 + \frac{\left(4\zeta_{Aj}^2 - 2a_1 - B_1\right)\beta_{Aj}^2 + \left(a_1^2 - B_2\right)\beta_{Aj}^4 - B_3\beta_{Aj}^6 - B_4\beta_{Aj}^8}{1 + B_1\beta_{Aj}^2 + B_2\beta_{Aj}^4 + B_3\beta_{Aj}^6 + B_4\beta_{Aj}^8}} \tag{2.106}$$

where $a_1(\alpha, \gamma_j)$ given by Eq. (2.102) points towards the directional dependency of such an approximate modal dynamic magnification factor on the varying angle of incidence of base excitation. The possible cause of this phenomenon is due to the fact that the position of the center of mass is not exact, because the small fraction of dead fluid-mass is not considered in the dynamic of the main system; however its effect is commonly negligible in practical cases.

References

- [2-1] Hochrainer M.J., Control of vibrations of civil engineering structures with special emphasis on tall buildings, Dissertation (in English), Vienna University of Technology, Vienna, Austria, 2001; <http://www.tuwien.ac.at/>.
- [2-2] Hochrainer M.J., Ziegler F., Control of tall building vibrations by sealed tuned liquid column dampers, *Structural Control and Health Monitoring*, 2006; **6/13**, 980-1002.
- [2-3] Fu Chuan, Effective damping of vibrations of plan-asymmetric buildings, Dissertation (in English), Vienna University of Technology, Vienna, Austria, 2008; <http://www.tuwien.ac.at/>.
- [2-4] Fu Chuan, Ziegler F., Vibration prone multi-purpose buildings and towers effectively damped by tuned liquid column gas dampers. *Asian J. Civil Engineering*, 2009; **10/1**, 21-56.
- [2-5] Ziegler F., *Mechanics of Solids and Fluids*, Corr. 2nd ed., Springer, New York, 1998.
- [2-6] Clough R.W., Penzien J., *Dynamics of Structures*, 2nd ed., McGraw-Hill, New York, 1993.
- [2-7] Chopra A.K., *Dynamics of Structures*, Prentice-Hall, New Jersey, 1995.
- [2-8] MATLAB, User Guide, Control Toolbox, MathWorks Inc., Version 7.8.0, 2009.

2. Single-storey Asymmetric Space Frame with TLCDs: Laboratory Model

- [2-9] Reiterer M., Damping of vibration-prone civil engineering structures with emphasis on bridges, Dissertation (in German), Vienna University of Technology, Austria, 2004, <http://www.tuwien.ac.at/>.
- [2-10] Reiterer M., Ziegler F., Control of pedestrian-induced vibrations of long-span bridges, *Structural Control and Health Monitoring*, 2006; **13/6**, 1003-1027.
- [2-11] Ziegler F., Special design of tuned liquid column gas dampers for the control of spatial structural vibrations, *Acta Mechanica*, 2008; **201**, 249-267.
- [2-12] Lindner-Silvester T., Schneider W., The moving contact line with weak viscosity effects-an application and evaluation of Shikhmurzaev's model, *Acta Mechanica*, 2005; **176**, 245-258.
- [2-13] Den Hartog J.P., *Mechanical vibrations*, 4th ed., McGraw-Hill, New York, 1956.

3 Experimental Verification of TLCGD Damping

3.1 Introduction

The state-of-the-art designed tuned liquid column-gas damper (TLCGD) increases the effective structural damping of vibration-prone buildings when subjected to dynamic loads like earthquakes or wind gusts. The effectiveness of the TLCGD is confirmed through experimentation by installing a TLCGD (secondary system) designed and tuned to the fundamental mode of vibration of the single-storey asymmetric space frame laboratory scaled model (i.e., 3 DOF main system: fully described in Section 2). The design and development of such a laboratory scaled structural model (str-model) is discussed along with its geometric and modal properties. The Section also includes the fabrication and installation of indigenously developed TLCGD to be installed in optimal position and direction on the str-model. The experimental procedure adopted for data acquisition and instrumentations required to measure the response of the coupled system (TLCGD installed on str-model) are also described to paint the full picture of the laboratory measurements. However, due to financial and laboratory constraints, the incorporation of novel base isolation units (design details in Section 4) for such a light weight str-model was not possible. The experimental results are compared with analytical solutions by simulating the experimental setup.

3.2 Design and development of the asymmetric structural model in view of base isolation

The simple single-storey space frame, laboratory scaled str-model consists of a “rigid” rectangular floor of size $a \times b = 400 \times 280 \text{mm}$ with the uniformly distributed floor mass

3. Experimental Verification of TLCD Damping

$m_S = 640\text{g}$ supported on four symmetrically arranged clamped-clamped elastic columns of height $l_c = 440\text{mm}$ placed at each corner as shown in Fig. 3.1.

Two thin aluminum rectangular plates having circular holes are joined by using spacer in between (a sandwich design) to form a light-weight and extremely stiff floor. The column numbered 1 is of larger diameter, M-6, with isotropic stiffness $k_{1y} = k_{1z} = k_1$ in y - and z -directions however, the other three columns are of one and the same diameter M-4 with isotropic stiffness $k_{2y} = k_{2z} = k_2$. Thus, column M-6 exhibits larger flexural stiffness due to which the centre of stiffness is distinct from the geometric centre O of the floor (i.e., the origin O of the Cartesian coordinate system).

The asymmetry of mass is created by introducing an additional point mass $m_1 = 100\text{g}$ at the upper right corner above the column numbered 1 (i.e., $e_y = a/2, e_z = b/2$) due to which centre of mass C_M is no more coincident with the geometric centre of the floor. Since the centre of mass C_M and the centre of stiffness C_S are not coincident for such an asymmetric structure, so even the uni-directional horizontal seismic (ground) excitation, in general, causes a three dimensional in-plane motion of the floor.

The bottom ends of the columns are rigidly clamped to the base-plate of similar sandwich design as that of the floor. The sliding system, shown in Fig. 3.2(a), consists of a rigid sliding-plate mounted on rails and hence is capable of moving forth and back when connected to the electromagnetic shaker (Brüel & Kjaer type 4808). The base-plate of the str-model is fixed on the sliding-plate so as to excite its base at any desired frequency or time record.

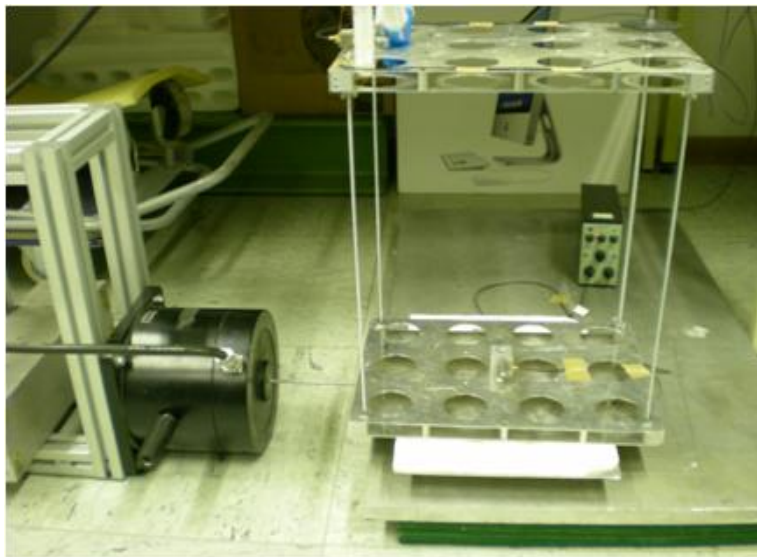
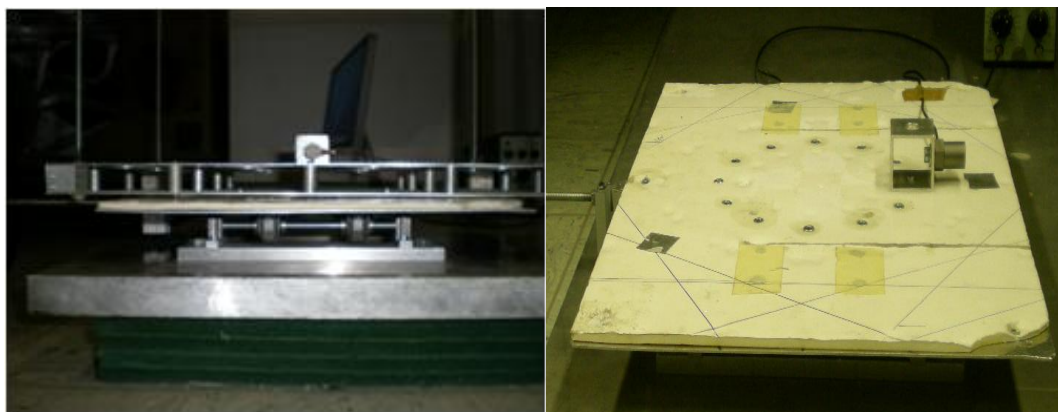


Fig. 3.1: Structural model on sliding plate attached to electromagnetic shaker (Brüel & Kjaer type-4808)

The task of base excitation on the str-model at various angles of incidence is managed by fixing the base-plate on the sliding-plate both having 12-peripheral holes with nut and bolt arrangement as shown in Fig. 3.2 (b). Hence, the relative position of the str-model can be changed at various angles by rotating it stepwise about the vertical x-axis with the interval of $\pi/6$.



(a)

(b)

Fig. 3.2: (a) base-plate of the structural model fixed to the sliding-plate by nut and bolt arrangement through 12-peripheral holes, (b) sliding-plate mounted on the rails and connected to the electromagnetic shaker.

3.2.1 Properties of the columns

The columns used to support the floor are threaded so as to adjust their lengths (if required), but its moment of inertia I and modulus of elasticity E are not exactly known. Therefore, a simple experiment is performed to determine the flexural stiffness EI of the columns. A certain length l_e of the column is taken to serve as a cantilever beam whose free-end deflection Δ_e for various lateral static loads F_e is measured experimentally by an inductive transducer (Kinex-251858) to determine the linear elastic flexural stiffness by $EI = F_e l_e^3 / 3\Delta_e$. These values are listed along with other properties of the columns in Table 3.1.

Table 3.1: Properties of the columns of the structural model.

Description of columns	Column 1 (M-6)	Column 2, 3&4 (M-4)
Flexural stiffness, $EI = F_e l_e^3 / 3\Delta_e$ [Nm ²]	4.978	0.924
Stiffness cc-column, $k = 12EI / l_c^3$ [N/m]	701.230	130.222
Measured mass of column, m_c [g]	80	36
Lumped mass of cc-column, $m_e = 13/35 m_c$ [g]	29.7	13.4
Euler critical buckling load, $F_{c,cr} = \pi^2 EI / l_c^2$ [N]	253.765	47.125
Axial compressive load applied, F_c [N]	-3.676	-2.436
Ratio of the applied load to the critical buckling load, $r_c = F_c / F_{c,cr} < 0.3$	0.014	0.052
Geometric correction for stiffness, P- Δ effect, $k_G = 6F_c / 5l_c$ [N/m]	-10.025	-6.645
Corrected stiffness, $\bar{k} = k + k_G$ [N/m]	691.205	123.577

The ratio of the flexural stiffness of the column M-6 to M-4 is $k_r = k_1/k_2 = 5.7$. As the load applied on each column is less than 30% of the respective critical buckling load so it is considered safe against buckling and allows a linear geometric correction of the flexural stiffness, see e.g., Ziegler^[3-1], page 604 and Clough-Penzien^[3-2], page 167. Hence, the corrected stiffness of the column is finally reduced under the influence of the usual normal force, see Table 3.1.

3.2.2 Properties of the structural model

As the laboratory scaled str-model is a light-weight structure therefore, the mass of the columns are lumped to the floor by using Hermite-shape function *H3* for the cc-beam, see e.g. Ziegler^[3-1] page 612. The mass of column M-4 (m_{e2}) is considered to be lumped at each corner however, the difference between lumped mass of column M-6 and M-4 ($\Delta m_e = m_{e1} - m_{e2}$) is added in m_1 to render the total point mass $\bar{m}_1 = m_1 + \Delta m_e$.

Therefore, the total mass of the floor becomes $m_t = m_S + \bar{m}_1 + 4m_{e2} = 877\text{g}$.

(i) Center of mass

The center of mass of the str-model is located at

$$y_M = \frac{\bar{m}_1 e_y}{m_t} = 14.2\text{mm}, z_M = \frac{\bar{m}_1 e_z}{m_t} = 17.3\text{mm}. \quad (3.1)$$

(ii) Mass moment of inertia

The mass moment of inertia about the vertical *x*-axis is,

$$I_x = m_S (a^2 + b^2) / 12 + m_S (y_M^2 + z_M^2) + \bar{m}_1 [(e_y - y_M)^2 + (e_z - z_M)^2] + \sum_{i=1}^4 m_{e2} [(e_{yi} - y_M)^2 + (e_{zi} - z_M)^2] = 22.5 \times 10^6 \text{ gmm}^2, i = \text{column number} \quad (3.2)$$

and radius of inertia is $r_x = \sqrt{I_x / m_t} = 160.3\text{mm}$.

(iii) Mass and stiffness matrices

Considering the displacements of the center of mass C_M in the state vector

$\bar{x}^T = [v_M \quad w_M \quad u_T]$, $u_T = \theta r_x$, the diagonal mass matrix and corrected symmetric

3. Experimental Verification of TLCDG Damping

stiffness matrix of the three degree of freedom (3-DOF) str-model are (TLCDG still not considered),

$$\underline{M} = m_t \begin{bmatrix} 1 & 0 & 0 \\ 0 & 1 & 0 \\ 0 & 0 & 1 \end{bmatrix}, \underline{\bar{K}} = \begin{bmatrix} \bar{k}_{11} & \bar{k}_{12} & \bar{k}_{13} \\ \bar{k}_{21} & \bar{k}_{22} & \bar{k}_{23} \\ \bar{k}_{31} & \bar{k}_{32} & \bar{k}_{33} \end{bmatrix} \quad (3.3)$$

where, the elements of the corrected stiffness matrix $\underline{\bar{K}}$ are

$$\bar{k}_{11} = \bar{k}_{y1} + 3\bar{k}_{y2}, \bar{k}_{22} = \bar{k}_{z1} + 3\bar{k}_{z2},$$

$$\bar{k}_{33} = \frac{1}{r_x^2} \left[(\bar{k}_{y1} + 3\bar{k}_{y2})(b^2/4 + z_M^2) + (\bar{k}_{z1} + 3\bar{k}_{z2})(a^2/4 + y_M^2) \right. \\ \left. + (\bar{k}_{y2} - \bar{k}_{y1})bz_M + (\bar{k}_{z2} - \bar{k}_{z1})ay_M \right]$$

$$\bar{k}_{12} = \bar{k}_{21} = 0, \bar{k}_{13} = \bar{k}_{31} = \left[(\bar{k}_{y1} + 3\bar{k}_{y2})z_M + (\bar{k}_{y2} - \bar{k}_{y1})b/2 \right] / r_x,$$

$$\bar{k}_{23} = \bar{k}_{32} = - \left[(\bar{k}_{z1} + 3\bar{k}_{z2})y_M + (\bar{k}_{z2} - \bar{k}_{z1})a/2 \right] / r_x.$$

(iv) Natural frequencies

The solution of the characteristic equation $\left[\underline{\bar{K}} - \omega_j^2 \underline{M} \right] \vec{\phi}_j = \vec{0}$, $j=1,2,3$ by calling the function *eig* in MATLAB^[3-3], renders the first three natural frequencies, $f_1 = 4.499\text{Hz}$, $f_2 = 5.556\text{Hz}$, $f_3 = 7.843\text{Hz}$ and the ortho-normalized modal matrix of the str-model is

$$\underline{\phi} = 10^{-3} \begin{bmatrix} -456.2 & 927.5 & -288.6 \\ 799.2 & 529.4 & 470.6 \\ -541.9 & 0.000 & 920.2 \end{bmatrix} \quad (3.4)$$

(v) Modal centers of velocity

The coordinates of the modal center of velocity for j -th mode are derived in terms of the components of the modal vectors $\vec{\phi}_j$, see e.g., Ziegler^[3-1], page 13, sufficiently small displacements and rotation of the floor understood, for details see Fu^[3-4] or Fu-Ziegler^[3-5],

$$y_{vj} = y_M - r_x \phi_{j2} / \phi_{j3}, z_{vj} = z_M + r_x \phi_{j1} / \phi_{j3}, \quad \phi_{j3} \neq 0. \quad (3.5)$$

The coordinates of the modal centers of velocity C_{vj} , $j=1,2,3$ are,

$$\vec{r}_{V1} = \begin{bmatrix} 251 \\ 152 \end{bmatrix} \text{mm}, \vec{r}_{V2} = 10^{10} \begin{bmatrix} -38 \\ 97 \end{bmatrix} \text{mm}, \vec{r}_{V3} = \begin{bmatrix} -68 \\ -29 \end{bmatrix} \text{mm} \quad (3.6)$$

i.e., mode number 2 is “translational”.

3.2.3 Corrected properties of structural model after TLCGD installation

In real buildings, the mass of the TLCGD-piping system and dead-mass of the water present inside the TLCGD is rather negligible when compared to the mass of the structure. But for such a laboratory scaled light-weight str-model, the static and modal properties are reasonably changed after the installation of TLCGD because of the added dead-mass, comparable to the mass of the str-model, and hence lower its natural frequencies. Therefore, it becomes necessary for the exact tuning of the TLCGD to update the following properties of the str-model.

(i) Center of mass

When a TLCGD and an accelerometer are attached at the left short edge on the str-model, the mass of TLCGD (i.e., measured mass of TLCGD piping system $m_p = 215\text{g}$ plus the dead mass of water inside, Eq. (2.81); $m_{fd} = m_f \left[1 - \kappa \bar{\kappa} \left(V_j^* / V_j \right)^2 \right] = 28\text{g}$, and the measured mass of accelerometer $m_{ac} = 57\text{g}$, renders the additional mass $m_A = m_p + m_{fd} + m_{ac} = 300\text{g}$ which is supposed to be concentrated at reference point A of the TLCGD (i.e., $e_{Ay} = -160\text{mm}$, $e_{Az} = 0$). Hence, the center of mass C_M with the total mass on the floor $\bar{m}_t = m_t + m_A = 1119.8\text{g}$ becomes, Eq. (3.1) properly updated,

$$\bar{y}_M = \frac{\bar{m}_t e_y + m_A e_{Ay}}{\bar{m}_t} = -23.6\text{mm}, \bar{z}_M = \frac{\bar{m}_t e_z + m_A e_{Az}}{\bar{m}_t} = 13.5\text{mm}. \quad (3.7)$$

Thus, significant shift of the center of mass is observed due to the additional dead mass in this str-model.

(ii) Mass moment of inertia

Equation (3.2) properly updated,

$$\bar{I}_x = I_x + m_A \left[(e_{Ay} - y_M)^2 + (e_{Az} - z_M)^2 \right] = 28.4 \times 10^6 \text{ gmm}^2, \quad \bar{r}_x = \sqrt{\bar{I}_x / \bar{m}_t} = 159.2 \text{ mm}. \quad (3.8)$$

Hence, moment of inertia and radius of inertia about vertical x -axis are also changed. The solution of the characteristic equation with updated mass matrix renders the reduced first three natural frequencies $f_1 = 3.598 \text{ Hz}$, $f_2 = 4.901 \text{ Hz}$, $f_3 = 7.668 \text{ Hz}$ and the ortho-normalized modal matrix of the str-model becomes,

$$\underline{\phi} = 10^{-3} \begin{bmatrix} -320.3 & 870.5 & -180.7 \\ 758.1 & 367.7 & 427.8 \\ -464.4 & 0.000 & 823.0 \end{bmatrix} \quad (3.9)$$

(iii) Modal centers of velocity

The coordinates of the modal centers of velocity C_{vj} , $j = 1, 2, 3$ are slightly shifted when Eq. (3.5) is properly updated,

$$\vec{r}_{V1} = \begin{bmatrix} 236 \\ 123 \end{bmatrix} \text{ mm}, \quad \vec{r}_{V2} = 10^{10} \begin{bmatrix} -45 \\ 106 \end{bmatrix} \text{ mm}, \quad \vec{r}_{V3} = \begin{bmatrix} -107 \\ -22 \end{bmatrix} \text{ mm} \quad (3.10)$$

The center of velocity for first mode C_{v1} lies just outside the floor plan, referring to the combined translational and rotational motion. The center of velocity for second mode C_{v2} lies far from the floor plan representing the dominant translational motion. However, C_{v3} lies within the floor plan, and C_{v3} is distinct from C_M , referring to a dominant rotational motion.

3.3 Optimal positioning of TLCDG

The TLCDG tuned to each rigid-body mode of the str-model should be placed on the floor keeping in view the normal distance of its trace to C_{vj} as large as possible within the floor plan, see Fu-Ziegler^[3-5], as illustrated in Fig. 3.3, for maximum kinetic energy absorption. The center of velocity for 1st mode C_{v1} lies just outside the floor plan, referring to moderate asymmetry: the dominant translational motion, therefore TLCDG1 is installed along left short edge (i.e., parallel to z -axis) to effectively damp the horizontal

vibrations for this mode. The TLCGD2 can be installed along the bottom long edge (i.e., parallel to y-axis) because the center of velocity for 2nd mode C_{v2} lies far from the floor plan representing the dominant translational motion. In addition, the center of velocity C_{v3} for the 3rd mode lies within the floor plan, and C_{v3} is distinct from C_M , therefore 3rd mode is excited as a dominant rotational motion. Hence, TLCGD3 can be installed along the right short edge (i.e., parallel to the z-axis). However, torsional tuned liquid column-gas dampers (TTLCGD), see Fu^[3-4] and Fu-Ziegler^[3-5], would be more effective to mitigate the torsional vibration of the 3rd mode.

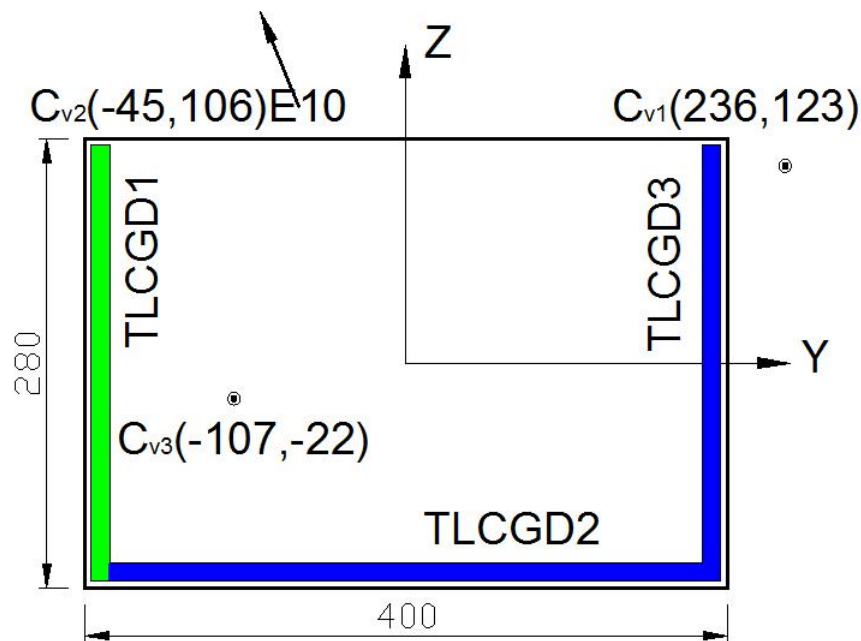


Fig. 3.3: Positioning of three TLCGDs: Here, \odot indicates the modal centres of velocity.

3.4 Design and development of TLCGD

To confirm the effectiveness of TLCGD experimentally, only single TLCGD (namely TLCGD 1 in Fig. 3.3) tuned to the updated first fundamental frequency of the str-model is practically installed to effectively damp the horizontal vibration of the first mode of the str-model.

The first effort towards the fabrication of laboratory scaled TLCGD involves the use of

3. Experimental Verification of TLCGD Damping

plexiglas pipe because of its light-weight and transparent material but the desired U-shape of TLCGD could not be formed by plexiglas. So the smooth 90-degree elbows were introduced at the turning positions but they had created unwanted edges offering turbulence and resistance to the flow of water at the junction inside the TLCGD. However, this problem was overcome by using a conventional flexible plastic pipe which could easily be formed to the required U-shape so as to keep the smooth flow of water inside TLCGD as shown in Fig. 3.5. The required volume of air above the water is managed sophisticatedly on each arm of the U-shaped pipe section by using a sealed light-weight plastic pipe (referred to as air-chamber) to create the gas-spring effect. The ends of the air-chamber pipes are connected to the Y-shaped valve, shown in Fig. 3.7, to facilitate the opening and closing (i.e., sealed or open ended liquid column damper) of liquid column damper in addition with the provision of changing the amount of water inside the TLCGD.

The geometrical dimension of TLCGD, the horizontal length of the liquid column $B = 280\text{mm}$ is selected to utilize maximum available length of the str-model along z-axis for its efficient design (i.e., higher κ value) and the vertical height of the liquid column, $H = 60\text{mm}$ is guided by Eq. (3.11), thus the ratio $B/L_{eff} = 0.7$.

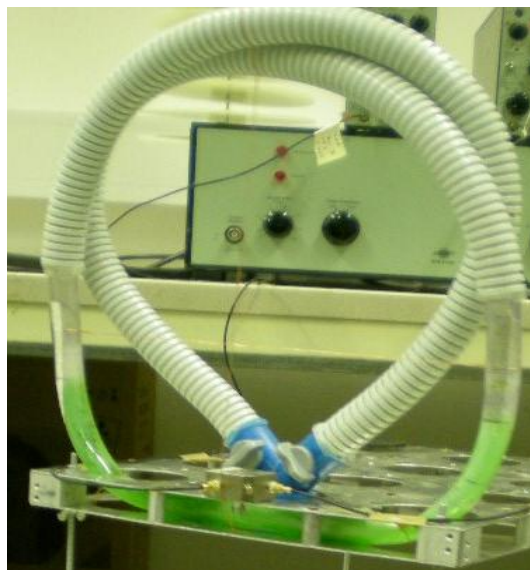


Fig. 3.4: TLCGD with required amount of water: green colour of water is due to dye for better visibility of its surface strokes.

The assembling of different parts of piping system of TLCGD is done with due care so as to maintain required gas (i.e., air) pressure above required water volume in its sealed design. Keeping the air at atmospheric pressure is manageable for the laboratory scaled self-made TLCGD saving any external compressor. The negative pressure by the expansion of the air is negligible because of a sufficiently small liquid stroke in TLCGD. The firm attachment of such a TLCGD on the floor of the str-model is also ensured to avoid any additional vibration induced by loose contact. The parameters of the gas-spring, the air-chamber volume and the equilibrium gas pressure, play a key role for rendering the optimal frequency of the TLCGD.

3.5 Experimental measurements

The experimental setup adopted for the verification of effectiveness of TLCGD is generally based on the nature of data acquisition system (DAQ). An accelerometer is attached at the center of the base-plate so as to measure the excitation acceleration at the base of the model and another biaxial accelerometer is attached very close to reference point A of TLCGD to measure the response in terms of acceleration along y - and z -axes as illustrated in Fig. 3.7. All the laboratory equipments for the experimentation are supplied by the Center of Mechanics and Structural Dynamics (CMSD), E2063, Institute of Building Construction and Technology of Vienna University of Technology. Somewhat relevant experiments had already been performed in the institute, e.g., for plane frame, see Kofler^[3-6] and for cable stayed bridges under wind excitation, see Achs^[3-7].

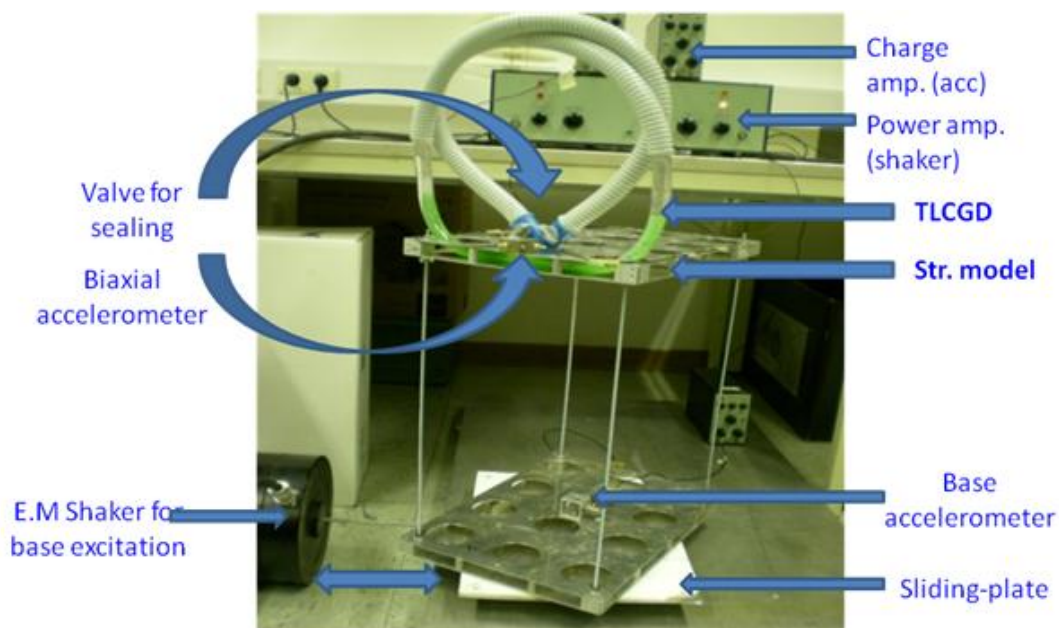


Fig. 3.5: Structural model with tuned TLCGD installed.

Electromagnetic shaker (Brüel & Kjaer type-4808) is connected to the sliding-plate at the base of the str-model so as to excite the base of the model at desired amplitude and frequency. The NI DAQ card-6062E installed in the laptop transmits the signal towards the shaker via the power amplifier (Brüel & Kjaer type-7212) through NI BNC-2090 connector. The response of the str-model measured by the accelerometers attached on it is first transmitted to the charge amplifiers (Brüel & Kjaer type-2635) and then acquired at the laptop by using same NI DAQ card-6062E via NI BNC-2090 connector as shown schematically in Fig. 3.6. Later on, NI USB-6221 DAQ also provided by CMSD Laboratory of Vienna University of Technology has replaced the NI DAQ card-6062E and NI BNC-2090 connector, to serve the same purpose with more convenient control and improved data acquisition. A program developed by using Labview Signal Express 3.0 of National Instruments controls the excitation of the shaker at prescribed frequency sweep rate and simultaneously acquires, and log the response of the model through the accelerometers attached on the str-model as illustrated schematically in Fig. 3.6.

3. Experimental Verification of TLCGD Damping

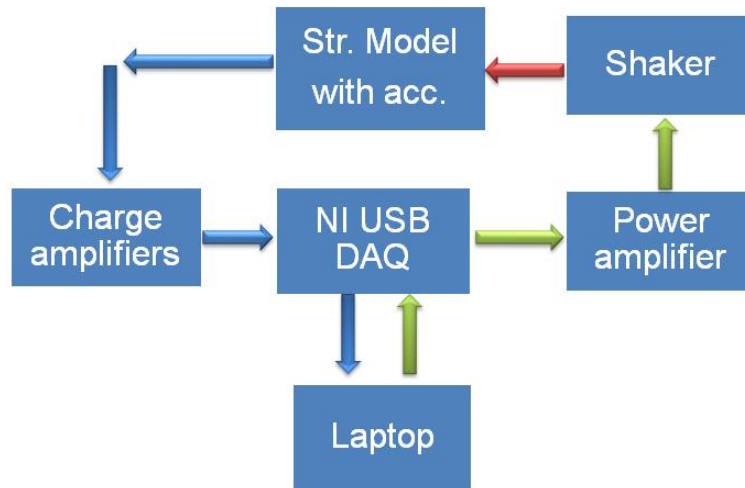


Fig. 3.6: Schematic flow of signals: green and blue arrows represent excitation to the shaker and response of the str-model respectively; connection of shaker to the str-model is shown by red arrow.

The response of the str-model equipped with the TLCGD is measured for both cases: the empty TLCGD piping system added (i.e., without water) and the properly tuned TLCGD (i.e., with required amount of water). The series of experimentations are performed by changing the relative position of the str-model with respect to the shaker axis direction (i.e., by rotating it stepwise about vertical axis) to record its response at various angles of incidence of the base excitation.

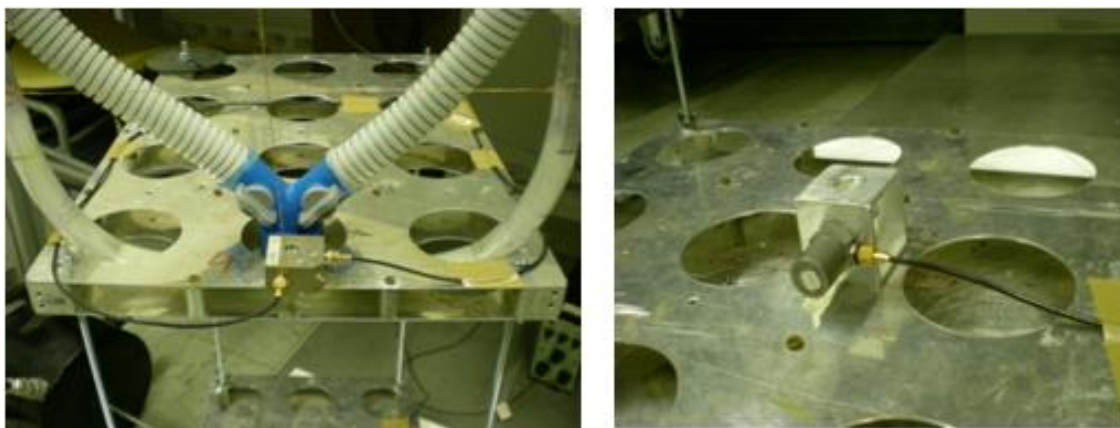


Fig. 3.7: Accelerometers at the floor and at the base-plate to measure the response and base excitation of the structural model respectively.

As it is not convenient in the laboratory to remove and reinstall the TLCGD-piping

system repeatedly therefore, it remains on the str-model and the required amount of water is added conveniently through the valve for the frequency tuning of TLCGD.

3.6 Experimental results

The frequency response function (FRF) is plotted from experimentally measured data for the str-model equipped with empty TLCGD-piping system, with detuned TLCD (not sealed) and with tuned TLCGD 1 installed. The acceleration measured along z-axis very close to reference point A of TLCGD 1 on the floor of the str-model is plotted over the excitation frequency at incidence angle of base excitation $\alpha = 90^0$ in Fig. 3.8.

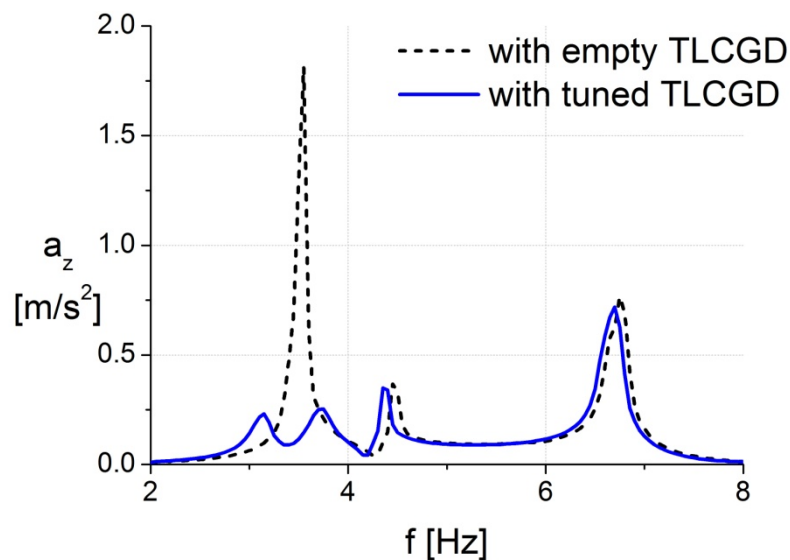


Fig. 3.8: Acceleration measured along z-axis at point A on the floor of the str-model with empty TLCGD-piping system and with tuned TLCGD, angle of incidence $\alpha = 90^0$

The three peaks in the measured response depict the first three natural frequencies of corresponding rigid body modes of the str-model (with empty TLCGD-piping system attached) as shown by dashed line in Fig. 3.8. The response is significantly damped when the TLCGD-piping system is filled with the required amount of water and hence tuned to the natural frequency of the first mode, as shown by slightly shifted solid blue line because of the dead mass of water. It is further mentioned that the response for the 2nd

3. Experimental Verification of TLCGD Damping

and 3rd modes is almost unaffected by the presence of TLCGD 1, as expected, because TLCGD 1 is tuned to the fundamental frequency of the first mode. However, the 2nd and 3rd modes can be damped by installing TLCGD 2 and TLCGD 3, tuned to the respective natural frequencies of these modes, at optimal position and direction, as illustrated in Fig. 3.3.

The FRF, ratio of acceleration measured very close to point A on the floor to the acceleration measured at the base-plate along z-axis a_z/a_0 , is plotted over the ratio of excitation frequency to the first natural frequency of the str-model f/f_1 both for empty TLCGD-piping system and tuned TLCGD, both installed on the str-model. The natural frequency of the str-model equipped with empty TLCGD-piping system is estimated as 3.575Hz and the modal damping of the str-model for the first mode is simply approximated as $\zeta_{S1} = 1/2FRF_{\max} = 0.45\%$ from the experimental FRF of the str-model equipped with empty TLCGD-piping system as illustrated in Fig. 3.9, see Fu-Ziegler^[3-5].

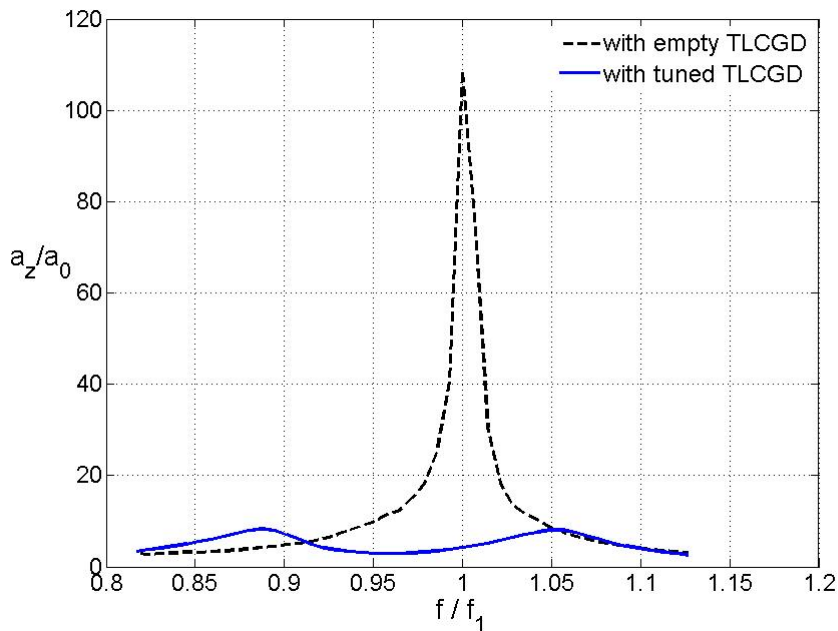


Fig. 3.9: FRF with empty TLCGD-piping system and with tuned TLCGD 1, angle of incidence $\alpha = 90^\circ$.

3. Experimental Verification of TLCGD Damping

In addition, the acceleration measured along z-axis at point A on the floor of the str-model keeping the valve open for the water filled TLCGD-piping system (i.e., open TLCD) is focused around the first natural frequency in Fig. 3.10. It is quite evident from the red dashed line in Fig. 3.10 that “open TLCD” does not damp the vibration of the str-model because of the fact that opening the valve eliminates the gas-spring effect resulting in a detuned TLCD, and its effect is not more than the added dead water mass on the floor, due to which the red dotted line is slightly shifted ($\Delta f = 0.05\text{Hz}$) towards the lower frequency.

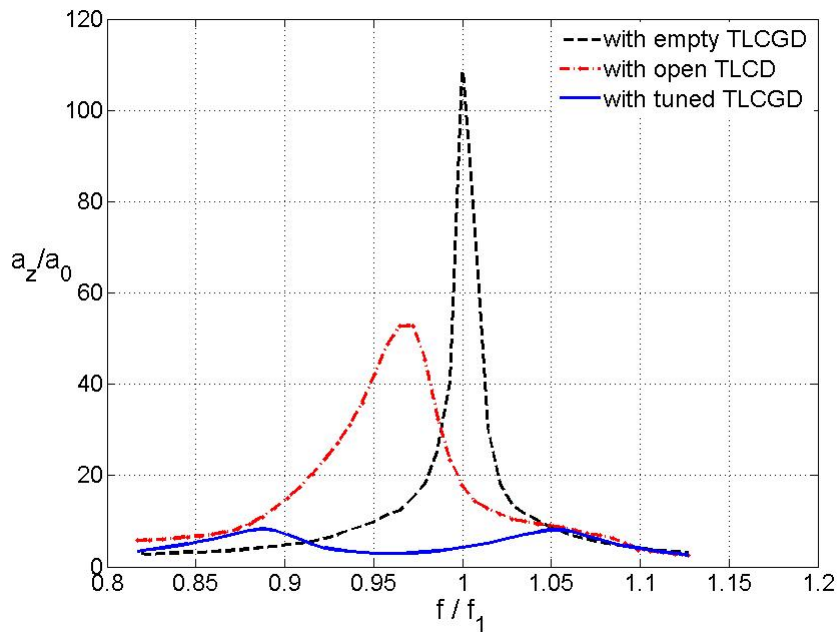


Fig. 3.10: FRF with empty TLCGD-piping system, open TLCD and with tuned TLCGD, angle of incidence $\alpha = 90^0$.

The modal participation factor L_{Sj} in Eq. (2.69), for $j=1$, is calculated at various angles of incidence, resulting in the critical angle of incidence close to $\alpha = 90^0$. Therefore, we focus on the results at the critical angle of incidence; however the FRFs plotted in Fig. 3.11 at various angle of incidence of base excitation with the interval of $\pi/6$ are also presented for TLCD, not sealed (detuned TLCD1) and sealed TLCGD (tuned TLCGD1).

3. Experimental Verification of TLCGD Damping

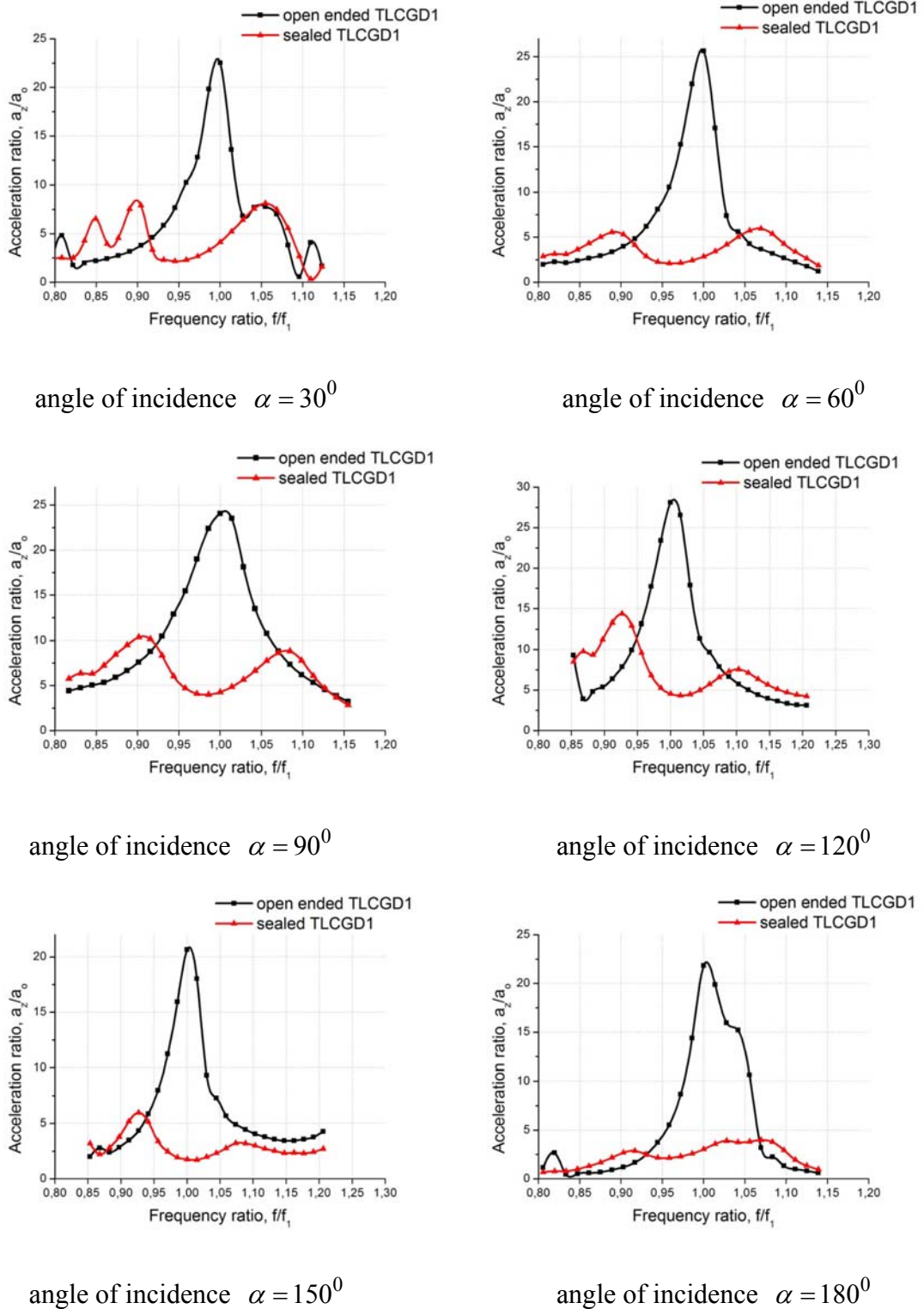


Fig. 3.11: FRF with open TLCGD 1 and tuned TLCGD 1 at various angles of incidence of base excitation.

3.7 Numerical Simulations

The simulation in Matlab is based on the measured mass and stiffness of the experimental str-model to calculate its natural frequencies and ortho-normalized modal vectors, see sub-section 3.2.3. The calculated natural frequency $f_l = 3.598$ Hz for the first mode is slightly higher (0.63%) than the experimentally measured natural frequency $f_l = 3.575$ Hz for the first mode pointing towards the slight decrease in stiffness of the str-model either due to the uncertainties in the measurement of the stiffness or the flexibility of the connection of the columns with the floor of the str-model. Since the modes of the str-model seem to be sufficiently separated, modal tuning of TLCD is conveniently performed by a transformation of the classical Den Hartog's formulas, see Den Hartog^[3-8], by means of the analogy between TMD and TLCD, see Hochrainer^[3-9] and Hochrainer-Ziegler^[3-10]. The fundamental mode is considered isolated, rendering a two degrees of freedom system (2-DOF) for which the time-reduced modally isolated linearized equation for the coupled TLCD-str-model, (i.e., Eq. (2.93) with $j=1$) renders the complex generalized coordinate $q_{1,2}$ and liquid stroke $u_{1,2}$ for the appropriate excitation frequency window and angle of incidence. The maximum liquid strokes in TLCD (i.e., $\max|u_0| = 3\text{mm}$) under time harmonic excitation are within following acceptable limits,

$$\max|u_0| \leq H/2 = 40\text{mm}, \max|u_0| \leq H_a/3 = 495\text{mm}. \quad (3.11)$$

and maximum liquid speed in TLCD is also well below the acceptable speed limit for application of piston theory $\max|\dot{u}_0| = 2\pi f_A \max|u_0| = 64\text{mm/s} < 10^4\text{mm/s}$, see Lindner-Silvester^[3-11] and Ziegler^[3-12].

The required large air volume V_0 in each arm of TLCD, a consequence of the low value of h_0/H_a , is managed within the long plastic pipes under atmospheric pressure.

The geometric dimensions of the TLCD and other resulting key parameters are collected in Table 3.2.

3. Experimental Verification of TLCGD Damping

Table 3.2: Design steps and parameters of TLCGD 1

Description of TLCGD 1	Values
Modal mass ratio, μ_j [%], Eq. (2.68), $m_j = 1$	8.7
Mass of water inside TLCGD, m_f [g]	56
Horizontal length of the liquid column, B [mm]	280
Vertical length of the liquid column, H [mm], Eq. (3.11)	60
Diameter of the TLCGD pipe, $d_H = d_B$ [mm]	14
Cross-sectional area of TLCGD pipe, $(A_H = A_B)$ [mm ²]	158.4
Effective length, $L_{eff} = L_1 = B + 2H$ [mm]	400
Geometry factor, $\kappa = \bar{\kappa}$, Eq. (2.28)	0.70
Optimal frequency ratio, δ_{opt} , Eq. (2.80)	0.94
Optimal absorber (TLCGD) frequency, $f_{A,opt} = f_S \delta_{opt}$ [Hz],	3.387
Optimal linear absorber damping, $\zeta_{A,opt}$ [%], Eq. (2.83), $\zeta_{Aj} = \zeta_{Aj}^*$	11.78
Eqv. math. pendulum length, L_0 [mm], Eq. (2.84)	22
$h_0/H_a = L_{eff}/2L_0 - \sin \beta$	8.232
Equilibrium pressure head, $h_0 = np_0/\rho g$ [m], $n=1.2$	12.232
Air volume, $V_0 = A_H H_a$ [dm ³]	0.235

The base excitation is assumed to be complex in the form $a_0 e^{i\omega t}$, where a_0 is the amplitude of the base acceleration. The three modal components of the approximate displacement at center of mass C_M along y -, z - and rotation about x -axes are

3. Experimental Verification of TLCGD Damping

$v_M = q_1\phi_{11}$, $w_M = q_1\phi_{12}$, $u_T = q_1\phi_{13}$ and their respective accelerations, $a_{yM} = -\omega^2 q_1\phi_{11}$, $a_{zM} = -\omega^2 q_1\phi_{12}$, $a_T = -\omega^2 q_1\phi_{13}$ when transformed to point A, by rigid body kinematics, see Ziegler^[3-1], page 14,

$$\bar{a}_A = \bar{a}_M + \ddot{\theta} \hat{r}_{AM} - \dot{\theta}^2 \bar{r}_{AM}, \quad (3.12)$$

where, $\theta = q_1\phi_{13}/r_S$, $\dot{\theta} = i\omega\theta$, $\ddot{\theta} = -\omega^2\theta$,

$$\hat{r}_{AM}^T = [-z_{AM} \quad y_{AM}], \quad y_{AM} = y_A - y_M, \quad z_{AM} = z_A - z_M.$$

The numerically calculated complex acceleration along z-axis, obtained from Eq. (3.12), of the modally isolated 2-DOF system is added to the real amplitude of the base acceleration a_0 along z-direction to render the complex resulting total acceleration a_z . The FRF expressed as the ratio of the absolute value of this complex resulting total acceleration $|a_z|$ to the base collinear acceleration a_0 is plotted over the ratio of excitation frequency in the relevant window around the first natural frequency both for empty TLCGD-piping system and tuned TLCGD 1 installed on the str-model in Fig. 3.12.

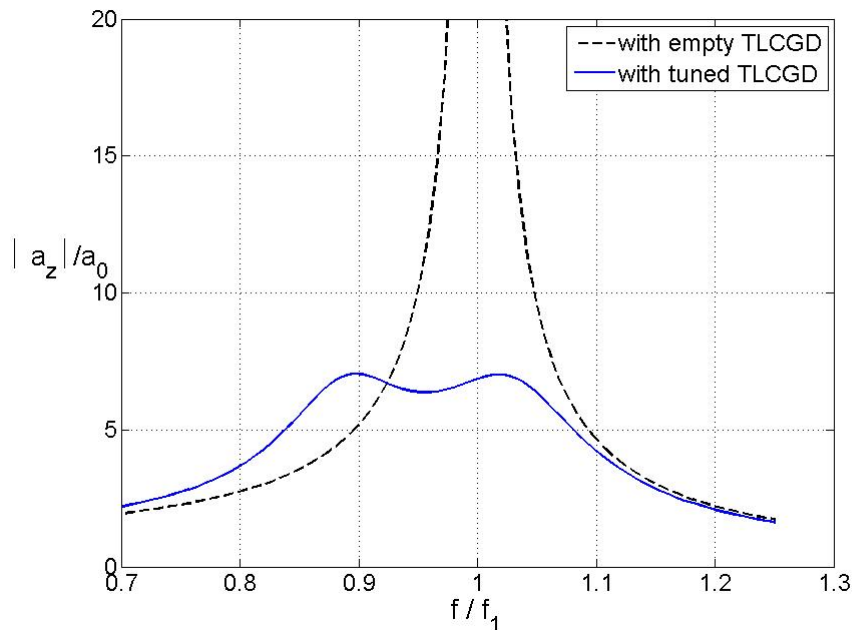


Fig. 3.12: FRF for the str-model with empty TLCGD-piping system (peak value=110) and with tuned TLCGD; angle of incidence $\alpha = 90^0$.

3.8 Comparison of experimental and simulated results

The simulated FRF for the case of tuned TLCGD 1 exhibits the higher damping than that from experimental FRF because of the fact that the damping imparted by the TLCGD 1 in the Laboratory is lower than Den Hartog's optimised damping for the simulated response as shown in Fig. 3.13.

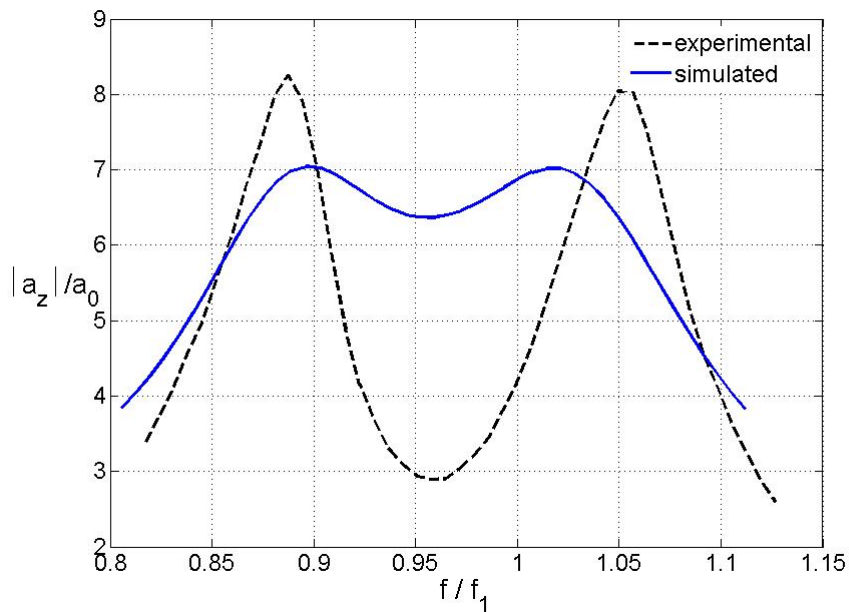


Fig. 3.13: FRF for the str-model with tuned TLCGD installed: damping in the experiment is not optimized, simulated response is with the optimal damping of TLCGD; angle of incidence $\alpha = 90^0$.

However, the simulated FRF gets closer to the experimental FRF for the case of tuned TLCGD 1 when the damping is approximated by using the experimentally determined damping coefficient $\zeta_{A,exp} = 6.1\% < \zeta_{A,sim} = 11.8\%$ as illustrated in Fig. 3.14.

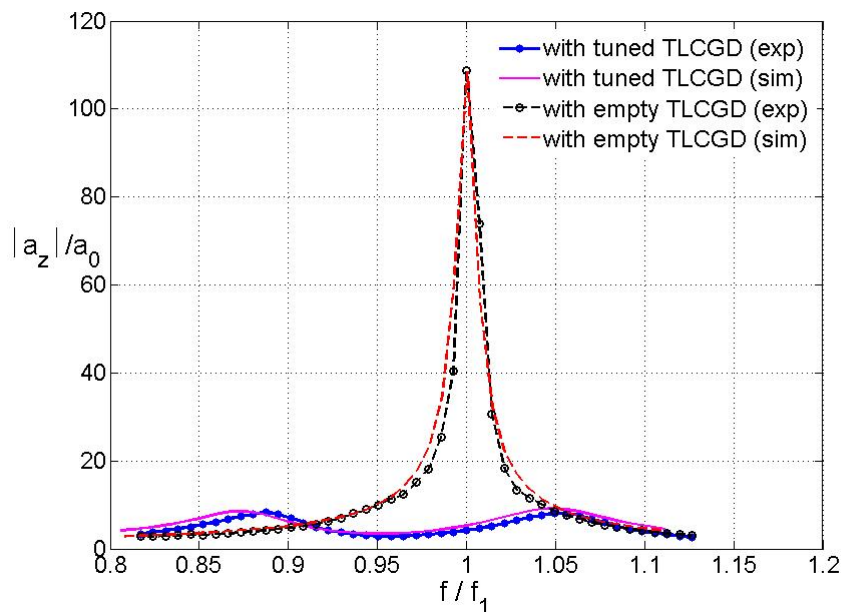


Fig. 3.14: FRF for the structural model with empty TLCGD-piping system and with frequency tuned TLCGD 1 installed; experimentally observed damping coefficient substituted; angle of incidence $\alpha = 90^0$.

It can be concluded from the above discussion that the results by numerical simulations are found to be in good agreement with those of the experimental output when substituting both the experimentally estimated damping coefficient of the str-model and that of the TLCGD 1 as confirmed in Fig. 3.14.

References

- [3-1] Ziegler F., Mechanics of Solids and Fluids, Corr. 2nd ed., Springer, New York, 1998.
- [3-2] Clough R.W., Penzien J., Dynamics of Structures, 2nd ed., McGraw-Hill, New York, 1993.
- [3-3] MATLAB, User Guide, Control Toolbox, MathWorks Inc., Version 7.8.0, 2009.
- [3-4] Fu Chuan, Effective damping of vibrations of plan-asymmetric buildings, Dissertation (in English), Vienna University of Technology, Vienna, Austria, 2008; <http://www.tuwien.ac.at/>.
- [3-5] Fu Chuan, Ziegler F., Vibration prone multi-purpose buildings and towers effectively damped by tuned liquid column gas dampers. Asian J. Civil Engineering, 2009; **10/1**, 21-56.
- [3-6] Kofler M., Eine experimentelle und numerische modelluntersuchung von ebenen rahmentragwerken mit U-rohrförmigen flüssigkeitsdämpfern, Master Thesis (in

3. Experimental Verification of TLCD Damping

- German), Vienna University of Technology, Vienna, Austria, 2000.
- [3-7] Achs G., Anwendung von flüssigkeitstilgern bei schrägseilbrücken im freivorbauzustand unter windanregung, Master Thesis (in German), Vienna University of Technology, Vienna, Austria, 2005.
- [3-8] Den Hartog J.P., Mechanical vibrations. 4th ed., McGraw-Hill, New York, 1956.
- [3-9] Hochrainer M.J., Control of vibrations of civil engineering structures with special emphasis on tall buildings, Dissertation (in English), Vienna University of Technology, Vienna, Austria, 2001; <http://www.tuwien.ac.at/>.
- [3-10] Hochrainer M.J., Ziegler F., Control of tall building vibrations by sealed tuned liquid column dampers, Structural Control and Health Monitoring, 2006; **6/13**, 980-1002.
- [3-11] Lindner-Silvester T., Schneider W., The moving contact line with weak viscosity effects-an application and evaluation of Shikhmurzaev's model, Acta Mechanica, 2005; **176**, 245-258.
- [3-12] Ziegler F., Special design of tuned liquid column-gas dampers for the control of spatial structural vibrations, Acta Mechanica, 2008; **201**, 249-267.

4 Novel Base Isolation System

4.1 Introduction

Earthquake poses serious threats to lives and the integrity of the infrastructure. As is the custom, a conventional strengthening of the structure to the code-related horizontal seismic forces was considered. However, this solution revealed considerable disadvantages because of construction expenditures for conventional strengthening of the structure and its foundation, Bachmann^[4-1]. Over the past decades, earthquake-resistant design of structures has been largely based on a ductility design concept worldwide. The performance of the intended ductile structures during major earthquakes (e.g. Northridge, 1944; Kobe, 1995; Chi-Chi, 1999. etc.), however, have proved to be unsatisfactory and indeed far below expectation, Wang-Yen^[4-2]. Therefore, to enhance structural safety and integrity against severe earthquakes, more effective and reliable techniques for aseismic design of structural control are demanded. Among the structural control schemes developed, seismic base isolation is one of the most promising strategies and thus became an increasingly applied structural design technique for buildings. The concept of isolating a structure from the shaking of the ground had long appealed to the imagination of inventors, but only in mid-1970's in New Zealand the elements of modern seismic isolation technology come together: quantitative ground motion and structural response criteria which could be met by a technology that reliably produced the necessary de-coupling of the structure from the foundation, increased damping and shifting of periods of vibration, Reitherman^[4-3]. Today, it is on the cutting edge of seismic resistance engineering, as evidence by the rapidly increasing number of buildings, both new construction and retrofit, using this earthquake resistant technique, Kelly^[4-4].

Base isolation system is a collection of structural elements which should substantially

decouple superstructure from its substructure resting on a shaking ground thus protecting a building or non-building structure's integrity. During earthquakes, the conventional structure without seismic isolation (i.e., fixed-base) is subjected to substantial storey-drifts, which may lead to damage or even collapse of the building. Whereas the isolated structure moves uniformly (like a rigid-body) with rather small accelerations, even if exposed to the strong motion phase of a severe earthquake, hence prevent most of the horizontal movement of the ground from being transmitted to the structure with deformation concentrated in the isolation bearings, as illustrated in Fig. 4.1. It is now generally accepted that a base-isolated building will perform better than a conventional fixed-base building in moderate and strong earthquakes, Kelly^[4-4].

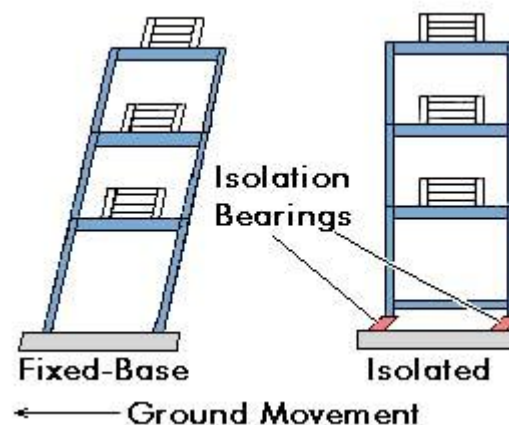


Fig. 4.1: Effect of base isolation.

Since base isolation act as a low-pass filter, it is commonly adopted for buildings with fixed-base fundamental frequency of more than about 1Hz (or buildings with less than about 10 stories), a rough estimate is given by $f_1 \approx 10/n_f$, where n_f is the number of floors or stories, see e.g., Flesch^[4-5], page 264. The lateral forces of the isolated building are not only reduced in magnitude but also fairly redistributed over the floors, which further mitigates the over turning moment of the structure.

4.1.1 Key concept of base isolation

The base isolation gives the structure a fundamental frequency that is much lower than its

fixed-base frequency (in other words: increases the period of vibration of the structure) and also much lower than the predominant frequencies of the ground motion so that the response is significantly reduced as demonstrated in Fig. 4.2. The first dynamic mode of the isolated structure involves deformation concentrated in the isolation bearings, the structure above being to all intents and purposes rigid. The higher modes which produce deformation in the structure are orthogonal to the first mode, and thus to the ground motion. These higher modes do not participate in the motion, so that if there is high energy in the ground motion at these higher frequencies, this energy cannot be imparted to the structure, Kelly^[4-4].

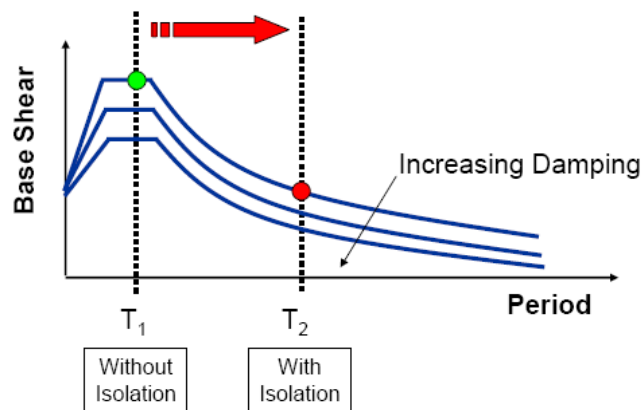


Fig. 4.2: Base isolation increases the period of the structure, Symans^[4-6].

4.1.2 Classical base isolation systems

The system that has been adopted most widely in recent years is typified by the use of elastomeric bearings. There are many elegant buildings worldwide, newly constructed or retrofit, by using such bearings as mentioned in literature review given in Section 1 of the thesis.

As mentioned earlier, the deformation during earthquake is concentrated in the isolation bearings and building above them moves rigidly. There are several tests performed in laboratories even on full-scale models to confirm their performance; Fig. 4.3 sharpens the imagination of the deformed shape of the elastomeric bearings.



Fig. 4.3: Deformed elastomeric bearing: (a) test of bearing used in the Indonesian demonstration building, Kelly^[4-7] (b) tested at the University of California San Diego Caltrans-SRMD (Seismic Response Modification Device) facility^[4-8].

The elastomeric bearings can further be classified into the following types based on the damping of the elastomers made of either natural rubber or neoprene;

- Low-damping natural or synthetic rubber
- High-damping natural rubber bearing
- Low-damping natural rubber with lead core (LRB)

Lead rubber bearings (LRB) have been invented in 1975 in New Zealand and used extensively in New Zealand, Japan and United States as well as in Europe, see Buckle-Mayaes^[4-9]. They are made by vulcanization bonding of sheets of rubber (low damping) to thin steel reinforcing plates and the energy dissipating lead core is placed in the center as shown in Fig. 4.4. Because the bearings are very stiff in the vertical (axial) direction and very flexible in the horizontal (shear) direction, under seismic loading the bearing layer isolates the building from the horizontal components of the ground movement while the vertical components are transmitted to the structure relatively unchanged.

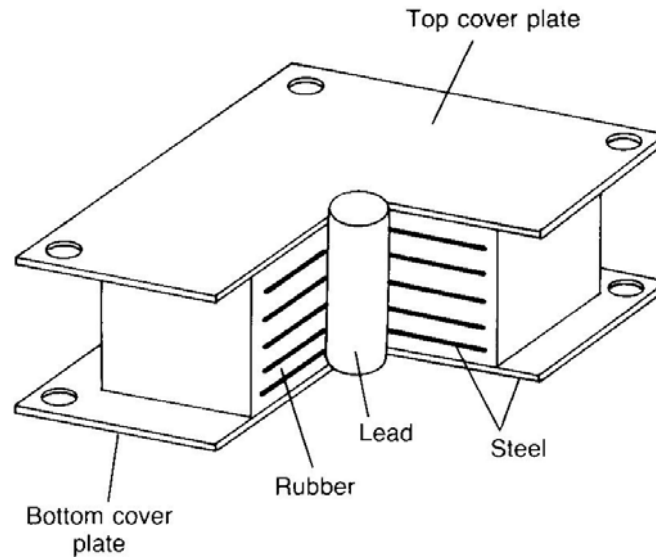


Fig. 4.4: Construction of LRB; top mounting plate not shown, Kunde-Jangid^[4-10].

LRB are put between the building and its foundation thus, the resulting fundamental mode should have a frequency below about 0.5 Hz. In that case the required damping of the resulting nearly rigid-body mode of the base-isolated building is supplied by the plastic deformation of a lead core placed in the center of the isolation element. This unit has a rather large ratio of the vertical to the horizontal stiffness; the latter in a rough approximation is given in terms of the rubber shear modulus G by $k_h = GA_r/n_r s_r$, where A_r and s_r are respectively, the cross-sectional area and the thickness of the n_r -times repeated rubber sheets, Ziegler-Khalid^[4-11].

However, lifetime problems, mainly caused by the increase of temperature, like reduction in yield stress with repeated cycling and plastic deformation of the lead core within the first occurrence of the earthquake or during the aftershocks are encountered. Therefore, it was strongly desired either some-how to improve the design philosophy of such bearings or to replace them by an advanced mechanism that could withstand the said problems so that the isolation mechanism remain effective and durable throughout the life of the structure.

4.2 Novel base isolation system

The lifetime problems related to the conventional isolation systems give way to the emergence of such an isolation system that could cope up with the above discussed problems. Consequently, keeping in view the extensive need and higher demand, a novel base isolation system is proposed to overcome the shortcomings of the conventional ones. The novel base isolation system can schematically be dividing into three main mechanical components: base isolation unit along with sliding elements and passive dampers schematically shown in Fig. 4.5.

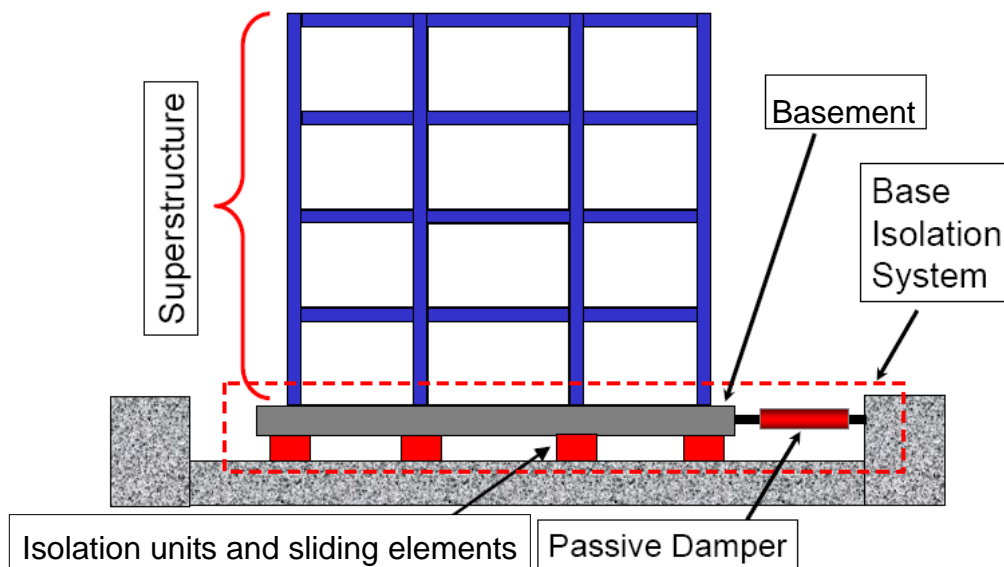


Fig. 4.5: Schematic representation of a novel base isolation system: isolation units, sliding element and passive damper.

The base isolation unit is an assembly of innovatively designed isolation elements, design details elaborated in next sub-section, acting as a low pass filter for isolating horizontal vibrations. The base isolation element, termed as spring-pendulum (SP) element, consists of an axially (vertical) pre-stressed helical steel spring combined with a pinned-pinned column (termed as upright-pendulum). The latter carries some portion of the dead weight and guides the motion of the rigid building, Ziegler-Khalid^[4-11]. The damping of the resulting fundamental modes of the building after base isolation is separately supplied by

the optimal arrangements of low-cost tuned liquid column-gas dampers (TLCGDs) in the building's basement. As static friction is missing in the TLCGD thus, it is provided by means of novel sliding elements with non-continuous energy dissipation. Such a novel base isolation system has hardly any maintenance cost and has a lifetime comparable to that of the building.

The idea of supplying the damping separately by means of sliding bearings for the base-isolated buildings is not new. For example, C. R. Drew Diagnostic Trauma Center California and Los Angeles City Hall contain 12 and 60 sliding bearings respectively, as mentioned in Section 1. Recently, Bachmann^[4-1] preferred to use elastomeric bearings made of reinforced rubber without having lead core placed in the peripheral basement walls under the columns for the seismic upgrading of a fire-brigade building in Basel, Switzerland. Whereas, the sliding bearings situated under the column-less partition walls provide damping and static friction. Hence, when following the current trends in the development of base isolation technology and Bachmann^[4-1] as a recent example, the damping is supplied separately by means of low-cost TLCGDs (having no moving mechanical parts) for base-isolated building; still the provision of the sliding elements becomes necessary to resist the loads by wind gusts and small seismic disturbances, say of traffic origin. Therefore, novel compatible sliding elements are designed, however without having continuous energy dissipation to achieve less wear and tear of the interface surfaces due to abrasive action. Thus, a limited horizontal force is transmitted analogously to the rigid-plastic lead core of the standard steel reinforced rubber isolation elements. The small amount of unavoidable frictional damping is considered in linearized form within the assigned light structural damping. The details of the sliding elements designed for single-storey asymmetric building are given in sub-section 4.5.2.3.

4.2.1 Design of novel base isolation element

The helical spring of the proposed SP element, see Fig. 4.6, is designed to have maximum vertical (axial) to horizontal (shear) stiffness; while the combined upright-pendulum carry some portion of the dead weight and also act as a means for transmitting any vertical base

acceleration. The base-isolated building in its low frequency modes is considered to be rigid when the isolation units are placed in-between the rigid building and its foundation. Such a base isolation element is functionally equivalent to a conventional one in extending structure's time period but with the additional advantageous features such as temperature-insensitivity and durability.

Considering a general asymmetric rigid building (idealised as 3-DOF space frame as discussed in Section 2) of total mass m_S to be base-isolated by means of N SP elements each having the same horizontal isotropic stiffness k_{1h} in y- and z-directions. The torsional stiffness of the SP element can be neglected since the angle of rotation about the vertical axis is extremely small under seismic excitation. The required period renders a first condition to be met in the design of the isolation element by choosing the resulting stiffness, see Ziegler-Khalid^[4-11],

$$T = 2\pi\sqrt{m_S/Nk_{1h}} \geq 2 \text{ s}. \quad (4.1)$$

The horizontal stiffness of the spring under shear is given by; see Parkus^[4-12], page 288,

$$k_{1h} = Ed \frac{(d/2D)^3}{n_t \left[1 + (4/3)(2+\nu)(l/D)^2 \right]}, \quad (4.2)$$

where, d is the diameter of the steel wire to form the helical spring of diameter D of length l having n_t active turns and ν is Poisson's ratio of the material of the spring.

The axial stiffness of the helical spring is noted for the sake of defining the proper axial pre-stress, see e.g., Wahl^[4-13], Nicholas^[4-14] or Ziegler^[4-15], page 385,

$$k_{1v} = Ed \frac{(d/2D)^3}{2(1+\nu)n_t}, \quad (4.3)$$

and the ratio of axial to shear stiffness should be maximized within proper design limits, Khalid-Ziegler^[4-16].

$$\lambda_{vh} = \frac{k_{1v}}{k_{1h}} = \frac{1 + (4/3)(2+\nu)(l/D)^2}{2(1+\nu)} \Rightarrow \max. \quad (4.4)$$

It is quite evident from Eq. (4.4), that the ratio λ_{vh} can be maximized just by adjusting the geometrical parameters, i.e., by increasing the l/D ratio).

4.2.1.1 Design details of the novel base isolation element

The various parts that form the SP element, made up of stainless steel, needs to be explained in detail because of its novel design. The upper and bottom mounting plates fixed with upper and lower foundation beams of the building respectively, are provided with studs (or flanges) of suitable diameter such that the helical spring can be firmly fitted on the outer periphery of these studs as illustrated in Fig. 4.6.

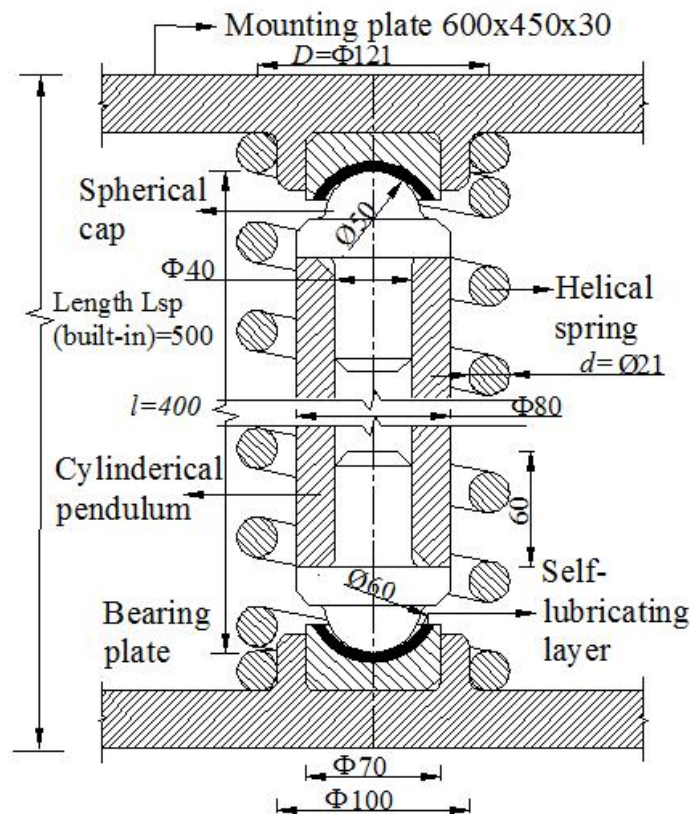


Fig. 4.6: Spring-pendulum (SP) element, dimensions (in mm) derived in sub-section 4.5.

Two similar bearing plates having (cup shaped) spherical surfaces lined with 5mm self-lubricating porous bronze layers, shown in black color in Fig. 4.6, are also fitted within these studs by making use of the shrink-fit technique. The upright-steel-pendulum

consisting of a hollow cylinder with spherical caps at both ends is pivoted (pinned-pinned) in-between the spherical cup shaped bearing plates and encapsulated by the axially pre-compressed helical spring as depicted in Fig. 4.6.

The required pre-compression of the helical spring dictates the load distribution on the helical spring and upright-pendulum as desired. The sliding of the spherical interfaces becomes convenient by use of the self-lubricating layers on the bearing plates when pendulum is tilted during the horizontal motion as a result of base excitations.

4.2.2 Static stability of base isolation element

When considering, at first in the design stage, the static stability of the pivoted upright-pendulum supported by the horizontal, shear stiffness of the helical spring, Fig. 4.6, a fraction of the dead-weight of the building is carried by the upright-pendulum and thus axial pre-stressing $k_{1v}(l_0 - l) > 0$ of the helical spring, compressed from its free length l_0 to pre-compressed length l , is required. Hence, the stability of N SP elements under dead-weight of the building $w_S = m_S g$ requires, when taking into account a fraction of the critical buckling load $k_{1h}l$ of a single element to be carried by the pendulum,

$$m_S g - Nk_{1v}(l_0 - l) = \lambda Nk_{1h}l, \quad 0 < \lambda < 1. \quad (4.5)$$

Rearranging Eq. (4.5) after dividing through by $Nk_{1h}l$ renders,

$$\frac{m_S g}{Nk_{1h}l} = \lambda + \lambda_{vh} \left(\frac{l_0}{l} - 1 \right), \quad (4.6)$$

where, the load factor λ used to define the required axial pre-stress of the spring must be positive to assure compressive axial force and is quantified when considering the vertical ground acceleration in next sub-section. Eq. (4.1) when substituted renders a universal equation (4.6) in base isolation. The design of the spring also depends on the load distribution mechanism for a SP element: a portion of the weight of the building is carried by the axially pre-stressed helical spring and the remaining part, for safety reasons

is supported by the upright-pendulum, Khalid-Ziegler^[4-16].

4.2.2.1 Quasi-static consideration for vertical ground motion

The quasi-static and conservative considerations render Eq. (4.7) when the expected maximum vertical ground acceleration a_{gv} is applied quasi-statically at the lower bearing,

$$m_s g (1 \pm a_{gv}/g) - Nk_{1h} \lambda_{vh} (l_0 - l) = \lambda_{gv} Nk_{1h} l, \quad 0 \leq \lambda_{gv} < 1 \quad (4.7)$$

where λ_{gv} is the load factor of the upright-pendulum.

Subtracting Eq. (4.5) from Eq. (4.7) yields

$$\pm a_{gv} = \frac{Nk_{1h}}{m_s} l (\lambda_{gv} - \lambda). \quad (4.8)$$

To have the same vertical ground acceleration a_{gv} both in upward and downward directions, λ_{gv} is limited either to 0.98 or zero, respectively, which defines the value of the load factor of the upright-pendulum under dead-weight load, $\lambda = 0.98/2 = 0.49$. Thus, with that acceptable value taken into account the axial pre-stress $(l_0 - l)$ is defined by Eq. (4.5) for the design of the base isolation (SP) elements for exemplary single-storey asymmetric building considered in sub-section 4.5.

Equation (4.1) renders the coefficient in Eqs. (4.6) and (4.8),

$$Nk_{1h}/m_s = (2\pi/T)^2, \quad (4.9)$$

and the condition on the period of base isolation, say $T = 2s$, further simplifies to $Nk_{1h}/m_s = \pi^2$. Therefore, consequently the maximum vertical ground acceleration results

$$\max a_{gv}/g = \lambda \pi^2 / g = 0.493l. \quad (4.10)$$

Therefore, it can be concluded that maximum vertical ground acceleration is directly related to the length of the upright-pendulum. However, when considering the base isolation (SP) element designed with $l = 400\text{mm}$ for exemplary single-storey

asymmetric building, the maximum vertical ground acceleration by such a conservative estimation is restricted to about $0.2g$. In case of higher values of vertical ground acceleration, another criterion is applied in the following sub-section to secure the novel base isolation unit.

4.2.2.2 Contact stability under vertical ground motion

Another conservative estimation of the effect of a ground acceleration peaking over a short time to the scaling factor $0.32g$ say of the El Centro seismogram is based on purely kinematical considerations of the ground movement during the time when the acceleration exceeds the critical acceleration of $0.2g$ (determined above) and by taking into account the simplified dynamics of the building during the phase of lost-contact of the pendulum with the bearings. The release of the spring force is roughly approximated by taking its mean value as constant.

During the downward motion, it is assumed that the upright-pendulum has lost the contact to the bearings just at the instant when the downward ground acceleration reaches the critical value of $0.2g$ within the peaking acceleration pulse. To save any numerical integrations, say of the pulse in the El Centro seismogram of duration $\Delta t_v = 0.22s$, a sine-half-wave pulse is substituted taking into account the maximum $a_{gv} = 0.32g$ also in the vertical direction. Thus,

$$a_v(t) = a_{gv} \sin \frac{\pi t}{\Delta t_v}, \quad 0 \leq t \leq \Delta t_v \quad (4.11)$$

renders the time elapsed $t_1 = 0.047s$ when the critical downward acceleration is reached.

The time instant when the ground acceleration takes on the same critical value is $t_2 = \Delta t_v - t_1$ (due to symmetry). During this short interval $t_2 - t_1 = \Delta t_v - 2t_1$, in such a purely kinematical and hence conservative formulation, the lower bearing and thus the ground covers a vertical downward distance of $\delta_{gv} = a_{gv} \frac{\Delta t_v}{\pi} (\Delta t_v - 2t_1) \approx 27mm$.

The upper bearing also moves downward with the building, with the crude approximated

acceleration assumed to be constant, i.e., considering the release of the spring force roughly equal to its mean value as a constant during this vertical downward motion,

$$a_{Sv}/g = 1 - \frac{Nk_{1h}}{m_S g} \lambda_{vh} (l_0 - l - \delta_{gv}/2) = 1 - \left(\frac{2\pi}{T}\right)^2 \frac{\lambda_{vh}}{g} (l_0 - l - \delta_{gv}/2) \quad (4.12)$$

Hence, the vertical distance travelled by the upper bearing is estimated,

$$\delta_{Sv} = \frac{a_{Sv} (\Delta t_v - 2t_1)^2}{2} \approx 29\text{mm} .$$

That approximate value is slightly larger than the vertical

distance travelled by the lower bearing. Therefore, the contact-stability is ensured and the upright-pendulum does not lose its contact with the bearings in such an intense vertical seismic forcing. Further, as pointed out in the sub-section 4.2.3, the expansion of the SP-unit is limited by a tensile-rod, thereby saving the unit even in the maximum allowed tilted configuration.

4.2.2.3 Static stability even including the post-buckling regime

To assure the static stability of the SP-element, i.e., to render a stable bifurcation in the upright position, we consider tilted equilibrium positions of the pendulum as well and determine the conditions for stability in such a post-buckling regime. The tilted pendulum has the shear tip deformation $\delta_{1h} = l \sin \varphi$ along with the vertical deflection $\delta_{1v} = l(1 - \cos \varphi)$ of the spring, Fig. 4.7.

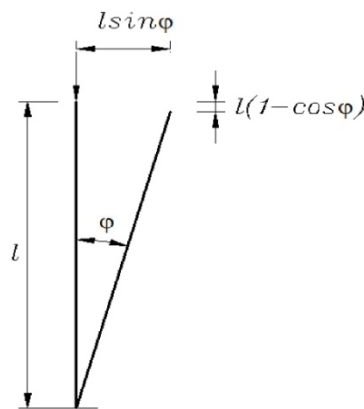


Fig. 4.7: Horizontal and vertical deflections at the tilted (equilibrium) position of the isolation element.

Thus, the strain energy in the spring due to shear and additional compression of the spring becomes

$$U_p = \frac{1}{2} k_{1h} \delta_{1h}^2 + \frac{1}{2} k_{1v} \delta_{1v}^2 \quad (4.13)$$

Equation (4.13) becomes by substituting the deflections,

$$U_p = l^2 \left\{ \frac{1}{2} (k_{1h} - k_{1v}) \sin^2 \varphi + k_{1v} (1 - \cos \varphi) \right\}. \quad (4.14)$$

The potential of the vertical force applied to the upright-pendulum is decreased,

$$W_p = -F_{1v} \delta_{1v} = -F_{1v} l (1 - \cos \varphi). \quad (4.15)$$

The potential energy, $E_p = U_p + W_p$ results by adding Eqs. (4.14) and (4.15),

$$E_p = l^2 k_{1h} \left\{ \frac{1}{2} (1 - \lambda_{vh}) \sin^2 \varphi + \lambda_{vh} (1 - \cos \varphi) \right\} - F_{1v} l (1 - \cos \varphi), \quad \frac{k_{1v}}{k_{1h}} = \lambda_{vh}. \quad (4.16)$$

The stationary value of the potential energy requires the resulting moment to vanish,

$$\frac{dE_p}{d\varphi} = M_{res} = k_{1h} l^2 \sin \varphi \left\{ (1 - \lambda_{vh}) \cos \varphi + \lambda_{vh} - \frac{F_{1v}}{k_{1h} l} \right\} = 0, \quad (4.17)$$

The roots of Eq. (4.17) are:

$\Rightarrow \sin \varphi = 0$, rendering the trivial root $\varphi = \varphi_0 = 0$; it refers to the vertical position of the pendulum, the relevant equilibrium for the SP-element.

$$\Rightarrow (1 - \lambda_{vh}) \cos \varphi + \lambda_{vh} - F_{1v}/k_{1h} l = 0, \quad (4.18)$$

determines the equilibrium in the post-buckling regime, $\varphi = \varphi_1 \neq 0$, however, actually is not relevant for the SP-element,

$$\cos \varphi_1 = \frac{\lambda_{vh} - F_{1v}/k_{1h} l}{\lambda_{vh} - 1} = \frac{\lambda_{vh} - \lambda}{\lambda_{vh} - 1} < 1, \quad (4.19)$$

since $\lambda = F_{1v}/k_{1h} l > 1$ is the load factor to render equilibrium in the post-buckling regime, considered just for stability considerations.

The Dirichlet stability condition (i.e., requiring a minimum of the potential energy) results by differentiating the resulting moment given by Eq. (4.17),

$$\frac{d^2 E_p}{d\varphi^2} = k_{1h} l^2 \left\{ \left(\lambda_{vh} - \frac{F_{1v}}{k_{1h} l} \right) \cos \varphi + (\lambda_{vh} - 1) (1 - 2 \cos^2 \varphi) \right\} \Big|_{\varphi=\varphi_0=0 \text{ or } \varphi=\varphi_1 \neq 0} > 0. \quad (4.20)$$

(i) The stability condition in the vertical relevant position, $\varphi = \varphi_0 = 0$ renders the critical buckling load, already mentioned above, Ziegler^[4-15], page 519,

$$F_{1v,cr} / k_{1h} l = \lambda_c = 1, \quad (4.21)$$

and the admissible dead-weight on the upright-pendulum $F_{1v} = \lambda k_{1h} l$, $\lambda < 1$. In addition, the maximum vertical ground acceleration is also considered to stay within the stability limit, see sub-section 4.2.2.1.

(ii) In a post-buckling regime, $\varphi = \varphi_1 \neq 0$, the Dirichlet stability condition becomes,

$$(\lambda_{vh} - \lambda) \cos \varphi_1 + (\lambda_{vh} - 1) (1 - 2 \cos^2 \varphi_1) > 0, \quad (4.22)$$

and simply reduces to the inequality,

$$1 - \cos^2 \varphi_1 > 0, \quad (4.23)$$

where stability of equilibrium positions require with $\lambda = \frac{F_{1v}}{k_{1h} l} > 1$, $\lambda_{vh} = \frac{k_{1v}}{k_{1h}} > 1$.

Hence, the Dirichlet stability condition is satisfied in the post-buckling regime in a sufficiently wide neighborhood of the vertical position.

Further, the stability at bifurcation point is also determined, the 2nd derivative of potential energy at the bifurcation point vanishes, $\lambda = \lambda_c = 1$,

$$\frac{d^2 E_p}{d\varphi^2} = l^2 k_{1h} \left\{ (\lambda_{vh} - \lambda) \cos \varphi - (\lambda_{vh} - 1) (2 \cos^2 \varphi - 1) \right\} \Big|_{\varphi=\varphi_0=0, \lambda=\lambda_c=1} = l^2 k_{1h} (1 - \lambda_c) = 0. \quad (4.24)$$

The 3rd derivative of the potential energy also vanishes at $\varphi = \varphi_0 = 0$,

$$\frac{d^3 E_p}{d\varphi^3} = k_{1h} l^2 \sin \varphi \left\{ 4(\lambda_{vh} - 1) \cos \varphi - (\lambda_{vh} - \lambda) \right\} \Big|_{\varphi=\varphi_0=0} = 0. \quad (4.25)$$

Consequently, the Dirichlet stability condition at the bifurcation point is decided by the 4th derivative of the potential energy,

$$\frac{d^4 E}{d\varphi^4} = k_{1h} l^2 \{ -(\lambda_{vh} - \lambda) \cos \varphi + 4(\lambda_{vh} - 1) \cos 2\varphi \}_{\varphi=\varphi_0=0, \lambda=\lambda_c=1} = 3k_{1h} l^2 (\lambda_{vh} - 1) > 0 \quad (4.26)$$

and thus requires the ratio of the stiffness of the helical spring to be larger than one, analogous to the condition in the post-buckling regime,

$$(\lambda_{vh} - 1) > 0 \Rightarrow \lambda_{vh} > 1 \quad (4.27)$$

This condition supports the requirement for the SP-element to maximize the ratio of vertical to horizontal stiffness, λ_{vh} .

4.2.3 Base isolation unit for asymmetric building

For the convenience of mounting the base isolation elements in the continuous foundations of the building described in sub-section 4.5.2, four SP elements are put in parallel action to form an assembly, termed as spring-pendulum (SP) unit, schematically sketched in Fig. 4.8. Thus, the building rests on such assembled units, number ($N/4$), to be arranged in equidistant manner along the perimeters in-between the rigid strip foundations of the building (masonry construction). The provision to consider safety columns is a standard strategy to support the building in case of any failure or mishap. Thus, for the exemplarily single-storey asymmetric building (numerically investigated in sub-section 4.5.2) four safety steel columns with 70mm axial clearance corresponding to maximum allowed $|\varphi| = 33^\circ$ tilt of the upright-pendulum, based on response of the building under El Centro 1940 scaled to 0.32g, in each assembled base isolation unit limit the further downward movement of the building and caters for the safety in the case of any mishap or malfunctioning of the SP elements.

However, the helical springs need to be pre-compressed at the assembly stage to keep the elements in their desired position so as to place the unit into the isolation gap in-between rigid foundations of the building.

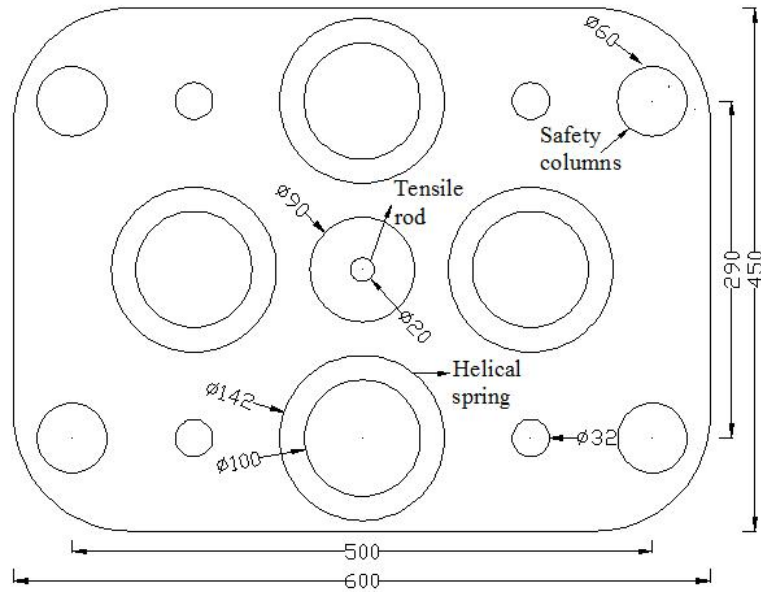


Fig. 4.8: Schematic plan of an assembled SP unit: four SP elements with four safety steel columns ($\Phi 60$), tensile-rod in central position acting in the pre-assembly stage is shown; dimensions (in mm) as per sub-section 4.5.2.

A sufficient axial compression of the springs can be achieved by means of a tensile-rod arrangement at the center of the unit, Fig. 4.8. The working of this arrangement can be comprehended from the Fig. 4.9; the tightening of the nut driven a certain allowed distance (limited length of the threads) on the tensile-rod creates tensile forces in the rod thus brings the mounting plates closer by compressing the four symmetrically arranged helical springs as required, namely just to keep the pendulum in contact with the bearing. However, in the built-in stage the rod becomes loose when the portion of the building's weight further compresses the helical spring axially. It remains loose if the pendulum is tilted during earthquake.

When implementing the base isolation system for a retrofit or even for new construction, a free “play” (i.e., expected ground displacement as per design earthquake) has to be provided for the base-isolated building for the purpose of free movement of the ground.

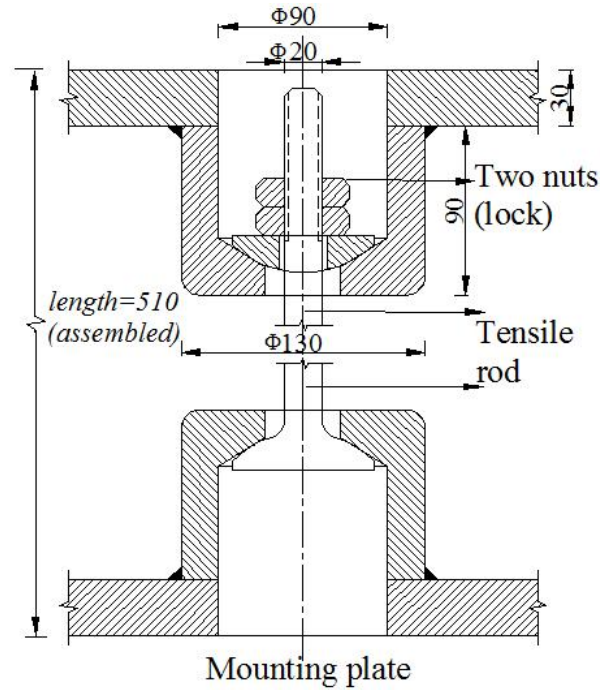


Fig. 4.9: Central tensile-rod arrangement for the axial compression of helical springs in the assembly stage, dimensions as of sub-section 4.5.2.

Referring to the exemplarily single-storey asymmetric building, see sub-section 4.5.2, the maximum horizontal displacement is 220mm when the building is excited under El Centro 1940 seismogram scaled to 0.32g. Additionally, in the range of the free plays, all supply conduits (tubes of water, waste, electricity cables etc.) must be made flexible for elongation and shortening, respectively through installation of flexible parts, see again Bachmann^[4-1].

4.2.4 Base isolation unit for skeletal structure

The base isolation unit consisting of four spring-pendulum (SP) elements is designed for the selected single-storey asymmetric building supported on continuous masonry walls with strip foundations as described in sub-section 4.2.3. However, if the building has a skeletal structure, its weight is transmitted to the ground by an arrangement of columns and the same design of the SP unit may serve the purpose with a proper concentration of the required number of SP elements. Thus, for example, if the same building as considered in sub-section 4.5.2, is supported on 20 columns, a total of 20 SP units each having 12 SP elements of one and the same design, sub-section 4.2.3, combined in

parallel action ($240/20$) are required. The arrangement of the 12 SP elements on two concentric circles of diameter 400mm and 600mm, respectively, with the upper and lower mounting plates of diameter 800mm, is illustrated in Fig. 4.10. Axial compression of the 12 helical springs in the assembled unit is achieved by means of a centrally built-in tensile-rod (say of size M-40), a design analogous to that of Fig. 4.8 in sub-section 4.2.3. The safety columns, however, are not included in the modified SP unit but are separately constructed outside of the unit; likewise to the classical standard constructions in base isolation with rubber bearings.

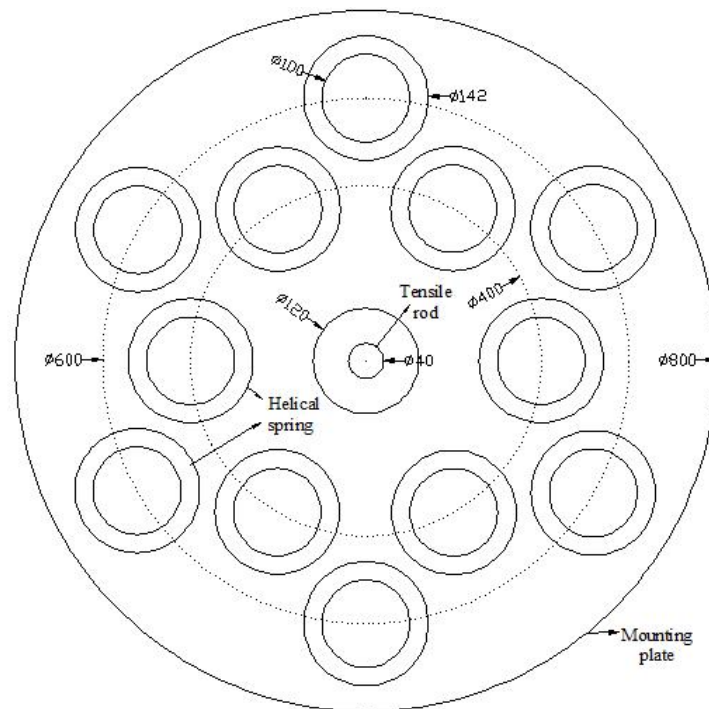


Fig. 4.10: Spring-pendulum (SP) unit having 12 SP elements arranged in two concentric circles; with tensile-rod in central position acting during assembly, see also Fig. 4.8. Safety columns outside of the unit are not shown.

The novel sliding elements as designed in sub-section 4.5.2.3 can be put between the shear walls of the skeletal building and their strip foundation since the horizontal forces transmitted to the ground are rather small, - for the classical system, see again Bachmann^[4-1].

4.3 Equation of motion for the base-isolated building

A simple single-storey rigid building of rectangular plan $a \times b$ with an asymmetrically placed intermediate wall, free-body diagram in Fig. 4.11, is base-isolated by putting a number of novel base isolation units underneath its rigid foundations. The SP unit is proposed to consist of four SP elements as discussed above but for convenience of formulation of the equations of motion, the horizontal restoring forces (Y_i, Z_i) along y - and z -axes, respectively by a single SP element located at point i are shown in Fig. 4.11.

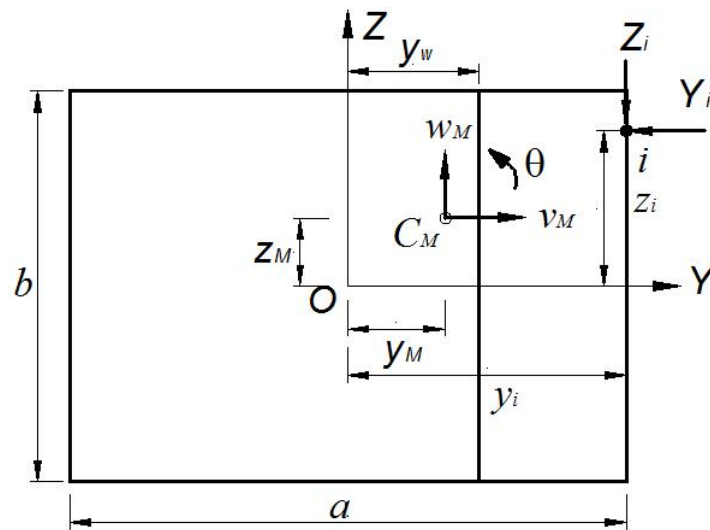


Fig. 4.11: Free-body diagram of base-isolated single-storey asymmetric building, restoring forces of a single base isolation (SP) element indicated.

The arbitrarily distributed mass of various structural elements of the building and in addition the asymmetrically located intermediate wall with eccentricity y_w create the mass asymmetry due to which center of mass C_M is off the geometric centre O of the plan of the building. Let $\vec{r}_M^T = [y_M \ z_M]$ denote the position vector of C_M as illustrated in Fig. 4.11. The asymmetric building of total mass m_S is considered under a single point horizontal seismic ground acceleration $a_g(t)$ with angle of incidence α to y -direction, thus $a_g \cos \alpha$ and $a_g \sin \alpha$ are the horizontal components of the seismic

ground acceleration in y - and z -directions. The lateral displacements of C_M of the building denoted by v_M and w_M along y - and z -axes, respectively and the rotational angle θ about the vertical x -axis define three degrees of freedom (3-DOF) in horizontal motion when the whole building is considered as rigid-body. The mass moment of inertia about the vertical x -axis of the building is $I_x = m_S r_x^2$, where r_x denotes the radius of inertia with respect to the center of mass C_M .

The building is base-isolated by means of symmetrically arranged novel SP units acting between ground and heavy foundation beams along its perimeters. These isolation units act as a low pass filter, thus the horizontal deformations caused by the horizontal component of an earthquake are concentrated in the isolation units and the resulting low frequency fundamental modes can be considered as the rigid-body modes of the building. The vertical motion of the building is a combination of the vertical component of the seismic forcing (no soil-structure interaction is considered) with a guided component from the horizontal motion. It is not further considered in this Section.

Consequently, the equations of horizontal motion are set up by means of conservation of momentum and of angular momentum about the vertical x -axis.

Let $\vec{r}_i^T = [y_i \quad z_i]$ be the position vector of an arbitrarily located single base isolation element of isotropic horizontal stiffness k_{1h} . The single restoring force supplied in the spring is $\vec{R}_i = -k_{1h} \delta \vec{r}_i$ and summation of the restoring forces supplied in all N springs render the resultant force,

$$\vec{R} = -k_{1h} \sum_{i=1}^N \delta \vec{r}_i. \quad (4.28)$$

Using rigid body kinematics, see e.g., Ziegler^[4-15], page 9,

$$\delta \vec{r}_i = \delta \vec{r}_M + \theta \hat{\vec{r}}_{iM} = \delta \vec{r}_M - \theta \hat{\vec{r}}_M + \theta \hat{\vec{r}}_i, \quad |\theta| \ll 1, \quad (4.29)$$

where, $\hat{\vec{r}}_{iM} = \vec{e}_x \times \vec{r}_{iM}$ is the positively rotated orthogonal vector to \vec{r}_{iM} . Hence, the

resultant restoring force becomes, isotropic shear stiffness understood,

$$\vec{R} = -k_{1h} \left\{ N(\delta\vec{r}_M - \theta\hat{\vec{r}}_M) + \theta \sum_{i=1}^N \hat{\vec{r}}_i \right\} = -k_{1h} \left\{ N \left(\begin{bmatrix} v_M \\ w_M \end{bmatrix} - \theta \begin{bmatrix} -z_M \\ y_M \end{bmatrix} \right) + \theta \sum_{i=1}^N \begin{bmatrix} -z_i \\ y_i \end{bmatrix} \right\}. \quad (4.30)$$

The y - and z -components of the resultant restoring force thus become

$$\begin{aligned} R_y &= \sum_{i=1}^N Y_i = -Nk_{1h}(v_M + \theta z_M) + \theta k_{1h} \sum_{i=1}^N z_i, \\ R_z &= \sum_{i=1}^N Z_i = -Nk_{1h}(w_M - \theta y_M) - \theta k_{1h} \sum_{i=1}^N y_i. \end{aligned} \quad (4.31)$$

The free-body diagram of single-storey asymmetric building under horizontal ground excitation as indicated in Fig. 4.11 is subjected to the basic laws of conservation of momentum and conservation of angular momentum about the vertical x -axis, see Ziegler^[4-15], page 400-411.

Conservation of momentum in the yz -plane of the building is,

$$m_S \vec{a}_M = \vec{R}, \quad \vec{a}_M = a_{ty} \vec{e}_y + a_{tz} \vec{e}_z, \quad a_{ty} = a_g \cos \alpha + \ddot{v}_M, \quad a_{tz} = a_g \sin \alpha + \ddot{w}_M, \quad (4.32)$$

where, a_{ty} and a_{tz} are the absolute accelerations of C_M in y - and z -directions,

respectively and \vec{R} is the resultant of the external forces. Hence, in y - and z -directions we respectively have,

$$m_S \ddot{v}_M + Nk_{1h} v_M + k_{1h} \left(Nz_M - \sum_{i=1}^N z_i \right) \theta = -m_S a_g \cos \alpha, \quad (4.33)$$

$$m_S \ddot{w}_M + Nk_{1h} w_M - k_{1h} \left(Ny_M - \sum_{i=1}^N y_i \right) \theta = -m_S a_g \sin \alpha. \quad (4.34)$$

The moment contribution of the single spring \vec{M}_i is, its torsional stiffness is neglected for extremely small rotations,

$$\vec{M}_i = \vec{r}_{iM} \times \vec{R}_i = -k_{1h} (\vec{r}_{iM} \times \delta\vec{r}_i), \quad (4.35)$$

and by substituting rigid body kinematics, Eq. (4.29),

$$\vec{M}_i = -k_{1h} \left[\vec{r}_{iM} \times \delta\vec{r}_M + \theta \vec{r}_{iM} \times (\vec{e}_x \times \vec{r}_{iM}) \right],$$

$$= -k_{1h} \left[\vec{r}_{iM} \times \delta \vec{r}_M + \theta \left((\vec{r}_{iM} \cdot \vec{r}_{iM}) \vec{e}_x - (\vec{r}_{iM} \cdot \vec{e}_x) \vec{r}_{iM} \right) \right]. \quad (4.36)$$

Using $(\vec{r}_{iM} \cdot \vec{r}_{iM}) = \vec{r}_{iM}^2 = \vec{r}_M^2 + \vec{r}_i^2 - 2(\vec{r}_M \cdot \vec{r}_i)$ and $(\vec{r}_{iM} \cdot \vec{e}_x) = 0$, Eq. (4.36) becomes,

$$\vec{M}_i = -k_{1h} \left[(\vec{r}_i - \vec{r}_M) \times \delta \vec{r}_M + \theta \left(\vec{r}_M^2 + \vec{r}_i^2 - 2(\vec{r}_M \cdot \vec{r}_i) \right) \vec{e}_x \right], \quad (4.37)$$

$$\vec{M}_i = -k_{1h} \left[-(\vec{r}_M \times \delta \vec{r}_M) + \theta \vec{r}_M^2 \vec{e}_x + (\vec{r}_i \times \delta \vec{r}_M) + \theta \left(\vec{r}_i^2 - 2\vec{r}_M \cdot \vec{r}_i \right) \vec{e}_x \right]. \quad (4.38)$$

Summation over N springs yields the resulting moment,

$$\vec{M} = -k_{1h} \left[N(\delta \vec{r}_M \times \vec{r}_M) + N\theta \vec{r}_M^2 \vec{e}_x - \delta \vec{r}_M \times \sum_{i=1}^N \vec{r}_i + \theta \left(\sum_{i=1}^N \vec{r}_i^2 - 2\vec{r}_M \cdot \sum_{i=1}^N \vec{r}_i \right) \vec{e}_x \right] \quad (4.39)$$

Substituting $\delta \vec{r}_M \times \vec{r}_M = (v_M z_M - w_M y_M) \vec{e}_x$ and $\delta \vec{r}_M \times \sum_{i=1}^N \vec{r}_i = \left(v_M \sum_{i=1}^N z_i - w_M \sum_{i=1}^N y_i \right) \vec{e}_x$

renders the axial moment about vertical x-axis,

$$\begin{aligned} M = k_{1h} & \left(-N z_M + \sum_{i=1}^N z_i \right) v_M + k_{1h} \left(N y_M - \sum_{i=1}^N y_i \right) w_M \\ & + k_{1h} \left(-N \left(y_M^2 + z_M^2 \right) - \left(\sum_{i=1}^N y_i^2 + \sum_{i=1}^N z_i^2 \right) + 2 \left(y_M \sum_{i=1}^N y_i + z_M \sum_{i=1}^N z_i \right) \right) \theta \end{aligned} \quad (4.40)$$

Conservation of angular momentum with respect to C_M about vertical x-axis is

$$\frac{d\vec{D}}{dt} = \vec{M}, \quad \vec{M} = M \vec{e}_x, \quad D = I_x \dot{\theta} \quad (4.41)$$

Hence, conservation of moment of momentum yields,

$$\begin{aligned} I_x \ddot{\theta} + k_{1h} & \left(N \left(y_M^2 + z_M^2 \right) + \left(\sum_{i=1}^N y_i^2 + \sum_{i=1}^N z_i^2 \right) - 2 \left(y_M \sum_{i=1}^N y_i + z_M \sum_{i=1}^N z_i \right) \right) \theta \\ & + k_{1h} \left(N z_M - \sum_{i=1}^N z_i \right) v_M - k_{1h} \left(N y_M - \sum_{i=1}^N y_i \right) w_M = 0 \end{aligned} \quad (4.42)$$

The three coupled mechanical conservation equations (4.33), (4.34) and (4.42) of (undamped) approximately rigid-body motion of the base-isolated building subjected to single point horizontal ground excitation, are written in matrix form,

$$\underline{M} \ddot{\vec{x}} + \underline{K} \vec{x} = -\underline{M} \vec{a}_g, \quad \vec{x}^T = [v_M \quad w_M \quad u_T], \quad \vec{a}_g^T = a_g [\cos \alpha \quad \sin \alpha \quad 0], \quad u_T = \theta r_x, \quad (4.43)$$

where, \underline{M} and \underline{K} are the diagonal mass- and the symmetric stiffness-matrix of the 3-DOF base-isolated building, respectively and \vec{x} is referred to the displacement vector of the center of mass; \vec{a}_g denotes the oblique single point horizontal seismic ground acceleration vector,

$$\underline{M} = m_S \begin{bmatrix} 1 & 0 & 0 \\ 0 & 1 & 0 \\ 0 & 0 & 1 \end{bmatrix}, \quad (4.44)$$

$$\underline{K} = \begin{bmatrix} Nk_{1h} & 0 & \frac{k_{1h}}{r_x} \left(Nz_M - \sum_{i=1}^N z_i \right) \\ 0 & Nk_{1h} & -\frac{k_{1h}}{r_x} \left(Ny_M - \sum_{i=1}^N y_i \right) \\ \frac{k_{1h}}{r_x} \left(Nz_M - \sum_{i=1}^N z_i \right) & -\frac{k_{1h}}{r_x} \left(Ny_M - \sum_{i=1}^N y_i \right) & k_{33} \end{bmatrix}, \quad (4.45)$$

$$k_{33} = \frac{k_{1h}}{r_x^2} \left(N(y_M^2 + z_M^2) + \left(\sum_{i=1}^N y_i^2 + \sum_{i=1}^N z_i^2 \right) - 2 \left(y_M \sum_{i=1}^N y_i + z_M \sum_{i=1}^N z_i \right) \right).$$

4.3.1 Modal analysis of base-isolated building

The solution of the eigen-value problem associated with the homogenous equation (2.1) when considering the diagonal mass- and symmetric stiffness matrices, renders the natural circular frequencies ω_j and ortho-normalized modal vectors $\vec{\phi}_j, j=1,2,3$ for the base-isolated building by requiring modal mass $m_j = \vec{\phi}_j^T \underline{M} \vec{\phi}_j = 1$. The coordinates of the modal centers of velocity $C_{Vj}, j=1,2,3$ are determined by Eq. (2.13), for details see Fu^[4-17] or Fu-Ziegler^[4-18]. The position of the modal center of velocity plays a key role in determining the effective location of the respective TLCGDs to be attached to the asymmetric building, as discussed in section 3.4. The modally tuned TLCGDs for the respective mode are placed in the basement of the base-isolated asymmetric building keeping in view the normal distance of its trace to modal center of velocity C_{Vj} as large as possible within the plan so as to absorb maximum kinetic energy, Fu-Ziegler^[4-18]. Thus,

the vibration induced by the horizontal ground excitation is damped by increasing the effective damping by means of the properly tuned and optimally placed TLCGDs; see Hochrainer-Ziegler^[4-19].

When considering the rigid-body modes of the asymmetric building in the design stage, each mode is considered isolated rendering the two degree of freedom (2-DOF) modally isolated coupled system (i.e., base isolated asymmetric building coupled with TLCGD) for the sake of modal tuning of the corresponding TLCGD, as described in sub-section 2.5, by the transformation of the classical Den Hartog's formulas, see Den Hartog^[4-20], by means of the analogy between TMD and TLCGD, for details, see Hochrainer^[4-21] and Hochrainer-Ziegler^[4-19].

4.4 Equations of motion for coupled system in state-space domain

Traditionally, dynamic systems have been described by second order differential equations because Newton's law as well as energy principles (e.g. Lagrange equations of motion, Hamilton's principle) render inertia proportional to acceleration. Alternatively, the state-space representation is a systematic approach adaptable for automated processing that is not only be used to represent the dynamical systems but also preferred for their dynamic investigations especially with respect to control theory.

4.4.1 Modally isolated 2-DOF coupled system in state space

Referring to the modally isolated 2-DOF coupled system by the virtue of modal approximations as explained in sub-section 2.4, for the similar case of base-isolated rigid building equipped with TLCGDs, the linearized modally approximated equations in matrix form, Eq. (2.76), is rewritten; light modal structural damping includes the linearized friction of the sliding elements,

$$\underbrace{\begin{bmatrix} 1 + \mu_j & \bar{\kappa}_j V_{\gamma j} \mu_{ff} \\ \kappa_j V_{\gamma j} & 1 \end{bmatrix}}_{\bar{M}_j} \begin{bmatrix} \ddot{q}_j \\ \ddot{u}_j \end{bmatrix} + \begin{bmatrix} 2\zeta_{Sj} \omega_{Sj} & 0 \\ 0 & 2\zeta_{Aj} \omega_{Aj} \end{bmatrix} \begin{bmatrix} \dot{q}_j \\ \dot{u}_j \end{bmatrix} + \begin{bmatrix} \omega_{Sj}^2 & 0 \\ 0 & \omega_{Aj}^2 \end{bmatrix} \begin{bmatrix} q_j \\ u_j \end{bmatrix} = - \begin{bmatrix} L_j \\ \kappa_j \cos(\alpha - \gamma_j) \end{bmatrix} a_g \quad (4.46)$$

and can be rearranged,

$$\begin{bmatrix} \ddot{q}_j \\ \ddot{u}_j \end{bmatrix} = -\bar{M}_j^{-1} \begin{bmatrix} 2\zeta_{Sj} \omega_{Sj} & 0 \\ 0 & 2\zeta_{Aj} \omega_{Aj} \end{bmatrix} \begin{bmatrix} \dot{q}_j \\ \dot{u}_j \end{bmatrix} - \bar{M}_j^{-1} \begin{bmatrix} \omega_{Sj}^2 & 0 \\ 0 & \omega_{Aj}^2 \end{bmatrix} \begin{bmatrix} q_j \\ u_j \end{bmatrix} - \bar{M}_j^{-1} \begin{bmatrix} L_j \\ \kappa_j \cos(\alpha - \gamma_j) \end{bmatrix} a_g$$

where, $\bar{M}_j = \begin{bmatrix} 1 + \mu_j & \bar{\kappa}_j V_{\gamma j} \mu_{ff} \\ \kappa_j V_{\gamma j} & 1 \end{bmatrix}$,

with abbreviations defined in sub-section 2.4 and 2.5. This system of second-order linear coupled differential equations, expressed by the generalized modal coordinate and the fluid stroke, can be straight forwardly converted to a first order state-space representation

by introducing the (4x1) modal state-vector $\bar{z}_j = [q_j \ u_j \ \dot{q}_j \ \dot{u}_j]^T$,

$$\begin{bmatrix} \dot{z}_1 \\ \dot{z}_2 \\ \dot{z}_3 \\ \dot{z}_4 \end{bmatrix}_j = \begin{bmatrix} 0 & 0 & 1 & 0 \\ 0 & 0 & 0 & 1 \\ -\bar{M}_j^{-1} \begin{bmatrix} \omega_{Sj}^2 & 0 \\ 0 & \omega_{Aj}^2 \end{bmatrix} & -\bar{M}_j^{-1} \begin{bmatrix} 2\zeta_{Sj} \omega_{Sj} & 0 \\ 0 & 2\zeta_{Aj} \omega_{Aj} \end{bmatrix} \end{bmatrix} \begin{bmatrix} z_1 \\ z_2 \\ z_3 \\ z_4 \end{bmatrix}_j + \begin{bmatrix} 0 \\ 0 \\ L_j \\ \kappa_j \cos(\alpha - \gamma_j) \end{bmatrix}_j a_g \quad (4.47)$$

thus, simply rewritten as

$$\dot{\bar{z}}_j(t) = \underline{A}_{rj} \bar{z}_j(t) + \underline{E}_g a_g(t) \quad (4.48)$$

where, $z_1 = q_j, z_2 = u_j, z_3 = \dot{q}_j, z_4 = \dot{u}_j$ and the system matrix $\underline{A}_{rj} = \underline{A}_j + \underline{B}_j \underline{R}_j$ is kept separated, to keep access to the absorber's (TLCGD) parameters,

$$\underline{A}_j = \begin{bmatrix} 0 & 0 & 1 & 0 \\ 0 & 0 & 0 & 1 \\ -\bar{M}_j^{-1} \begin{bmatrix} \omega_{Sj}^2 & 0 \\ 0 & 0 \end{bmatrix} & -\bar{M}_j^{-1} \begin{bmatrix} 2\zeta_{Sj} \omega_{Sj} & 0 \\ 0 & 0 \end{bmatrix} \end{bmatrix}, \underline{B}_j = \begin{bmatrix} 0 & 0 & 0 & 0 \\ 0 & 0 & 0 & 0 \\ -\bar{M}_j^{-1} \begin{bmatrix} 1 & 0 \\ 0 & 1 \end{bmatrix} & -\bar{M}_j^{-1} \begin{bmatrix} 1 & 0 \\ 0 & 1 \end{bmatrix} \end{bmatrix}$$

$$R_j = \begin{bmatrix} 0 & 0 & 0 & 0 \\ 0 & \omega_{Aj}^2 & 0 & 0 \\ 0 & 0 & 0 & 0 \\ 0 & 0 & 0 & 2\zeta_{Aj}\omega_{Aj} \end{bmatrix}, E_{gj} = \begin{bmatrix} 0 \\ 0 \\ L_j \\ -\bar{M}_j^{-1} \left[\kappa_j \cos(\alpha - \gamma_j) \right] \end{bmatrix}. \quad (4.49)$$

The modally approximated state equation (4.48) is formally solved for $\bar{z}_j(t)$ when subjected to ground acceleration $a_g(t)$,

$$\bar{z}_j(t) = (A_j + B_j R_j)^{-1} (\bar{z}_j(t) - E_{gj} a_g(t)). \quad (4.50)$$

Inserting a time-harmonic forcing, $\bar{z}_j(t) = \bar{z}_{j0} e^{i\omega t}$ and $a_g(t) = a_g e^{i\omega t}$ into Eq. (4.48)

the time-reduced modal equation for TLCGD-main system results

$$\bar{z}_{j0} = (i\omega I - A_j)^{-1} E_{gj} a_g. \quad (4.51)$$

The modally approximated state equations, Eq. (4.48) and (4.51) in time and frequency domain respectively, make the numerical investigations of the modally isolated 2-DOF coupled system conveniently possible to get the approximate solution in state-space domain.

4.4.2 Modally coupled system in state-space

As a matter of fact, the equations of motion for three degree of freedom (3-DOF) structure (i.e., base-isolated asymmetric building: main system) with three TLCGDs (i.e., secondary system) render modal coupling when modal approximations are no longer considered. Thus, incorporating the damping matrix of the main system and the control force term due to the TLCGDs in Eq. (2.1), we get

$$M\ddot{x} + C\dot{x} + Kx = -M\ddot{a}_g + P\bar{F}, \quad (4.52)$$

$$\bar{F}^T = [\bar{F}_1^T \quad \bar{F}_2^T \quad \bar{F}_3^T], \quad \bar{F}_j^T = -[F_{A_jj} \quad F_{A_zj} \quad M_{xj}/r_x]$$

where C is such a damping matrix of the base-isolated building that keeps the modal vectors orthogonal; \bar{F}^T is the control force vector and $P = [P_1 \quad P_2 \quad P_3]$;

$P_j = \text{diag}[1 \quad 1 \quad 1]$ is the position matrix of the TLCGDs.

The displacement vector \bar{x} of center of mass of base-isolated building is expanded into

modal series $\bar{x} = \sum_{j=1}^3 \bar{\phi}_j q_j$ on the left hand side of Eq. (4.52) considering the rigid-body

motion. Therefore, the term $\sum_{j=1}^3 \bar{\phi}_j \ddot{q}_j$ takes the form $\bar{\phi} \ddot{\bar{q}}$ when expanded for rigid-body

modes, thus Eq. (4.52) becomes

$$\underline{M} \bar{\phi} \ddot{\bar{q}} + \underline{C} \bar{\phi} \dot{\bar{q}} + \underline{K} \bar{\phi} \bar{q} = -\underline{M} \bar{a}_g + \underline{P} \bar{F} \quad (4.53)$$

The control force vector $\bar{F}_j^T = -[F_{Ayj} \quad F_{Azj} \quad M_{xj}/r_x]$ is written for j -th TLCDG when \ddot{v}_M , \ddot{w}_M and \ddot{u}_T , i.e.,

$$\ddot{v}_M = \phi_{11} \ddot{q}_1 + \phi_{12} \ddot{q}_2 + \phi_{13} \ddot{q}_3, \quad \ddot{w}_M = \phi_{21} \ddot{q}_1 + \phi_{22} \ddot{q}_2 + \phi_{23} \ddot{q}_3, \quad \ddot{u}_T = \phi_{31} \ddot{q}_1 + \phi_{32} \ddot{q}_2 + \phi_{33} \ddot{q}_3, \quad (4.54)$$

are substituted in Eqs. (2.46), (2.47) and (2.60) to render,

$$\bar{F}_j = -\underline{M}_{ff} \left(\underline{T}_j \bar{\phi} \ddot{\bar{q}} + \bar{T}_j \bar{a}_g + \bar{\kappa}_j \underline{\gamma}_j \ddot{u}_j \right), \quad j = 1, 2, 3 \quad (4.55)$$

$$\text{where, } \underline{T}_j = \begin{bmatrix} 1 & 0 & -(z_{Aj} - z_M)/r_x \\ 0 & 1 & (y_{Aj} - y_M)/r_x \\ -(z_{Aj} - z_M)/r_x & (y_{Aj} - y_M)/r_x & T_{j33} \end{bmatrix},$$

$$T_{j33} = \frac{1}{r_x^2} \left[(z_{Aj} - z_M)^2 + (y_{Aj} - y_M)^2 + \bar{\kappa}_{Tj} H_j^2 \right],$$

$$\bar{T}_j = \begin{bmatrix} 1 & 0 & 0 \\ 0 & 1 & 0 \\ -(z_{Aj} - z_M)/r_x & (y_{Aj} - y_M)/r_x & 0 \end{bmatrix}, \quad \underline{M}_{ff} = \text{diag}(m_{ff}, m_{ff}, m_{ff}),$$

$$\bar{\delta}_j^T = \begin{bmatrix} \cos \gamma_j & \sin \gamma_j & \begin{bmatrix} -\cos \gamma_j (z_{Aj} - z_M)/r_x \\ +\sin \gamma_j (y_{Aj} - y_M)/r_x \end{bmatrix} \end{bmatrix},$$

$$\underline{\gamma}_1 = [\bar{\delta}_1 \quad \bar{0} \quad \bar{0}], \quad \underline{\gamma}_2 = [\bar{0} \quad \bar{\delta}_2 \quad \bar{0}], \quad \underline{\gamma}_3 = [\bar{0} \quad \bar{0} \quad \bar{\delta}_3].$$

Thus, Eq. (4.56) results when the linearized control forces produced by several TLCDGs are written in a hyper-matrix notation,

$$\bar{F} = -\underline{M}_f \left(\underline{T} \bar{\phi} \ddot{\bar{q}} + \bar{T} \bar{x}_g + \bar{\kappa} \underline{\gamma} \ddot{u} \right), \quad (4.56)$$

where, $\underline{T}^T = [\underline{T}_1 \quad \underline{T}_2 \quad \underline{T}_3]$, $\bar{\underline{T}}^T = [\bar{\underline{T}}_1 \quad \bar{\underline{T}}_2 \quad \bar{\underline{T}}_3]$, $\underline{\gamma}^T = [\underline{\gamma}_1 \quad \underline{\gamma}_2 \quad \underline{\gamma}_3]$,

$$\bar{\underline{\kappa}}^T = \text{diag} [\bar{\kappa}_1, \bar{\kappa}_1, \bar{\kappa}_1, \bar{\kappa}_2, \bar{\kappa}_2, \bar{\kappa}_2, \bar{\kappa}_3, \bar{\kappa}_3, \bar{\kappa}_3],$$

$$\underline{M}_f = \text{diag} [m_{f1}, m_{f1}, m_{f1}, m_{f2}, m_{f2}, m_{f2}, m_{f3}, m_{f3}, m_{f3}],$$

$\bar{\underline{u}}^T = [u_1 \quad u_2 \quad u_3]$ samples the fluid strokes.

Hence, Eq. (4.53) for base-isolated building with three TLCGDs installed in terms of the favorable generalized coordinates becomes,

$$\left(\underline{M} \underline{\phi} + \underline{P} \underline{M}_f \underline{T} \underline{\phi} \right) \ddot{\underline{q}} + \underline{P} \underline{M}_f \bar{\underline{\kappa}} \ddot{\underline{u}} + \underline{C} \underline{\phi} \dot{\underline{q}} + \underline{K} \underline{\phi} \underline{q} = - \left(\underline{M} + \underline{P} \underline{M}_f \bar{\underline{T}} \right) \bar{\underline{a}}_g. \quad (4.57)$$

The linearized equation of relative fluid flow in TLCGD number j , (Eq. 2.33) is

$$\ddot{u}_j + 2\zeta_{Aj} \omega_{Aj} \dot{u}_j + \omega_{Aj}^2 u_j = -\kappa_j \left\{ \begin{array}{l} \left(\ddot{v}_M - (z_{Aj} - z_M) \ddot{\theta} \right) \cos \gamma_j \\ + \left(\ddot{w}_M + (y_{Aj} - y_M) \ddot{\theta} \right) \sin \gamma_j + a_g \cos(\alpha - \gamma_j) \end{array} \right\}. \quad (4.58)$$

Substituting the modal expansions of \ddot{v}_M , \ddot{w}_M and \ddot{u}_T given by Eq. (4.54) into Eq.

(4.58) for each of three TLCGDs, render a set of equations written in matrix notation,

$$\underline{I} \ddot{\underline{u}} + \underline{C}_f \dot{\underline{u}} + \underline{K}_f \underline{u} = -\underline{\kappa} \underline{T}_f \underline{\phi} \ddot{\underline{q}} - \underline{\kappa} \underline{\gamma}_f \bar{\underline{a}}_g, \quad (4.59)$$

where, $\underline{C}_f = \text{diag} [2\zeta_{A1} \omega_{A1}, 2\zeta_{A2} \omega_{A2}, 2\zeta_{A3} \omega_{A3}]$ denotes the linearized absorber

damping matrix; $\underline{K}_f = \text{diag} [\omega_{A1}^2, \omega_{A2}^2, \omega_{A3}^2]$ denotes the stiffness matrix of TLCGDs,

$$\underline{\kappa} = \text{diag} [\kappa_1, \kappa_2, \kappa_3], \quad \underline{T}_\gamma = \underline{\gamma}_c \underline{T}_z + \underline{\gamma}_s \underline{T}_y, \quad \underline{\gamma}_c = \text{diag} [\cos \gamma_1, \cos \gamma_2, \cos \gamma_3],$$

$$\underline{\gamma}_s = \text{diag} [\sin \gamma_1, \sin \gamma_2, \sin \gamma_3],$$

$$\underline{\gamma}_f = \begin{bmatrix} \cos \gamma_1 & \sin \gamma_1 & 0 \\ \cos \gamma_2 & \sin \gamma_2 & 0 \\ \cos \gamma_3 & \sin \gamma_3 & 0 \end{bmatrix}, \quad \underline{T}_z = \begin{bmatrix} 1 & 0 & -(z_{A1} - z_M)/r_x \\ 1 & 0 & -(z_{A2} - z_M)/r_x \\ 1 & 0 & -(z_{A3} - z_M)/r_x \end{bmatrix}, \quad \underline{T}_y = \begin{bmatrix} 0 & 1 & (y_{A1} - y_M)/r_x \\ 0 & 1 & (y_{A2} - y_M)/r_x \\ 0 & 1 & (y_{A3} - y_M)/r_x \end{bmatrix}.$$

The equations of motion for coupled TLCGD-main system by substituting the linearized control force and rearranging terms, Eq. (4.57) and (4.59) are assembled in matrix form,

$$\begin{bmatrix} \underline{M}\underline{\phi} + \underline{P}\underline{M}_f\underline{T}\underline{\phi} & \underline{P}\underline{M}_f\underline{\kappa}\underline{\gamma} \\ \underline{\kappa}\underline{T}_\gamma\underline{\phi} & \underline{I} \end{bmatrix} \begin{Bmatrix} \ddot{\underline{q}} \\ \ddot{\underline{u}} \end{Bmatrix} + \begin{bmatrix} \underline{C}\underline{\phi} & \underline{0} \\ \underline{0} & \underline{C}_f \end{bmatrix} \begin{Bmatrix} \dot{\underline{q}} \\ \dot{\underline{u}} \end{Bmatrix} + \begin{bmatrix} \underline{K}\underline{\phi} & \underline{0} \\ \underline{0} & \underline{K}_f \end{bmatrix} \begin{Bmatrix} \underline{q} \\ \underline{u} \end{Bmatrix} = - \begin{bmatrix} \underline{M} + \underline{P}\underline{M}_f\underline{T} \\ \underline{\kappa}\underline{\gamma}_f \end{bmatrix} \underline{\ddot{a}}_g \quad (4.60)$$

and can be written as follows

$$\begin{Bmatrix} \ddot{\underline{q}} \\ \ddot{\underline{u}} \end{Bmatrix} = -\underline{\bar{M}}^{-1} \begin{bmatrix} \underline{C}\underline{\phi} & \underline{0} \\ \underline{0} & \underline{C}_f \end{bmatrix} \begin{Bmatrix} \dot{\underline{q}} \\ \dot{\underline{u}} \end{Bmatrix} - \underline{\bar{M}}^{-1} \begin{bmatrix} \underline{K}\underline{\phi} & \underline{0} \\ \underline{0} & \underline{K}_f \end{bmatrix} \begin{Bmatrix} \underline{q} \\ \underline{u} \end{Bmatrix} - \underline{\bar{M}}^{-1} \begin{bmatrix} \underline{M} + \underline{P}\underline{M}_f\underline{T} \\ \underline{\kappa}\underline{\gamma}_f \end{bmatrix} \underline{\ddot{a}}_g, \quad (4.61)$$

$$\text{where, } \underline{\bar{M}} = \begin{bmatrix} \underline{M}\underline{\phi} + \underline{P}\underline{M}_f\underline{T}\underline{\phi} & \underline{P}\underline{M}_f\underline{\kappa}\underline{\gamma} \\ \underline{\kappa}\underline{T}_\gamma\underline{\phi} & \underline{I} \end{bmatrix}. \quad (4.62)$$

This system of second order differential equations is converted to first order state-space representation by introducing a state hyper-vector $\underline{\bar{z}} = [\underline{\bar{q}}^T \underline{\bar{u}}^T \dot{\underline{\bar{q}}}^T \dot{\underline{\bar{u}}}^T]^T$ of order $2(N_S + N_A)$, where N_S is the degree of freedom of the main system (i.e., 3-DOF base-isolated asymmetric building) and N_A is the number of TLCGDs installed (e.g. three), see e.g. Ziegler^[4-15] page 438,

$$\dot{\underline{\bar{z}}}(t) = (\underline{A} + \underline{B}\underline{R})\underline{\bar{z}}(t) + \underline{E}_g \underline{\ddot{a}}_g(t), \quad (4.63)$$

where, in a hyper-matrix notation, the main system matrix again remains separated,

$$\underline{A} = \begin{bmatrix} \underline{0} & \underline{0} & \underline{I} & \underline{0} \\ \underline{0} & \underline{0} & \underline{0} & \underline{I} \\ -\underline{\bar{M}}^{-1} \begin{bmatrix} \underline{K}\underline{\phi} & \underline{0} \\ \underline{0} & \underline{0} \end{bmatrix} & -\underline{\bar{M}}^{-1} \begin{bmatrix} \underline{C}\underline{\phi} & \underline{0} \\ \underline{0} & \underline{0} \end{bmatrix} & \underline{0} & \underline{0} \end{bmatrix}, \quad \underline{B} = \begin{bmatrix} \underline{0} & \underline{0} & \underline{0} & \underline{0} \\ \underline{0} & \underline{0} & \underline{0} & \underline{0} \\ -\underline{\bar{M}}^{-1} \begin{bmatrix} \underline{I} & \underline{0} \\ \underline{0} & \underline{I} \end{bmatrix} & -\underline{\bar{M}}^{-1} \begin{bmatrix} \underline{I} & \underline{0} \\ \underline{0} & \underline{I} \end{bmatrix} & \underline{0} & \underline{0} \end{bmatrix}$$

$$\underline{R} = \begin{bmatrix} \underline{0} & \underline{0} & \underline{0} & \underline{0} \\ \underline{0} & \underline{K}_f & \underline{0} & \underline{0} \\ \underline{0} & \underline{0} & \underline{0} & \underline{0} \\ \underline{0} & \underline{0} & \underline{0} & \underline{C}_f \end{bmatrix}, \quad \underline{E}_g = \begin{bmatrix} \underline{0} \\ \underline{0} \\ -\underline{\bar{M}}^{-1} \begin{bmatrix} \underline{M} + \underline{P}\underline{M}_f\underline{T} \\ \underline{\kappa}\underline{\gamma}_f \end{bmatrix} \end{bmatrix}. \quad (4.64)$$

The state equation (4.63) is solved for $\underline{\bar{z}}_j(t)$ to render the response of the coupled system in time domain when subjected to ground acceleration $\underline{a}_g(t)$. Since generalized modal coordinates have been chosen, the coupling refers to the action of the TLCGDs only. The calculation of the structural response for the linearized system is straight forward, once a dynamic description in the state-space, Eq. (4.63), is available.

MATLAB^[4-22] provides efficient time integration subroutine like *lsim*, which simulates the time response of continuous linear time invariant systems to arbitrary input (e.g., a recorded earthquake seismogram).

In addition, steady-state solution $\bar{z}(t) = \bar{z}_0 e^{i\omega t}$, assuming the ground excitation to be time-harmonic $\bar{a}_g(t) = \bar{a}_g e^{i\omega t}$ becomes,

$$\bar{z}_0(\alpha, \omega) = [i\omega I - (\underline{A} + \underline{B}\underline{R})]^{-1} \underline{E}_g \bar{a}_g. \quad (4.65)$$

The state equation (4.65) renders the solution of the fully coupled system in frequency domain.

The optimal natural frequency and the damping ratios of the fine tuned TLCGDs are calculated by minimizing the following performance index in state-space domain, corresponding to the minimum of the area under the resonance curve,

$$J = \int_{-\infty}^{\infty} \bar{z}_S^T(\omega) \underline{S} \bar{z}_S(\omega) d\omega = 2\pi \bar{b}^T \bar{P} \bar{b}^T \rightarrow \text{Minimum}, \quad (4.66)$$

where $\bar{z}_S = [\bar{q}^T \quad \dot{\bar{q}}^T]^T$ represents the main structure's state-vector expressed in generalized modal coordinates. $\bar{b} = \underline{E}_g \bar{a}_g$ is the excitation vector; \bar{P} is consequently the solution of the algebraic Lyapunov matrix equation,

$$(\underline{A} + \underline{B}\underline{R})^T \bar{P} + \bar{P}(\underline{A} + \underline{B}\underline{R}) = -\underline{S}, \quad (4.67)$$

evaluated by means of the software MATLAB^[4-22], where \underline{S} is the positive semi-definite weighing diagonal matrix chosen to pronounce the displacements 10 times over velocities. The minimization of performance index J is performed numerically by calling the function *fminsearch* of the MATLAB^[4-22] Optimization Toolbox. *fminsearch* quickly finds the minimum of the scalar function J of several variables, when substituting Den Hartog's modal tuning parameters as initial estimates.

4.5 Application with numerical examples

The dynamic response of the base-isolated structures subjected to horizontal ground

excitation is investigated numerically in frequency and time domain by using state-space representation. Both, a simple five-storey plane frame, a benchmark given in Chopra^[4-23], page 744, and the single-storey asymmetric building, see section 4.3, are investigated under earthquake excitation when equipped with the novel base isolation system (i.e., SP units along with sliding elements and TLCGDs).

4.5.1 Base-isolated plane frame

Referring to the benchmark five-storey plane frame as considered by Chopra^[4-23], page 744, sketch in Fig. 4.12, it is worthily notified that the storey-drifts (relative deformation among various floors) are negligible when frame is base isolated. Such a typical base-isolated frame is also worked-out by Hochrainer-Ziegler^[4-19] with unnecessary large amount of water ($\mu = m_f / M = 3\%$) in the TLCGD placed in the basement of the frame.

The purpose of reconsidering such a simple frame in this Section is to confirm the behavior of the frame as “rigid” after base isolation because of the small storey-drifts of the various floors (e.g., deformation of even the top floor is almost same as that for the new basic mode of the isolated frame) as illustrated by mode shapes of the base-isolated frame in Fig. 4.13(b).

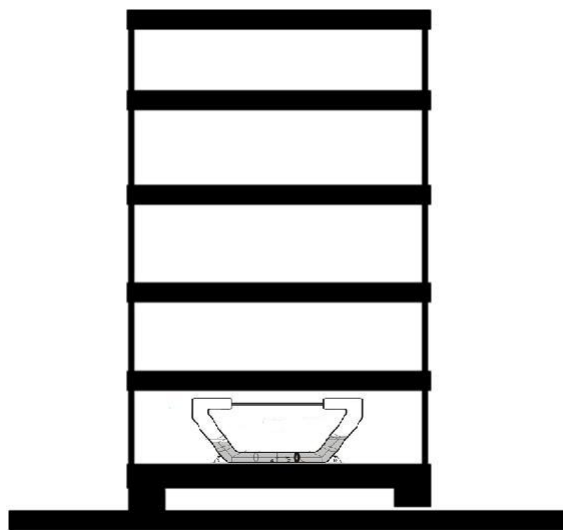


Fig. 4.12: Five-storey benchmark frame, Chopra^[4-23], base-isolated along with TLCGD in the basement, sliding elements not shown.

The numerical investigations in state-space are performed to improve the results with respect to damping supplied by TLCGD by using the minimum required mass ratio to achieve its optimal design.

4.5.1.1 Modal analysis and installation of TLCGD

The modal analysis of the fixed-base five-storey frame depicts the relative deformation of various floors corresponding to its modes of vibrations, first and second modes are shown in Fig. 4.13(a), for details, see Hochrainer-Adam^[4-24]. The top (5th) floor experiences the maximum deformation 1.049 whereas the first floor is at 0.299 when vibrating in its first mode as sketched in Fig. 4.13(a).

The base isolation introduces a base-slab of one and same mass $m = 45344\text{kg}$ rendering a 6-DOF system of total mass $m_S = (5 + 1) \times m = 272064\text{kg}$. Homogeneous field stiffness and stiffness of the base isolation units are chosen such that the same period results as given in Chopra^[4-23]. It is quite evident from the mode shapes in Fig. 4.13 that most of the deformations are in the isolation units and the frame above behaves like a rigid-body. Hence, it can be concluded that the contribution of modal deformation is negligible for the base-isolated frame. Even, the 2nd mode shape of base-isolated frame (6-DOF) exhibits a node almost at the center, thus creating an additional virtual stiffness of the frame.

When working with multi-storey structures, the floor level at which the absorber is installed must be chosen carefully, since it highly influences the TLCGD performance. In case of base-isolated structure, the mode shape of the new basic mode with contribution of modal deformation negligibly small, the optimal position of TLCGD sits in the basement of the frame as drawn in Fig. 4.12. Consequently, the dead-fluid mass must not be minimized and vertical upright sections of the TLCGD piping system become well suited.

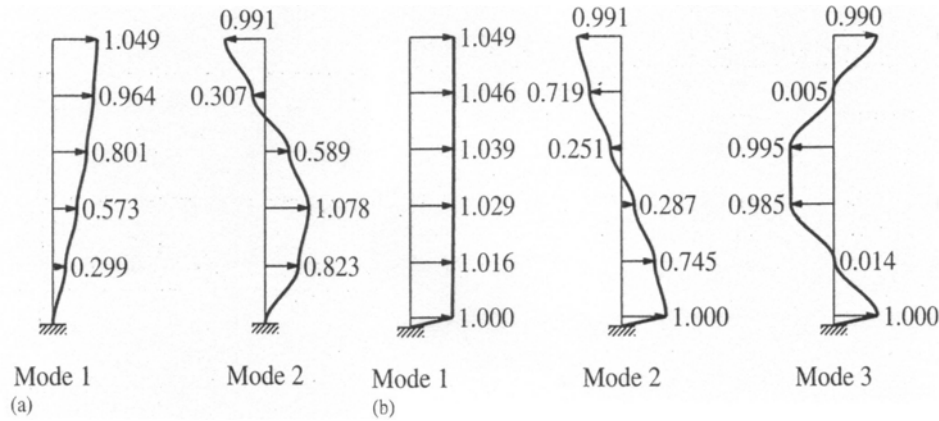


Fig. 4.13: Changing the natural mode shapes of five-storey plane frame by base isolation, Chopra^[4-23]: (a) fixed-base (b) base-isolated.

4.5.1.2 TLCGD design parameters

The vertical height ($H = 2.5\text{m}$) of the liquid column of TLCGD is guided by limiting conditions on the maximum liquid strokes in TLCGD. It is ensured that latter (i.e., $\max|u_0| = 1.24\text{m}$), when base-isolated frame is excited by El Centro 1940 seismogram scaled to $0.32g$, must be under admissible limits; $\max|u_0| \leq 2/3 H = 1.67\text{m}$, $\max|u_0| \leq H_a/3 = 1.35\text{m}$. In addition, the maximum speed of the fluid interface to the gas in the TLCGD should also be within acceptable limits for the application of the piston theory: $\max|\dot{u}_0| = \omega_A \max|u_0| = 3.8\text{m/s} \leq 10\text{m/s}$, see again Ziegler^[4-25].

The structural modal damping of such a base-isolated frame is extremely low, even with linearized frictional damping of the novel sliding elements included, and assumed to be 0.01% for the basic mode. The geometrical dimensions of the TLCGD and other resulting key parameters are collected in Table 4.1.

Table 4.1: Parameters of the TLCGD placed in the basement of plane frame.

TLCGD Parameters	Values
Mass of water inside TLCGD, m_f [kg]	2721
Mass ratio, $\mu = m_f/m_S$ [%]	1

Horizontal length of the liquid column, B [m]	8.0
Vertical height of the liquid column, H [m]	2.5
Effective length, $L_{eff} = B + 2H$ [m]	13
B / L_{eff}	0.615
Angle of inclined pipe section, β [rad] (might be vertical)	$\pi/4$
Inner diameter, circular TLCGD pipe, [m]	0.516
Geometry factor, $\kappa = \bar{\kappa}$, Eq. (2.28)	0.89
Optimal frequency ratio, δ_{opt} , Eq. (2.80)	0.991
Optimal absorber frequency, $f_{A,opt} = \delta_{opt} f_S$ [Hz]	0.488
Optimal linear damping coefficient, $\zeta_{A,opt}$ [%], Eq. (2.83), $\zeta_{A_j} = \zeta_{A_j}^*$	5.41
Eqv. math. pendulum length, L_0 [m], Eq. (2.84)	1.042
$h_0/H_a = L_{eff}/2L_0 - \sin \beta$	5.53
Equilibrium pressure head, $h_0 = np_0/\rho g$ [m], $n = 1$	22.43
Gas volume, $V_0 = A_H H_a$ [m ³]	0.849
Dead fluid-mass, $m_{fd} = m_f (1 - \kappa \bar{\kappa})$ [kg], Eq. (2.81)	578.4

4.5.1.3 Simulation results

The base-isolated shear frame subjected to the ground excitation equipped with Den Hartog's tuned TLCGD in the basement is simulated for further dynamic investigations both in frequency and time domain by using the state-space approach. The dynamics of shear frame influenced by TLCGD are also investigated by Hochrainer-Adam^[4-24].

The 6-DOF (w_1, w_2, \dots, w_6) base-isolated frame with single TLCGD installed at proper location (i.e., in the basement of the frame with control force substituted accordingly) is

described by the set of matrix equations in terms of real co-ordinates, see Hochrainer-Ziegler^[4-19] in their hyper-matrix form,

$$\bar{M}_S \begin{Bmatrix} \ddot{\bar{w}} \\ \ddot{\bar{u}} \end{Bmatrix} + \begin{bmatrix} \bar{C} & \bar{0} \\ \bar{0} & \bar{C}_f \end{bmatrix} \begin{Bmatrix} \dot{\bar{w}} \\ \dot{\bar{u}} \end{Bmatrix} + \begin{bmatrix} \bar{K} & \bar{0} \\ \bar{0} & \bar{K}_f \end{bmatrix} \begin{Bmatrix} \bar{w} \\ \bar{u} \end{Bmatrix} = \begin{bmatrix} \bar{M}\bar{r}_S + \bar{L}\bar{M}_f\bar{i} \\ \bar{\kappa}\bar{i} \end{bmatrix} a_g, \quad (4.68)$$

The sparse position matrix is $\bar{L}^T = [1 \ 0 \ 0 \ 0 \ 0 \ 0]$ with dimension 6×1 apparent in (4.68), enters the generalized mass matrix with dimension 7×7 for the said case,

$$\bar{M}_S = \begin{bmatrix} \bar{M} + \bar{L}\bar{M}_f\bar{L}^T & \bar{L}\bar{M}_f\bar{\kappa} \\ \bar{\kappa}\bar{L}^T & \bar{I} \end{bmatrix}$$

where \bar{M} , \bar{C} and \bar{K} are mass, light damping and stiffness matrix of the plane frame and \bar{M}_f , \bar{C}_f , \bar{K}_f , $\bar{\kappa}$, $\bar{\kappa}$ are the diagonal matrices of 1×1 for the single TLCGD installed.

To make the tools of control theory applicable, equation (4.68) is converted to state-space representation by means of a state hyper-vector $\bar{z} = [\bar{w} \ \bar{u} \ \dot{\bar{w}} \ \dot{\bar{u}}]^T$ of order $2(6+1)=14$, see e.g. Ziegler^[4-15] page 438; modal expansion with the possibility of modal truncation is saved here when dealing with a rather small system,

$$\dot{\bar{z}}(t) = (\bar{A} + \bar{B}\bar{R})\bar{z}(t) + \bar{e}_g a_g(t), \quad (4.69)$$

where, in a hyper-matrix notation, the main system matrix of order 14×14 remains separated,

$$\bar{A} = \begin{bmatrix} \bar{0} & \bar{0} & \bar{I} & \bar{0} \\ \bar{0} & \bar{0} & \bar{0} & \bar{I} \\ -\bar{M}_S^{-1} \begin{bmatrix} \bar{K} & \bar{0} \\ \bar{0} & \bar{0} \end{bmatrix} & -\bar{M}_S^{-1} \begin{bmatrix} \bar{C} & \bar{0} \\ \bar{0} & \bar{0} \end{bmatrix} \end{bmatrix}, \quad \bar{B} = \begin{bmatrix} \bar{0} & \bar{0} & \bar{0} & \bar{0} \\ \bar{0} & \bar{0} & \bar{0} & \bar{0} \\ -\bar{M}_S^{-1} \begin{bmatrix} \bar{I} & \bar{0} \\ \bar{0} & \bar{I} \end{bmatrix} & -\bar{M}_S^{-1} \begin{bmatrix} \bar{I} & \bar{0} \\ \bar{0} & \bar{I} \end{bmatrix} \end{bmatrix}, \quad (4.70)$$

with $\bar{e}_g = \begin{bmatrix} \bar{0} & \bar{0} & -\bar{M}_S^{-1} \begin{bmatrix} \bar{M}\bar{r}_S + \bar{L}\bar{M}_f\bar{i} \\ \bar{\kappa}\bar{i} \end{bmatrix} \end{bmatrix}^T$ of order 14×1 and

$\bar{R} = \text{diag}[\bar{0} \ \bar{K}_f \ \bar{0} \ \bar{C}_f]$ of order 14×14 contains the linear TLCGD design parameters, subjected possibly to fine tuning.

The state equation (4.69) is solved for $\bar{z}_j(t)$ to get the response of the coupled system

in time domain when subjected to excitation $a_g(t)$. In addition, steady-state solution $\bar{z}(t) = \bar{z}_0 e^{i\omega t}$, assuming the ground excitation to be time-harmonic $a_g(t) = a_g e^{i\omega t}$ becomes,

$$\bar{z}_0(\alpha, \omega) = [i\omega \underline{I} - (\underline{A} + \underline{B}\underline{R})]^{-1} \bar{e}_g a_g. \quad (4.71)$$

The optimal natural frequency and the damping ratio of the fine tuned TLCGD are calculated by minimizing the same performance index as given by Eq. (4.66), where $\bar{z}_S = [\bar{w} \quad \dot{\bar{w}}]^T$ represents the main structure's state-vector of dimension 12×1 . $\bar{b} = \bar{e}_g a_g$ is the excitation vector. For this case, *fminsearch* quickly finds the minimum of the scalar function J of two critical variables of the TLCGD, when substituting Den Hartog's modal tuning parameters $x_0 = [\omega_A; \zeta_A]$ as initial estimates. The optimization results in a slight decrease of the natural frequency whereas the damping coefficient of the fluid flow is significantly reduced.

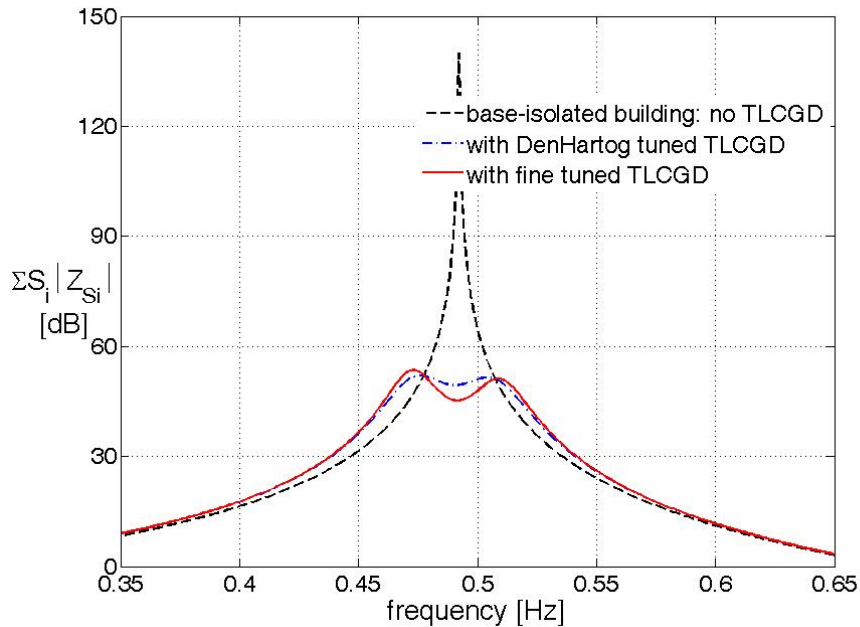


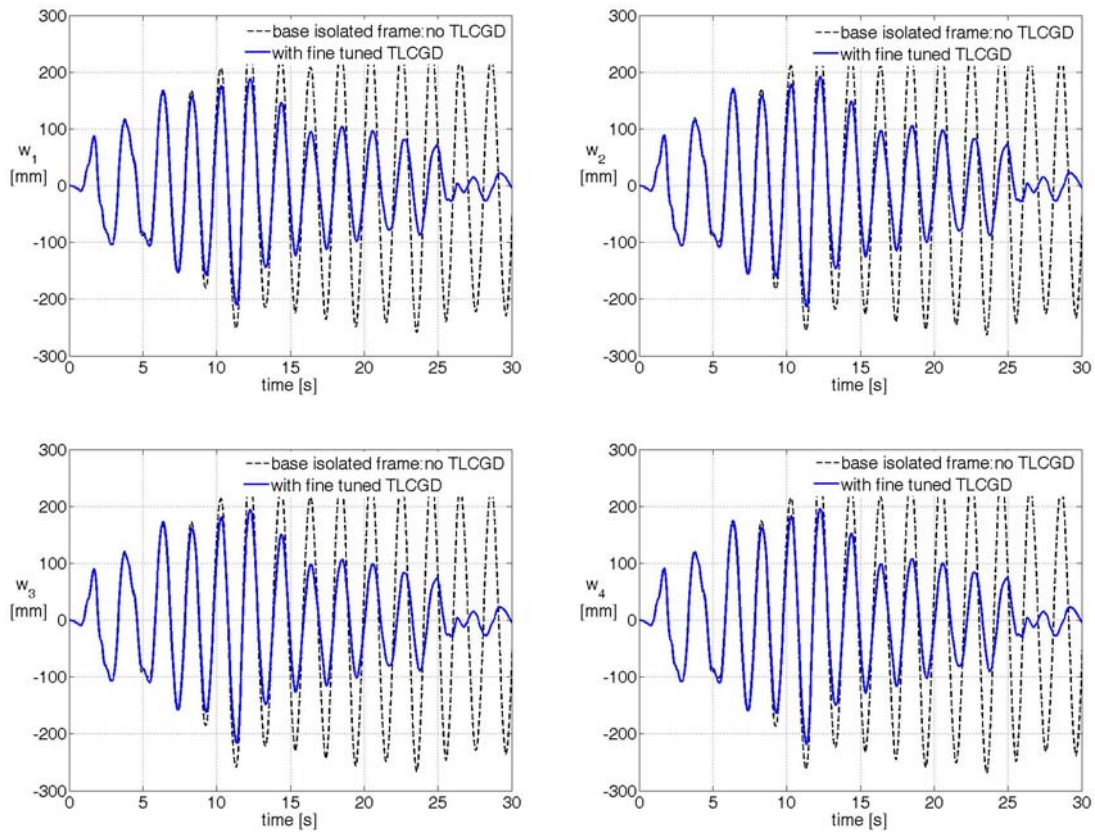
Fig. 4.14: Weighed sum of amplitude response function for the base-isolated plane frame.

4. Novel Base Isolation System

The weighed sum $\sum_{i=1}^{12} S_i |z_{Si}(\omega)|$ of the amplitude response function of building's states

for the original and optimized system, in the logarithmic decibel scale, defined by $x[dB] = 20 \log x$ is illustrated in Fig. 4.14. Thus, the frequency response of the base-isolated frame with TLCGD is tremendously reduced at the fundamental resonant peak, which confirms the effective damping supplied by TLCGD.

The displacements of each floor of the base-isolated frame subjected to El Centro seismogram scaled to 0.32g with fine tuned TLCGD attached and without any TLCGD is illustrated in Fig. 4.15.



4. Novel Base Isolation System

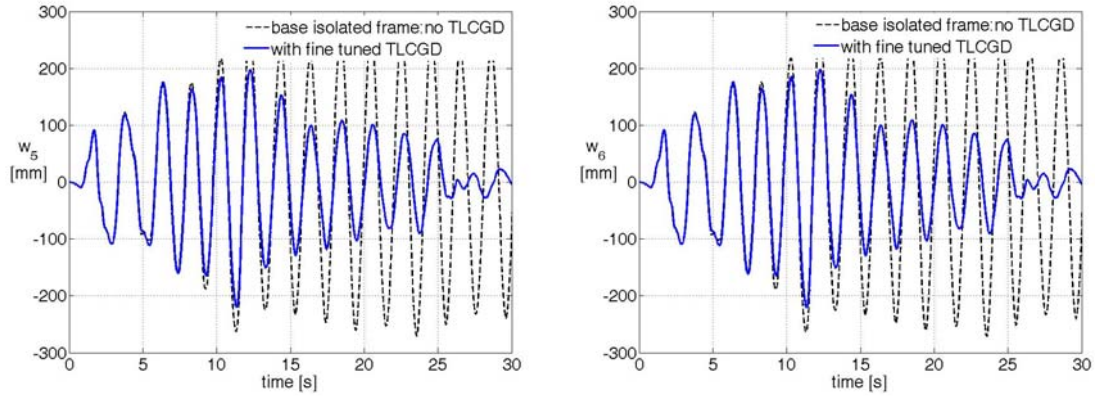
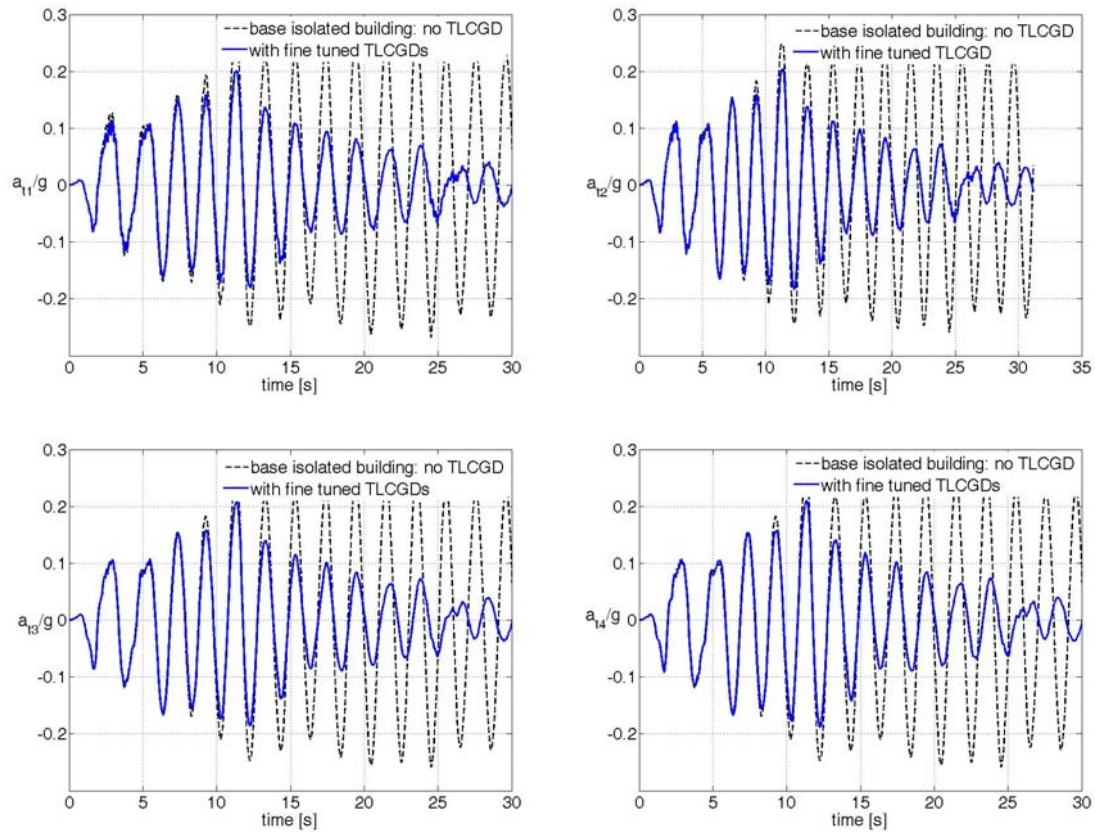


Fig. 4.15: Displacements of floors (base slab to sixth floor, w_1, w_2, \dots, w_6) of base-isolated building forced by El Centro seismogram scaled to $0.32g$.

The response in terms of total acceleration of each floor of the base-isolated frame excited by El Centro 1940 seismogram scaled to $0.32g$ is calculated by $a_{ii} = a_i + a_g$, $i = 1, 2, \dots, 6$ and plotted in Fig. 4.16 for each floor of the frame.



4. Novel Base Isolation System

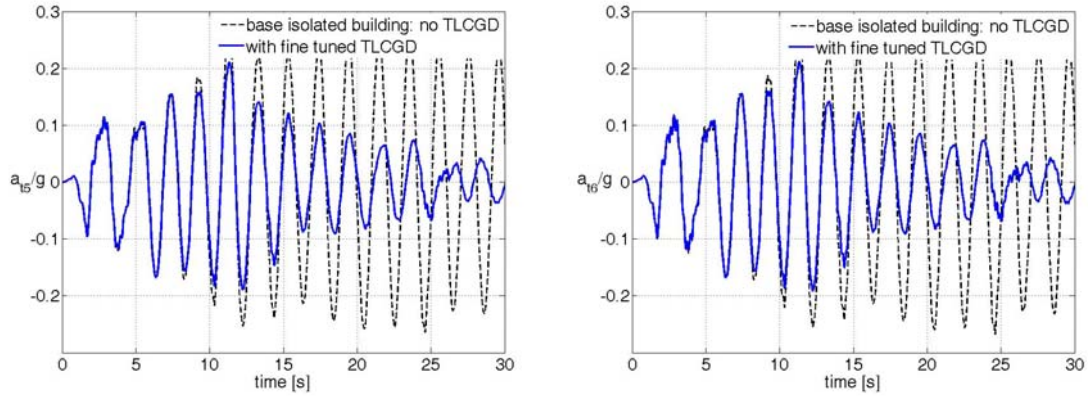


Fig. 4.16: Total acceleration (as a fraction of g) of the floors (base slab to sixth floor, $a_{t1}, a_{t2}, \dots, a_{t6}$) of the base-isolated frame forced by El Centro seismogram scaled to $0.32g$.

It is quite evident from Fig. 4.15 and Fig. 4.16 that vibration response of the base-isolated frame is effectively damped by means of the TLCGD installed at the basement of the frame even by using less amount of water mass (i.e., low mass ratio) as compared to that considered by Hochrainer^[4-21]. The resulting time response of the liquid in TLCGD with maximum value 1.2m, Fig. 4.17 is an evidence of the vibrations (thus kinetic energy) transmitted to the water inside TLCGD.

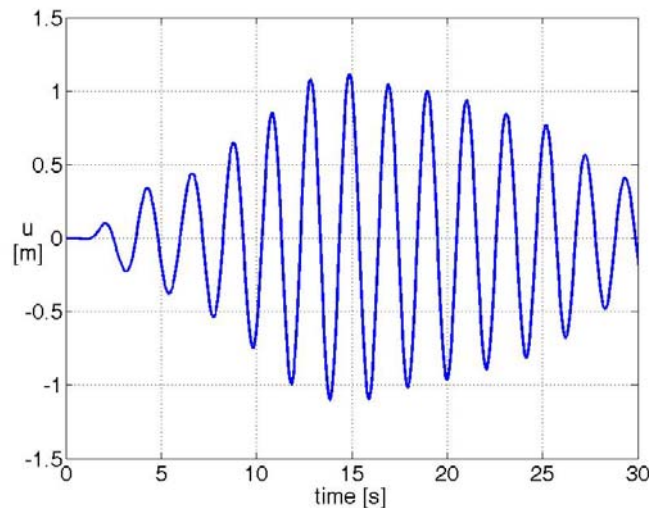


Fig. 4.17: Liquid stroke in TLCGD under El Centro seismogram scaled to $0.32g$.

However, the corresponding maximum liquid speed in the TLCGD must be within

acceptable speed limit; $\max |u_0| = \omega_A \max |u_0| = 3.71 \text{ m/s} \leq 10 \text{ m/s}$ to keep the interface between liquid and gas intact as specified by Ziegler^[4-25].

4.5.2 Base-isolated single-storey asymmetric building

A simple single-storey asymmetric building as discussed in sub-section 4.3 is also exemplarily considered for the dynamic investigations. The building consists of rectangular-plan $a \times b = 12 \times 8 \text{ m}$ rigid base and top floors of combined mass $m_F = 118331 \text{ kg}$ having exterior walls of mass $m_W = 84434 \text{ kg}$ and an asymmetrically located ($y_w = 2 \text{ m}$) intermediate wall of mass $m_w = 18822 \text{ kg}$ in-between the rigid floors along with additional concentrated (point) mass $m_1 = 22159 \text{ kg}$ placed at the right upper corner ($y_1 = 6 \text{ m}$, $z_1 = 4 \text{ m}$), illustrated in Fig. 4.11. Thus, the distribution of the total mass $m_S = m_F + m_W + m_w + m_1 = 243746 \text{ kg}$ creates the mass-asymmetry and center of mass C_M is located by considering the static mass-moments at

$$\begin{aligned} y_M &= (m_1 y_1 + m_w y_w) / m_S = 1.071 \text{ m} \\ z_M &= (m_1 z_1 + m_w z_w) / m_S = 0.556 \text{ m} \end{aligned} \quad (4.72)$$

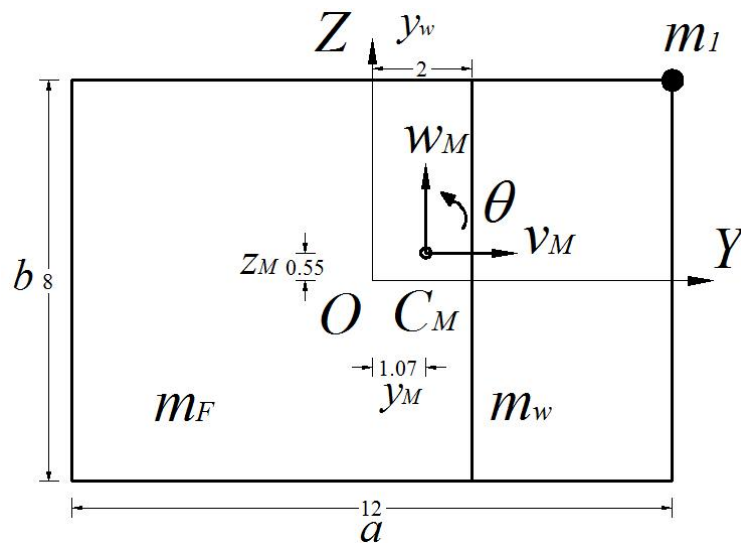


Fig. 4.18: Scaled plan of asymmetric building, dimensions in meter.

The mass moment of inertia about the vertical x -axis of the building is

$$I_x = m_S r_x^2 = 5.274 \times 10^6 \text{ kgm}^2, r_x = 4.652 \text{ m}. \quad (4.73)$$

Such an asymmetric building is base-isolated by introducing symmetrically arranged N spring-pendulum (SP) elements along the perimeters (i.e., $N = 2N_a + 3N_b$), between its heavy rigid foundation beams and the ground. Actually, they are assembled in isolation units each having four SP elements as discussed in sub-section 4.2.3. Thus, the coefficients of the symmetric stiffness matrix, given by Eq. (4.45), take the form for the selected rectangular-plan,

$$k_{11} = k_{22} = Nk_{1h},$$

$$k_{33} = \frac{Nk_{1h}}{r_x^2} \left[y_M^2 + z_M^2 + \frac{N_b}{2N} (a^2 + 2y_w^2 - 4y_w y_M) + \frac{N_a}{2N} b^2 + \frac{3}{N} \sum_{i=1}^{N_b} z_i^2 + \frac{2}{N} \sum_{i=1}^{N_a} y_i^2 \right],$$

$$k_{12} = k_{21} = 0, \quad k_{13} = k_{31} = Nk_{1h} z_M / r_x, \quad k_{32} = k_{23} = Nk_{1h} y_M (N_b y_w / N y_M - 1) / r_x, \quad (4.74)$$

resulting in the following numerical values of the elements of the stiffness matrix for the asymmetric building under consideration isolated by means of $N = 240$ SP elements,

$$\underline{K} = 10^6 \begin{bmatrix} 2.406 & 0 & 0.288 \\ 0 & 2.406 & -0.381 \\ 0.288 & -0.381 & 6.387 \end{bmatrix} \text{ N/m}.$$

When there are $N = 240$ SP elements, the averaged load on each SP element is $w_1 = m_S g / N = 9.96 \text{ kN}$.

4.5.2.1 Modal analysis and installation of TLCGDs

Solving the linear eigen-value problem, Eq. (2.1), e.g., by using the tool *eig* in MATLAB^[4-22] with the given mass and stiffness matrices for the asymmetric building, renders the set of three ortho-normalized modal vectors and the associated natural frequencies, say around 0.5Hz,

$$\begin{bmatrix} f_1 = 0.494 \\ f_2 = 0.500 \\ f_3 = 0.818 \end{bmatrix} \text{ Hz}, \quad \underline{\phi} = 10^{-3} \begin{bmatrix} 1.211 & 1.617 & 0.143 \\ 1.606 & 1.220 & 0.190 \\ 0.238 & -2.15 \times 10^{-15} & 2.011 \end{bmatrix} \quad (4.75)$$

4. Novel Base Isolation System

For small displacements, 3×1 modal vectors $\vec{\phi}_j$ determine the modal centers of velocity $C_{Vj}, j=1,2,3$ by using Eq. (2.13),

$$\vec{r}_{v1} = \begin{bmatrix} -30.313 \\ -23.119 \end{bmatrix} \text{m}, \quad \vec{r}_{v2} = 10^{15} \begin{bmatrix} 2.643 \\ -3.503 \end{bmatrix} \text{m}, \quad \vec{r}_{v3} = \begin{bmatrix} 1.510 \\ 0.888 \end{bmatrix} \text{m}, \quad (4.76)$$

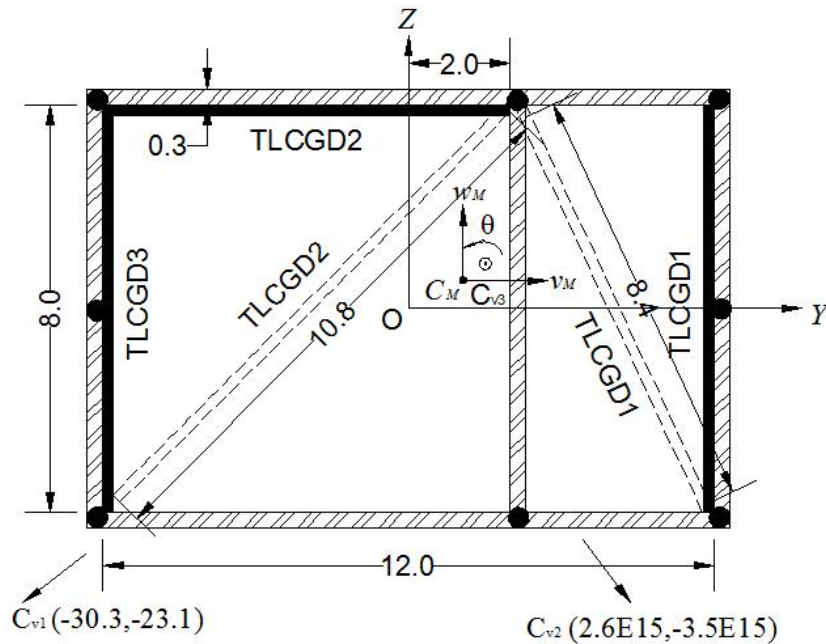


Fig. 4.19: Scaled plan of base-isolated asymmetric building with alternative arrangements of three TLCGDs; eight novel sliding elements are indicated by circles.

The modal centers of velocity, as illustrated in Fig. 4.19, lie outside of the plan for the 1st and 2nd rigid-body modes of the building, indicating a dominant translational motion that refers to a moderate asymmetry of the building. Whereas C_{v3} for the 3rd mode falls within the plan, however distinct from C_M , indicating a dominant rotational seismically forced motion thus referring to strong asymmetry of the building for this mode. The placement of the modally tuned TLCGDs becomes optimal with normal distance to the modal centers of velocity maximum; see again Fu-Ziegler^[4-18]. Fig. 4.19 illustrates the orientation of three TLCGDs in the plan of asymmetric building; alternative diagonal arrangement of TLCGD1 and TLCGD2 shown by dashed lines, is preferred because of their better performance than that of those placed parallel to the outer perimeter.

4.5.2.2 Design steps of base isolation element for asymmetric building

The required period of the base-isolated rigid building, Eq. (4.1), renders the first condition to be met in the design of the isolation (SP) element by choosing the resulting horizontal stiffness. The diameter d of the wire of the spring is calculated by Eq. (4.2) when the horizontal (shear) stiffness k_{1h} , required diameter D , number of turns n_t in its length l and material properties (i.e. modulus of elasticity E , Poisson’s ratio ν) of the selected helical steel spring are known.

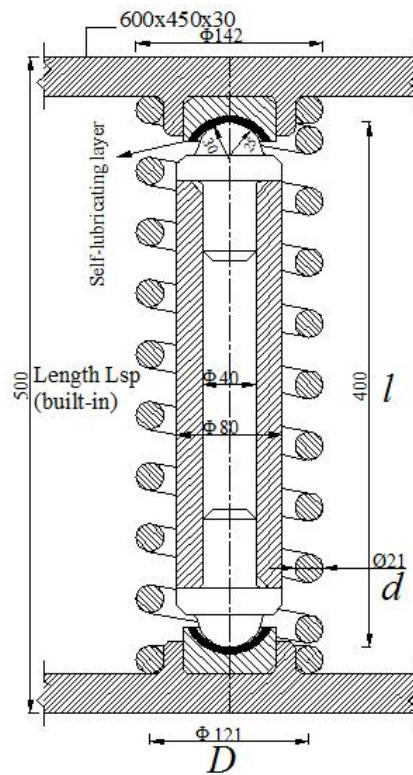


Fig. 4.20: Novel spring-pendulum (SP) element: pivoted upright-pendulum is encapsulated by axially prestressed helical spring.

The key parameters of the helical spring are listed in Table 4.2. Thus, the axial (pre-stress) stiffness given by Eq. (4.3) is about 13-times the horizontal stiffness for the selected steel spring (i.e. $\lambda_{vh} = 13.1$) so as to serve as a low pass filter. The material properties i.e., modulus of elasticity $E = 204GPa$ and Poisson’s ratio $\nu = 0.3$ are well-known for the steel spring.

Table 4.2: Key parameters of base isolation (SP) element.

Parameters	Values
Horizontal stiffness of helical spring, k_{1h} [N/mm], Eq. (4.1)	10.02
Length of helical spring, l [mm]	400
Number of active turns/coils of helical spring, n_t	8
Outer spring diameter, D_e [mm]	142
Diameter of the wire of helical spring, d [mm], Eq. (4.2)	21
Vertical stiffness of helical spring, k_{1v} [N/mm], Eq. (4.3)	130.95
Vertical to horizontal stiffness ratio, $\lambda_{vh} = k_{1v}/k_{1h}$, Eq. (4.3)	13.06
Mean diameter of spring, $D = D_e - d$ [mm]	121
Spring index, $C = D/d$	5.8
Pre-compression, δ_v [mm], Eq. (4.5) for load factor $\lambda = 0.49$	61
Free spring length, $l_0 = l + \delta_v$ [mm]	461
Critical buckling load, $F_{1v,cr} = k_{1h}l$ [kN], $\lambda_c = 1$, Eq. (4.21)	4.01
Force in upright-pendulum, $F_{1v} = \lambda F_{1v,cr}$, $\lambda = 0.49$ [kN]	1.96
Force in spring due to axial pre-stress, $F_{1r} = k_{1v}(l_0 - l)$ [kN]	8.00
Vertical deflection at $ \varphi = 33^\circ$, $\delta_{1v} = l(1 - \cos \varphi)$ [mm]	70
Length of spring, when tilted, $l_1 = l - \delta_{1v}$ [mm]	330
Allowance before solid, $l_a = l_1 - l_s$, [mm], $l_s = n_t d = 168\text{mm}$	162

4.5.2.3 Design of novel sliding element for asymmetric building

For the single-storey asymmetric building under consideration where the damping is supplied separately by means of TLCGDs, the purpose of the sliding elements is just to resist the loads by wind gusts and small seismic disturbances. The average stagnation pressure $p_{av} = 150 \text{ N/m}^2$, corresponding to the average wind speed of $v_{av} = 15.5 \text{ m/s}$,

$p_{av} = \rho_a v_{av}^2 / 2$, see Ziegler^[4-15], page 486, renders the horizontal wind force $F_w = 9 \text{ kN}$

acting on the larger face of the building.

A novel sliding element consists of a circular steel plate of diameter $\Phi_{ls} = 200\text{mm}$ coated with 5mm bronze layer in contact with another circular steel plate of diameter $\Phi_{us} = 680\text{mm}$ connected to the upper foundation beam of the building so as to establish a bronze-steel interface between upper and lower sliding plates. Therefore, considering the coefficient of static friction at the interface (bronze-steel contact) $\mu = 0.2$, the normal force $R_v = F_w/\mu = 45\text{kN}$ dictates the total number of sliding elements required to be placed in-between the rigid foundation beams of the asymmetric base isolated building. The contact at the bronze-steel interface is maintained by a pre-compressed conical spring. The appropriate pre-compression δ_v of the conical spring underneath the lower sliding plate, providing the necessary static friction against the sliding, requires

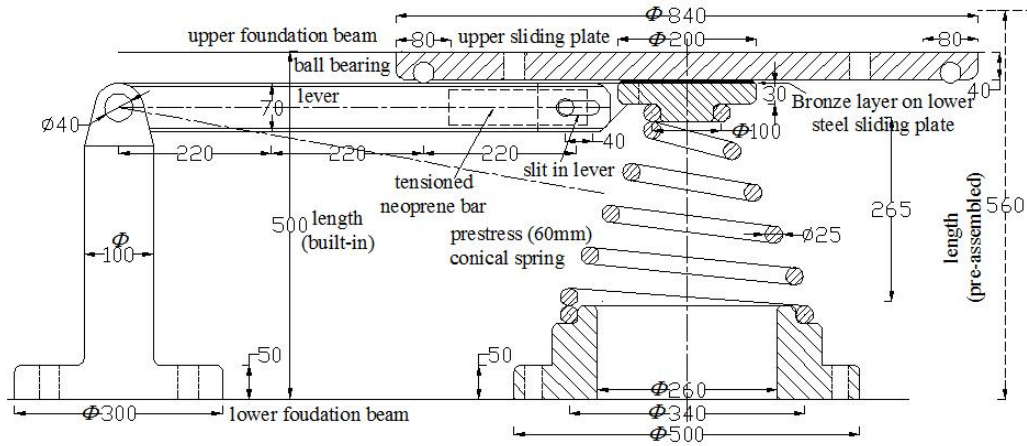
$$n_s k_{1v} \delta_v = R_v \quad (4.77)$$

where n_s is the number of sliding elements and k_{1v} is the axial stiffness of one conical spring. Choosing the sufficient number $n_s = 8$ of sliding elements to be arranged as illustrated in Fig. 4.19, we get the required vertical stiffness of one conical spring $k_{1v} = 93.75\text{ N/mm}$, Eq. (4.77). The conical spring is adopted to take the advantage of its less solid height and is designed as a linear spring with constant spring rate whereas the pitch is variable so that all coils come to touch each other at the same time when pressed to solid. Thus, the averaged diameter D of the conical spring results for the required stiffness, Eq. (4.3). The design and other key parameters of the conical spring are listed in Table 4.3 and its scaled sketch is drawn in Fig. 4.21 with its top and bottom diameters whose arithmetic mean renders the averaged diameter.

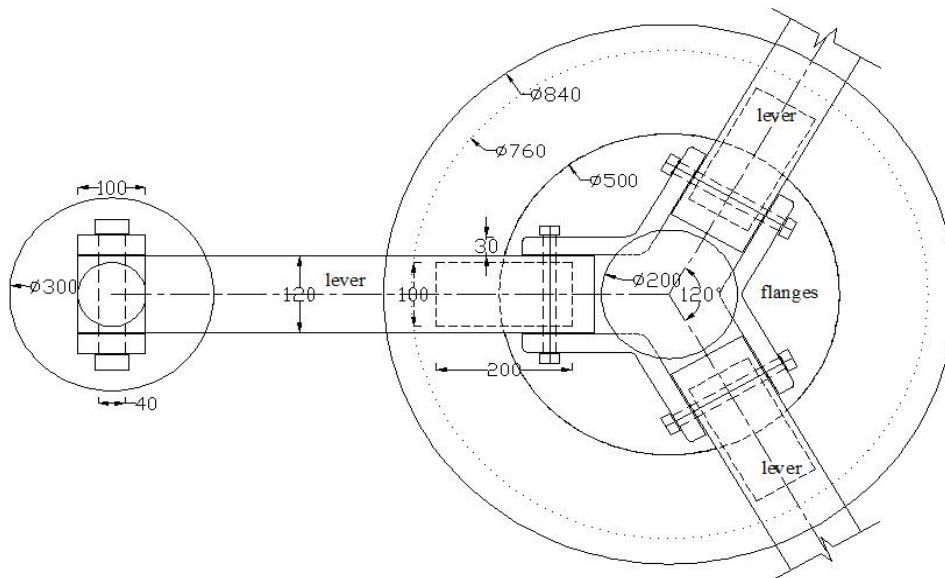
In case of a sufficiently strong earthquake, the foundation beams of the rigid asymmetric building experience a relative horizontal motion associated with the vertical downward movement of the building. It is also desired that the sliding elements should not offer continuous friction by the abrasive contact (i.e., no continuous frictional energy

4. Novel Base Isolation System

dissipation in this horizontal movement) which can be achieved if the contact at the bronze-steel interface is released.



(a)



(b)

Fig. 4.21: Scaled sketch of compatible novel sliding element without continuous energy dissipation, (a) Elevation (b) Plan; all dimensions are in mm.

For this purpose, a lever system consisting of three mechanical levers at 120° apart as illustrated in Fig. 4.21(b) is proposed to magnify the vertical motion of the building. The levers of sufficient length $L_l = 720\text{mm}$ with thin-walled sandwich cross-section, scaled sketched in Fig. 4.21, are designed to serve the purpose. The one end of the lever is

hinged-support on the lower foundation beam whereas the other end is connected to the extended flanges of the lower sliding plate by means of a bolt in a proper slit as illustrated in Fig. 4.21. Thus, the wind forces in static friction are transmitted to the ground mainly by compressive axial force in the lever (metal contact of the bolt in the slit). The pre-stressed neoprene spring (a bar of about 200 mm length) within the hollow lever is pre-tensioned with the bolt at the lower sliding plate-bearing. A ring at the periphery of upper sliding plate (moving with the building) contains densely packed ball bearings and is attached to the upper foundation beam of the building such that the ball bearings just touch the levers under some local admissible clearance.

The working of the lever is simple and can be grasped for instance; during the horizontal movement due to earthquake, the ball bearing slides on the lever and the associated vertical downward movement simply pushes the lever down as required. Thus, the tip of the lever connected to the lower sliding plate forces it to an amplified downward movement by further compressing the conical spring and hence the contact at the bronze-steel interface is released. The bolt in the bearing at the lower sliding plate moves vertically downward, consequently it slides in the slit provided in the lever side walls.

Table 4.3: Parameters of conical spring and lever.

Parameters	Values
Number of active turns/coils of conical spring, n_t	4
Vertical stiffness of conical spring, k_{1v} [N/mm],	93.75
Diameter of the wire of conical spring, d [mm]	25
Average diameter of conical spring, D [mm], Eq. (4.3)	220
Spring index, $C = D/d$	8.68
Required full deflection of the spring [mm]	218
Pre-compression, δ_v [mm]	60
Force under pre-compression $F_{1r} = k_{1v}\delta_v$ [kN]	5.63

Free length of conical spring, $l_0 = l_s + \delta_{1v} + \delta_v + l_a$, [mm] $l_a = 22\text{mm} = \text{allowance before solid}$, $l_s = d = 25\text{mm}$	325
Length of the conical spring, $l = l_0 - \delta_v$ [mm]	265
Length of lever, L_l [mm]	720
Cross-sectional area of lever, $A_l = (2b_l + 2h_l)t_l$ [mm ²] (thin walled sandwich cross-section ($b_l = 120$, $h_l = 60\text{mm}$, $t_l = 5\text{mm}$))	1800
Critical force in lever, $F_{l,cr} = k_{1v}L_l$ [kN]	67.5
Normal stress, $\sigma_l = F_{l,cr}/A_l$ [MPa]	37.5
Virtual static friction coefficient, $\mu = F_{l,cr}/F_{1r}$	12

Therefore, the properly designed sliding elements not only supply the necessary static friction against the wind load but also do not cause any continuous energy dissipation in the relative horizontal movement under seismic excitation. Buckling of the levers safe the element against any unexpected horizontal overloads.

4.5.2.4 TLCGD design parameters

The geometric dimensions of TLCGDs; the horizontal length of the liquid column B is selected to utilize maximum available length on the plan of the base-isolated building in the optimal orientation for the respective TLCGD for its efficient design (i.e., higher κ value) and the vertical height of the liquid column H of TLCGD is guided by limiting conditions;

$$\max|u_0| \leq 2/3 H, \max|u_0| \leq H_a/3. \quad (4.78)$$

The maximum liquid strokes in each TLCGD (i.e., $\max|u_0|$) when subjected to El Centro 1940 seismogram scaled to 0.32g are ensured to be within admissible limits given by Eq. (4.78) and in addition, the maximum liquid speed in the TLCGD is also within acceptable speed limit for the application of the piston theory (i.e. to keep the interface between liquid and gas intact), $\max|\dot{u}_0| = \omega_A \max|u_0| \leq 10 \text{ m/s}$, see again Ziegler^[4-22].

The fluid-mass (of water) is chosen as $m_{f1} = 5000\text{kg}$, $m_{f2} = 4200\text{kg}$ and

4. Novel Base Isolation System

$m_{f3} = 1000\text{kg}$ inside the three TLCGDs. The structural modal damping of such a base-isolated building is extremely low even with linearized frictional damping of the novel sliding elements included thus, assumed to be constant 0.5% in each mode. The geometrical dimensions of the TLCGDs and other resulting key parameters at corresponding modally critical angles of incidence $\alpha_{cr} = 125^\circ, 40^\circ, 125^\circ$ are collected in Table 4.4.

Table 4.4: Parameters of the diagonally orientated TLCGD1 and TLCGD2, and the z-parallel TLCGD3.

Description	TLCGD1	TLCGD2	TLCGD3
Orientation and position of TLCGDs	$\gamma_1 = 115^\circ$ A(4,0)	$\gamma_2 = 45^\circ$ A(-1.9,0)	$\gamma_3 = 90^\circ$ A(-6,0)
Mass of water in TLCGD, m_f [kg]	5000	4200	500
Modal mass ratio, μ_j [%], $m_j = 1$, Eq. (2.68)	2.25	1.72	0.6
Horizontal length of the liquid column, B [m]	8.4	10.8	8
Vertical height of the liquid column, H [m]	1.65	1.75	0.5
Effective length, $L_{eff} = B + 2H$ [m]	11.7	14.3	9.0
B / L_{eff}	0.718	0.755	0.889
Inner diameter, circular TLCGD pipe, [mm]	737	612	266
Geometry factor, $\kappa = \bar{\kappa}$, Eq. (2.28)	0.72	0.755	0.889
Optimal frequency ratio, δ_{opt} , Eq. (2.80)	0.983	0.987	0.995
Optimal absorber frequency, $f_{A,opt} = \delta_{opt} f_S$ [Hz]	0.4861	0.4933	0.8142
Optimal linear damping coefficient, $\zeta_{A,opt}$ [%], Eq. (2.83), $\zeta_{Aj} = \zeta_{Aj}^*$	6.51	6.02	3.97
Equivalent math. pendulum length, L_0 [m], Eq. (2.84)	1.053	1.021	0.375

$h_0/H_a = L_{eff}/2L_0 - \sin \beta$	4.557	6.003	11.004
Equilibrium pressure head, $h_0 = np_0/\rho g$, $n = 1$, [m]	13.76	15.80	12.232
Gas volume, $V_0 = A_H H_a$ [m ³]	1.291	0.773	0.062
Dead fluid-mass $m_f \left(1 - (\kappa V^*/V)^2\right)$ [kg], Eq. (2.81)	2436.5	1804.3	105

Because of the low frequencies of the base-isolated structures under consideration (i.e., around 0.5Hz both for plane frame and single-storey asymmetric building) the gas compression might be close to isothermal conditions and thus becomes linear for the associated liquid strokes, hence we use $n = 1$ as listed in Table 4.1 and Table 4.4.

4.5.2.5 Dimensioning of TLCGD piping

For the sake of simplicity, a straight circular cylindrical pipe with radius r and wall thickness $t \ll r$ is considered for the dimensioning of TLCGDs piping system. The hoop stress σ_h (pressure-vessel formula) due to the internal gauge pressure p_g is determined by, see Ziegler^[4-15], page 91,

$$\sigma_h = \frac{p_g r}{t}. \quad (4.79)$$

Considering the larger liquid stroke, $\max|u| = H_a/3$ for safety reasons during the compression phase of the gas (i.e., upward liquid stroke); the maximum dynamic gas pressure p' is defined by assuming an adiabatic gas compression from the equilibrium state,

$$p' = p_0 \left(\frac{\rho'}{\rho_0} \right)^n, \quad n = 1.4. \quad (4.80)$$

Since, the amount of gas remains constant during the compression,

$$\rho_0 V_0 = \rho' (V_0 - \max|u| A_H), \quad V_0 = A_H H_a, \quad (4.81)$$

the gas volume is reduced. By substituting the upward liquid stroke $\max|u| = H_a/3$, the gas density is increased to

$$\rho' = 3/2 \rho_0. \quad (4.82)$$

Substituting Eq. (4.82) into Eq. (4.80) yields the absolute gas pressure acting at the displaced interface

$$p' = 1.76 p_0. \quad (4.83)$$

Therefore, the maximum absolute pressure becomes in a quasi-static consideration

$$(p_{abs})_{\max} = p' + \rho g (H + H_a/3). \quad (4.84)$$

The corresponding gauge pressure is

$$p_{g \max} = (p_{abs})_{\max} - p_{atm}, \quad p_{atm} = 1 \times 10^5 \text{ N/m}^2, \quad (4.85)$$

to be substituted in Eq. (4.79) to render the wall thickness of the cylindrical pipe. The maximum tensile hoop stress σ_h is set equal to the admissible stress, for steel $\sigma_a = 15 \text{ N/mm}^2$. The results along with other key parameters of the three TLCD piping systems are summarized in Table 4.5.

However, when considering the same liquid stroke, $\max|u| = H_a/3$, during the expansion phase of the gas (i.e., downward stroke), the gas volume is increased, - updating Eq. (4.81),

$$\rho_0 V_0 = \rho'' (V_0 + \max|u| A_H), \quad V_0 = A_H H_a. \quad (4.86)$$

The gas density decreases with respect to the equilibrium state,

$$\rho'' = 3/4 \rho_0. \quad (4.87)$$

The absolute dynamic gas pressure at the displaced interface equals the minimum absolute pressure in such a quasi-static consideration and becomes, by updating Eq. (4.80),

$$(p_{abs})_{\min} = p'' = 0.67 p_0, \quad (4.88)$$

Thus, the corresponding gauge pressure is calculated analogous to Eq. (4.85),

$$p_{g\min} = (p_{abs})_{\min} - p_{atm}. \quad (4.89)$$

Consequently, a sufficiently large value of the equilibrium gas-pressure is required to keep the gauge pressure positive for the expansion phase - to be preferred in practice - and thus, to avoid compressive hoop stress in the thin-walled pipe.

The critical buckling pressure for thin-walled long cylinders under uniform radial external pressure is, see Young^[4-26], page 690,

$$p_{cr} = \frac{E}{4(1-\nu^2)} \left(\frac{t}{r} \right)^3. \quad (4.90)$$

For that extreme liquid stroke, negative gauge pressures, i.e., external pressures, are possibly acceptable if far below the critical buckling pressure, Eq. (4.90), see Table 4.5.

Finally, the dead mass of the piping system is also approximately estimated with wall thickness known, choosing same wall thickness $t = 5\text{mm}$ for all three TLCGDs for design reasons, also listed Table 4.5, and by assuming a constant circular cylindrical cross-section over their entire length, i.e. including the gas vessels. The density of steel $\rho_p = 7.8 \times 10^3 \text{ kg/m}^3$ is inserted in Eq. (4.91).

$$m_p = \rho_p 2\pi r t (B + 2H + 2H_a). \quad (4.91)$$

The dead fluid-mass, calculated in Table 4.4 and also listed in Table 4.5, is larger than the mass of piping system for TLCGD1 and TLCGD2; however for TLCGD3, it turns out to be smaller, see Table 4.5. The wall thickness and the estimated dead mass of the piping system are listed along with other key parameters for the three TLCGDs in Table 4.5.

Table 4.5: Dimensioning of circular steel piping for TLCGDs.

Description	TLCGD1	TLCGD2	TLCGD3
$h'_0 = h_0/n$, $n = 1$ [m], Table 4.4	13.76	15.80	12.23
H_a [m], Table 4.4	3.020	2.632	1.111
H [m], Table 4.4	1.65	1.75	0.50

4. Novel Base Isolation System

B [m], Table 4.4	8.4	10.8	8.0
$p' = 1.76p_0$, 10^{-5} [N/m ²], (4.83)	2.38	2.73	2.12
$(p_{abs})_{\max}$, 10^{-5} [N/m ²], Eq. (4.84)	2.64	2.99	2.20
$p_{g \max}$, 10^{-5} [N/m ²], Eq. (4.85)	1.64	1.99	1.20
Pipe diameter, $2r$ [mm], Table 4.4	737	612	266
Wall thickness, t [mm], Eq. (4.79)	4.05	4.06	1.1
Design wall thickness, t [mm]	5	5	5
Piping mass, m_p [kg], Eq. (4.91), $t = 5\text{mm}$	1602	1467	366
Dead fluid-mass, [kg], Table 4.4	2436	1804	105
$(p_{abs})_{\min} = p'' = 0.67p_0$, 10^{-5} [N/m ²]	0.902	1.041	0.802
$p_{g \min}$, 10^{-5} [N/m ²], Eq. (4.89)	-0.1	0.04	-0.2
Critical buckling pressure, p_{cr} 10^{-5} [N/m ²], Eq. (4.90)	1.41	2.44	29.8
Stability against buckling	$ -0.1 \ll 1.41$	$0.04 \ll 2.44$	$ -0.2 \ll 29.8$

However, the final dimensions of cylindrical steel pipes must be changed according to their commercial availability. By considering the dead mass of the piping system, the peaks of resonance curves are slightly shifted towards lower frequencies. These reductions of the eigen frequencies are not considered in this dissertation except in the in-situ testing of the lab-model. Large parts of the piping system can possibly be incorporated in the structural carrying system, i.e. without contributing additional mass to the main system.

4.5.2.6 Simulated results

The base-isolated asymmetric building subjected to the ground excitation is simulated for

numerical investigations when novel base isolation system (i.e., SP units with sliding elements and the TLCGDs) is incorporated.

(a) Modally isolated 2-DOF coupled system

The dynamic response of the modally isolated 2-DOF coupled system (i.e., base-isolated building equipped with TLCGDs) subjected to horizontal ground excitation is determined numerically both in frequency and time domain. Modal tuning of each TLCGD is performed by applying Den Hartog's optimization formulas, analogy between TMD and TLCGD understood. Further, the natural frequency and the damping ratio are optimized to render fine tuned TLCGDs on similar lines as described in sub-section 4.4 (i.e., minimization of performance index, Eq. (4.66)) but with the slight difference in defining the modal performance index J_j for the modally isolated system under consideration; and $\bar{z}_{Sj} = [q_j \quad \dot{q}_j]^T$ represents the main structure's modal state-vector, $\bar{b}_j = E_{zgj} a_g$ is the excitation vector. In this simple case, *fminsearch* quickly finds the minimum of the modal scalar function J_j of two variables, when substituting Den Hartog's modal tuning parameters $x_{0j} = [\omega_{Aj} \quad \zeta_{Aj}]$ as initial estimates. As a result of this optimization, the frequencies are slightly lowered whereas the damping ratios are significantly reduced. The modally approximated state equation (4.48) is solved for $\bar{z}_j(t)$ for a seismogram $a_g(t)$ (e.g., El Centro 1940 scaled to 0.32g acting close to the critical angle of incidence) for each mode $j = 1, 2, 3$. Thus, the dynamic response in terms of generalized modal displacement q_j for modally isolated 2-DOF coupled system and the corresponding liquid stroke u_j in corresponding TLCGDs are determined.

(i) Dynamic response with modally tuned TLCGD1:

Considering TLCGD1, modally tuned to the fundamental mode and placed along the semi-diagonal of right portion of the asymmetric building's plan, Fig. 4.19, and the frequency response function in terms of modal dynamic magnification factor both for the main system (i.e., base-isolated building) alone, Eq. (2.92), and for the modally isolated

2-DOF coupled TLCGD-fundamental mode system, Eq. (2.105), are plotted in Fig. 4.22. The maximum value of modal DMF_l for base-isolated building alone reaches to 100 as its structural damping is assumed to be 0.5%. The effective damping supplied by TLCGD1, approximated by $\zeta_{eff1} = 1/2DMF_{1max}$ is about 4%. However, the shifting of the curve towards left is evidence of the dead fluid-mass of TLCGD1 added to the main system.

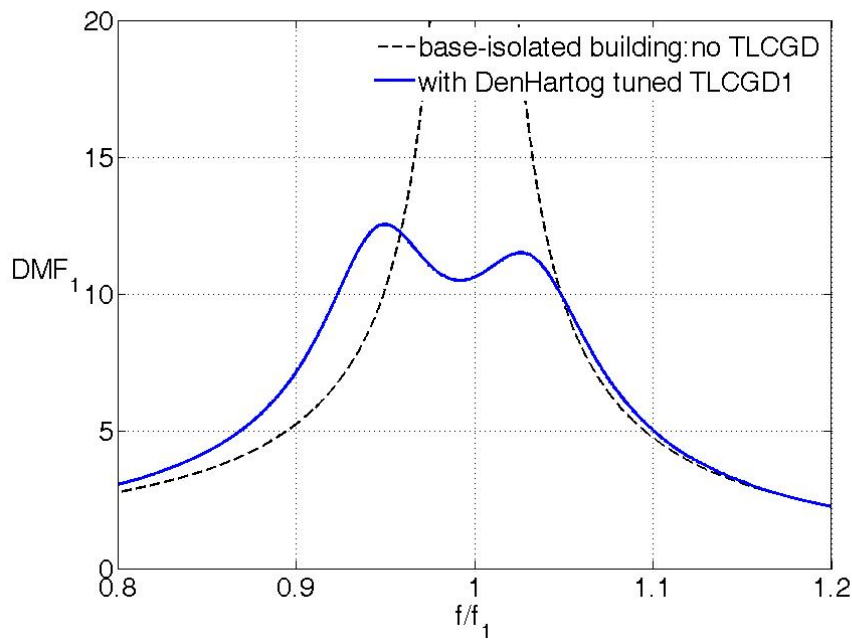


Fig. 4.22: Modal dynamic magnification factor (DMF_l) for base-isolated building alone and with TLCGD1 installed; the effective damping is increased from 0.5 to 4%.

The gain in dB , shown in Fig. 4.23, as weighed sum $\sum_{i=1}^2 S_{j_i} |z_{S_{j_i}}(\omega)|$ of the amplitude response function for the base-isolated building with TLCGD1 attached, ground acceleration at critical angle of incidence $\alpha_{cr1} = 125^0$, confirms the effective damping and results are even improved by fine tuning of TLCGD1 in state-space domain.

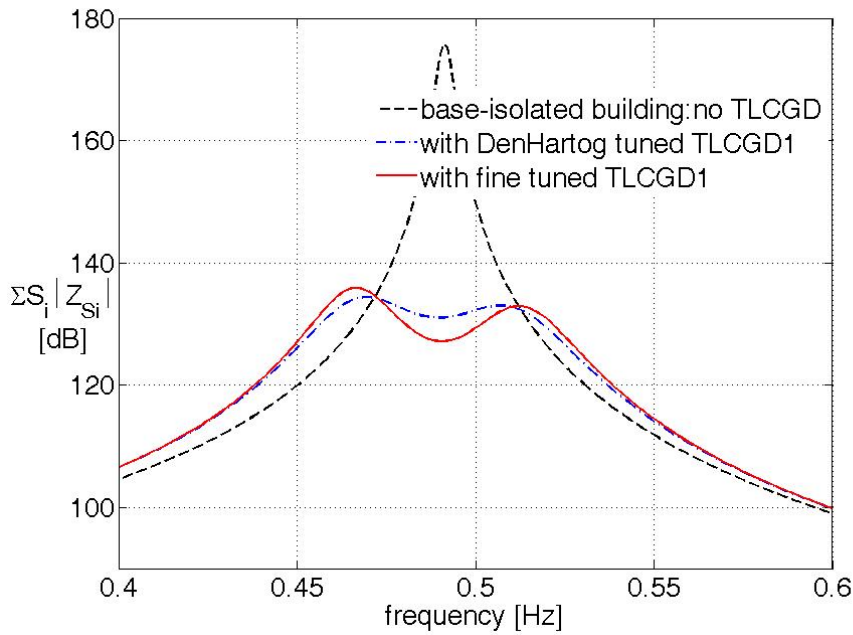


Fig. 4.23: Weighed sum of amplitude response function for the base-isolated building with TLCGD1 attached and without any TLCGD, $\alpha_{cr1} = 125^0$.

The dynamic response in terms of modal displacement q_1 and the corresponding liquid stroke u_1 in TLCGD1 (with maximum value, $u_{1max} = 0.81m$) are given over time in Fig. 4.24.

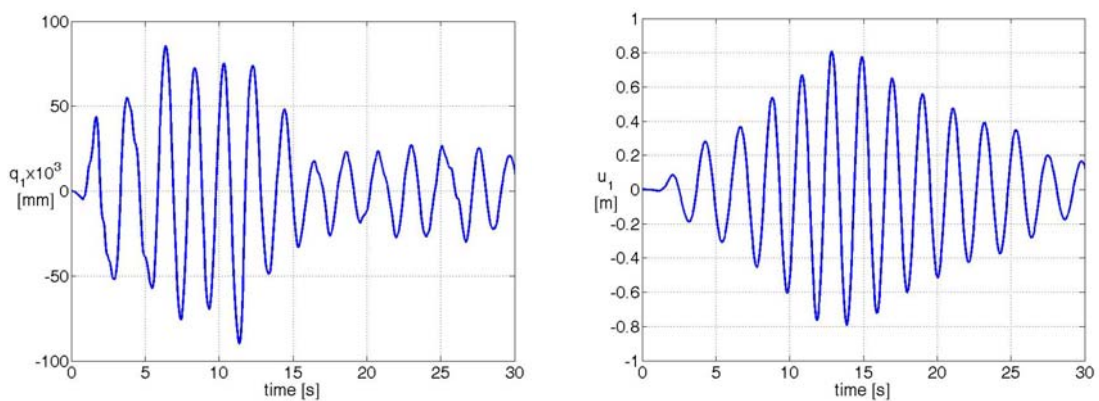


Fig. 4.24: Time response under El Centro seismogram scaled to 0.32g, (a) Modal displacement q_1 of base-isolated building (b) Liquid stroke u_1 in TLCGD1.

The approximate horizontal displacements of center of mass C_M of the base-isolated

4. Novel Base Isolation System

building are calculated by $v_{M1} = q_1\phi_{11}$ and $w_{M1} = q_1\phi_{12}$ and plotted in Fig. 4.25 for base-isolated building equipped with fine tuned TLCGD1 and without any TLCGD. And the approximate horizontal total accelerations (as fraction of g) of center of mass of base-isolated building are also illustrated in Fig. 4.26.

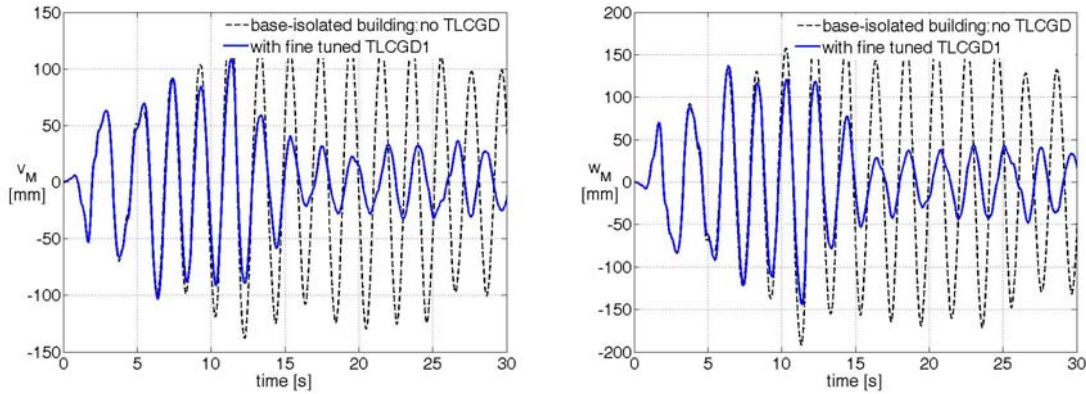


Fig. 4.25: Approximate horizontal displacements of center of mass of base-isolated building under the action of El Centro seismogram scaled to $0.32g$.

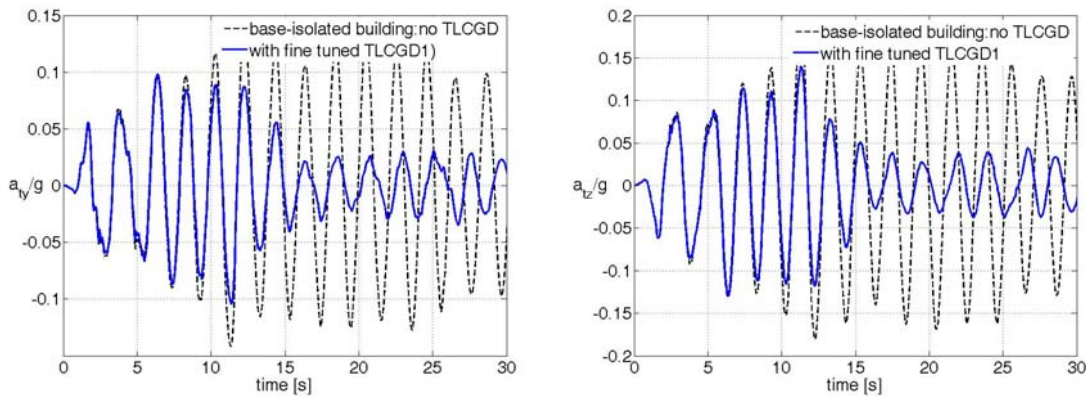


Fig. 4.26: Approximate horizontal total acceleration (as fraction of g) of center of mass of base-isolated building under the action of El Centro seismogram scaled to $0.32g$.

(ii) Dynamic response with modally tuned TLCGD2:

The results of the analogously modally isolated 2-DOF coupled system by considering TLCGD2 installed to the building, Fig. 4.19, subjected to same El Centro seismogram at critical angle of incidence $\alpha_{cr2} = 40^0$, are obtained on similar lines as discussed above for TLCGD1.

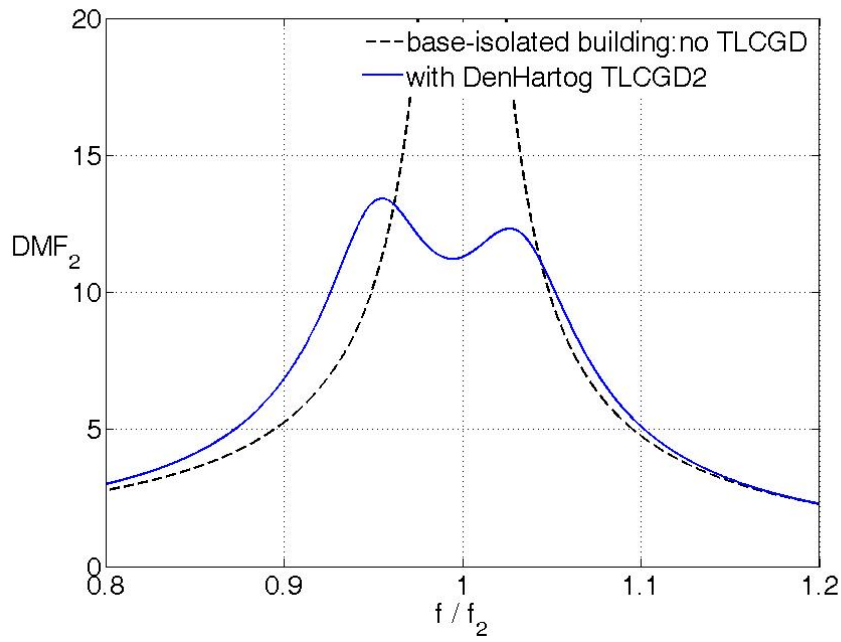


Fig. 4.27: Modal dynamic magnification factor (DMF_2) for base-isolated building alone and with TLCGD2 installed; the effective damping is increased from 0.5 to 3.73%.

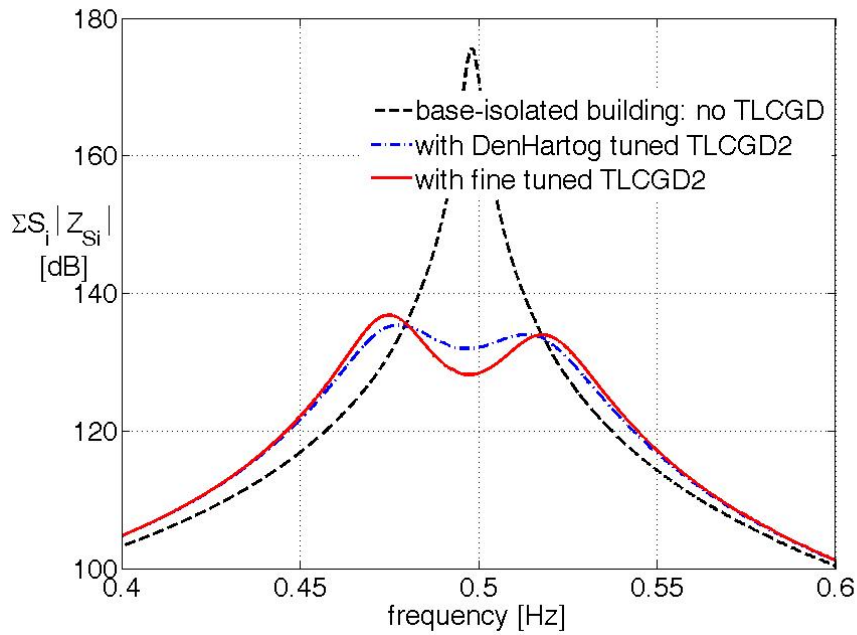


Fig. 4.28: Weighed sum of amplitude response function for the base-isolated building with TLCGD2 attached and without any TLCGD, $\alpha_{cr2} = 40^\circ$.

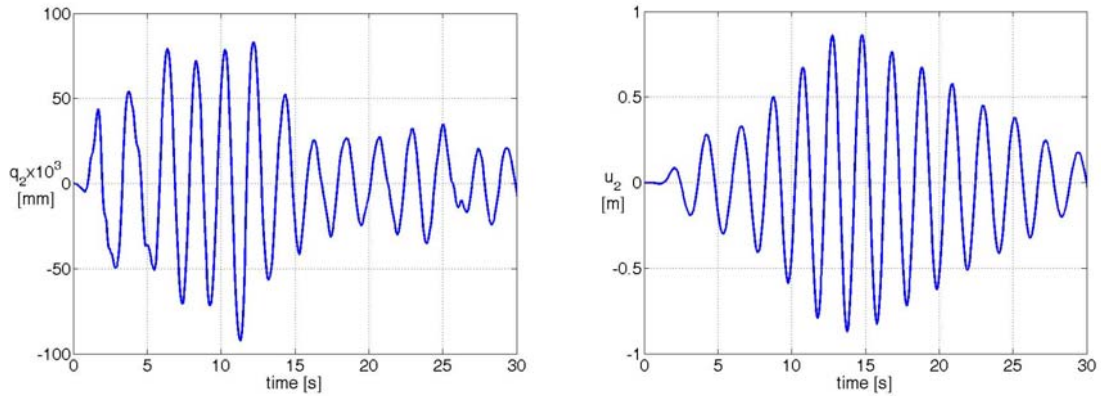


Fig. 4.29: Time response under El Centro seismogram scaled to $0.32g$ (a) Modal displacement q_2 of base-isolated building (b) Liquid stroke u_2 in TLCGD2, $u_{2max} = 0.77m$.

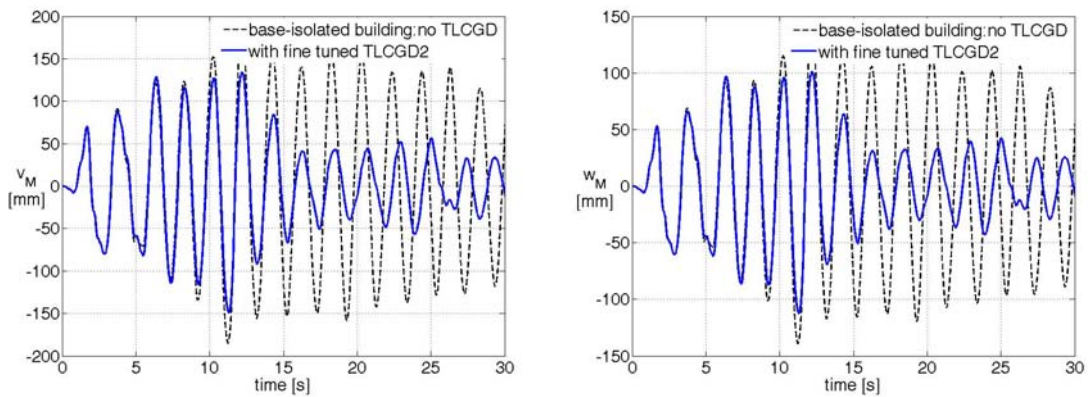


Fig. 4.30: Approximate horizontal displacements of center of mass of base-isolated building equipped with TLCGD2 under El Centro seismogram scaled to $0.32g$.

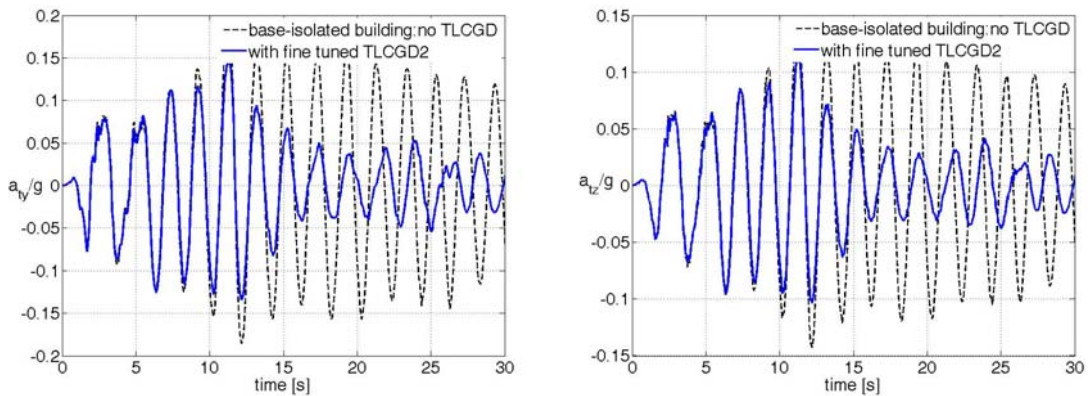


Fig. 4.31: Approximate horizontal total acceleration (as fraction of g) of center of mass of base-isolated building equipped with TLCGD2 under El Centro seismogram scaled to $0.32g$.

(iii) Dynamic response with modally tuned TLCGD3:

The results of the modally isolated 2-DOF coupled system by considering modally tuned TLCGD3 installed on the asymmetric building, Fig. 4.19, subjected to El Centro at

critical angle of incidence $\alpha_{cr3} = 125^0$ are also presented on similar lines as discussed above for TLCGD1 and TLCGD2.

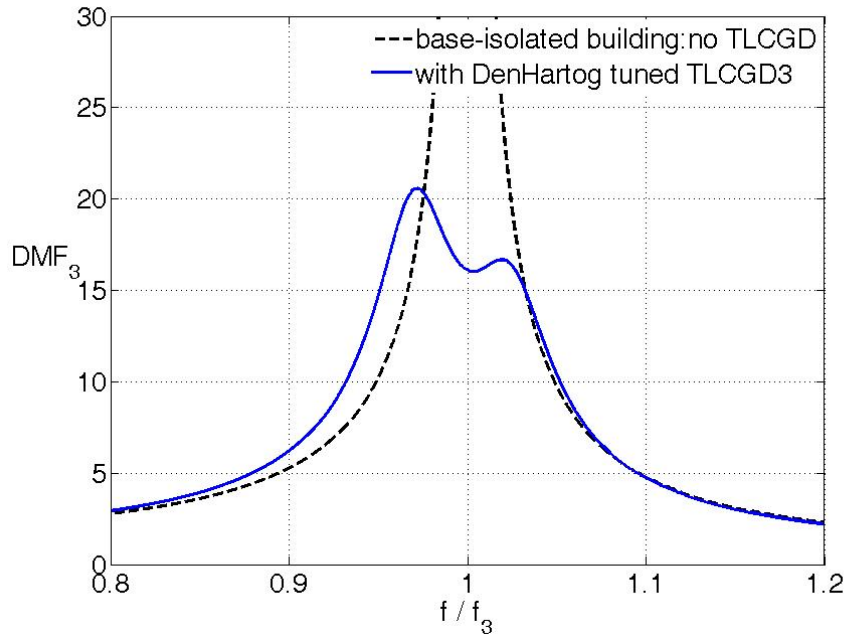


Fig. 4.32: Modal dynamic magnification factor (DMF_3) for base-isolated building alone and with TLCGD3 installed; the effective damping is increased from 0.5 to 2.43%.

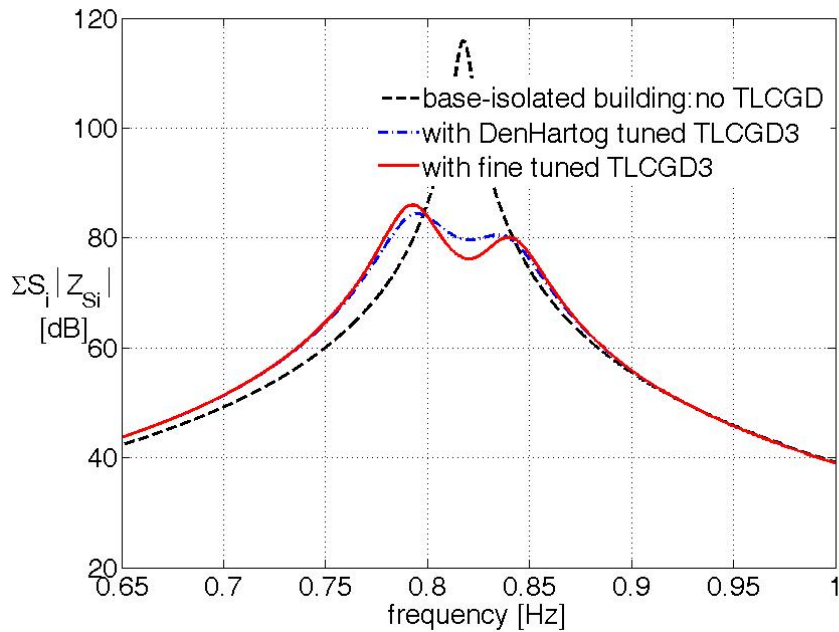


Fig. 4.33: Weighed sum of amplitude response function for the base-isolated building with TLCGD3 attached and without any TLCGD, $\alpha_{cr3} = 125^0$.

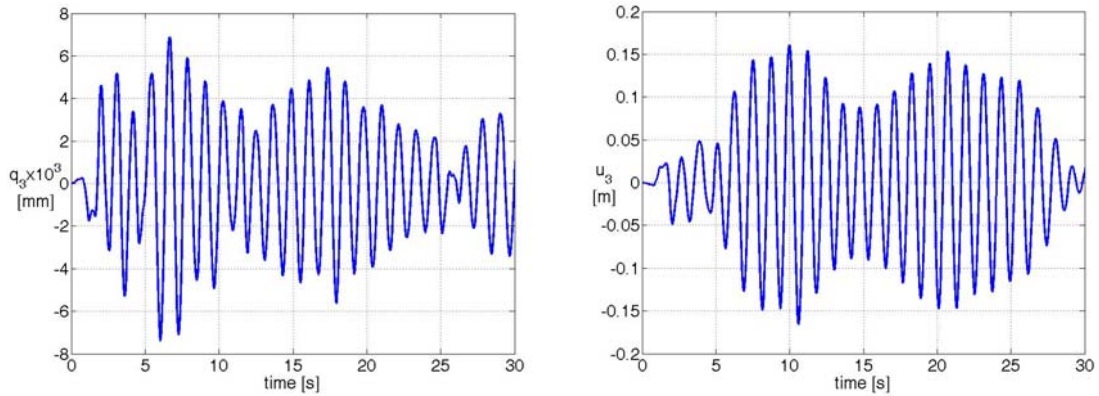


Fig. 4.34: Time response under El Centro seismogram scaled to $0.32g$ (a) Modal displacement q_3 of base-isolated building (b) Liquid stroke u_3 in TLCGD3, $u_{3max} = 0.15m$.

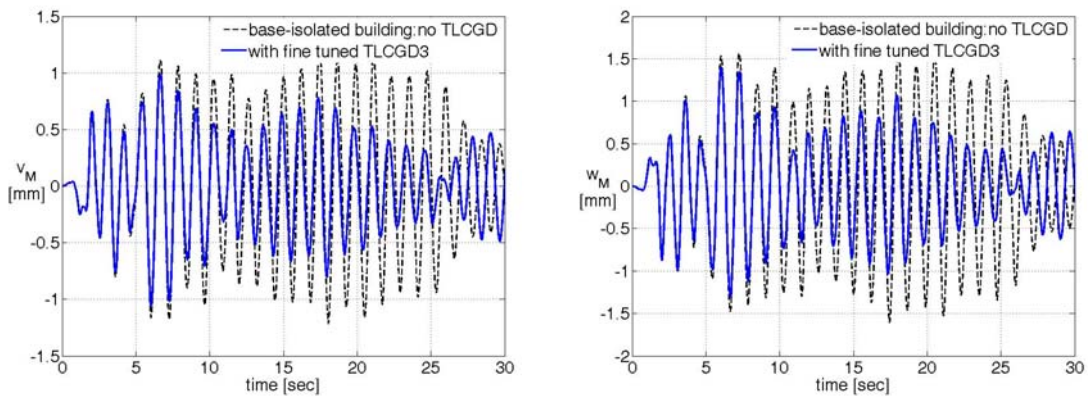


Fig. 4.35: Approximate horizontal displacements of center of mass of base-isolated building equipped with TLCGD3 under El Centro seismogram scaled to $0.32g$.

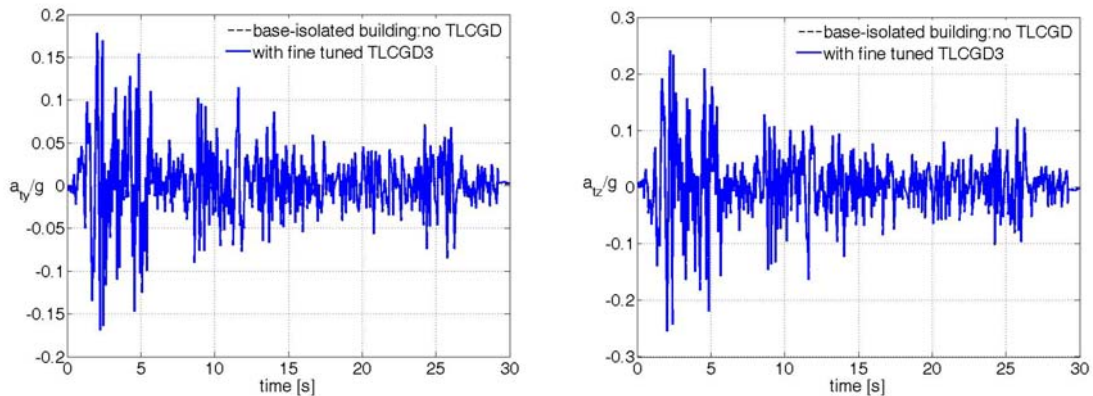


Fig. 4.36: Approximate horizontal total acceleration (as fraction of g) of center of mass of base-isolated building equipped with TLCGD3 under El Centro seismogram scaled to $0.32g$.

The beat phenomenon observed in the response, Fig. 4.34 is related to the inefficiency of the “linear” TLCGD when exposed to a dominating rotational oscillation. Substitution of a torsional TTLCGD, see Fu^[4-17] or Fu-Ziegler^[4-18] is recommended. However, excitation of mode 3 is rather small.

(b) Modally coupled 6-DOF system

The equations of motion for three degree-of-freedom structure (e.g., 3-DOF asymmetric building) with three TLCGDs render 6-DOF modally coupled system. The equations of motion are preferably transformed to generalized coordinates such that the coupling is only by the control forces of the TLCGDs. Further, if required, such an approach conveniently allows modal truncation in larger multi-degree-of-freedom (MDOF) systems.

The natural frequencies and the damping ratios are optimized for the sake of fine tuning of the TLCGDs by similar fashion as described in sub-section 4.4, i.e., by minimizing the performance index with the difference that $\bar{z}_S = [\bar{q}^T \quad \dot{\bar{q}}^T]^T$ represents the main structure's state-vector. $\bar{b} = E_g \bar{a}_g$ is the excitation vector. Here also, *fminsearch* of MATLAB^[4-22] quickly finds the minimum of the scalar function J of six variables, when substituting Den Hartog's modal tuning parameters $x_0 = [\omega_{A1}, \omega_{A2}, \omega_{A3}, \zeta_{A1}, \zeta_{A2}, \zeta_{A3}]$ as initial estimates. The optimization results in a slight decrease of the natural absorber frequencies whereas the damping coefficients of the fluid flow are significantly reduced.

The weighed sum $\sum_{i=1}^6 S_i |z_{Si}(\omega)|$ of the amplitude response function of building's states

for the original and optimized system is illustrated in Fig. 4.37. Thus, the frequency response of the base-isolated building with 3-TLCGDs (TLCGD1, TLCGD2 diagonal and TLCGD3 z-parallel; see Fig. 4.19) is tremendously reduced at resonant peaks, which confirm the effective damping supplied by TLCGDs.

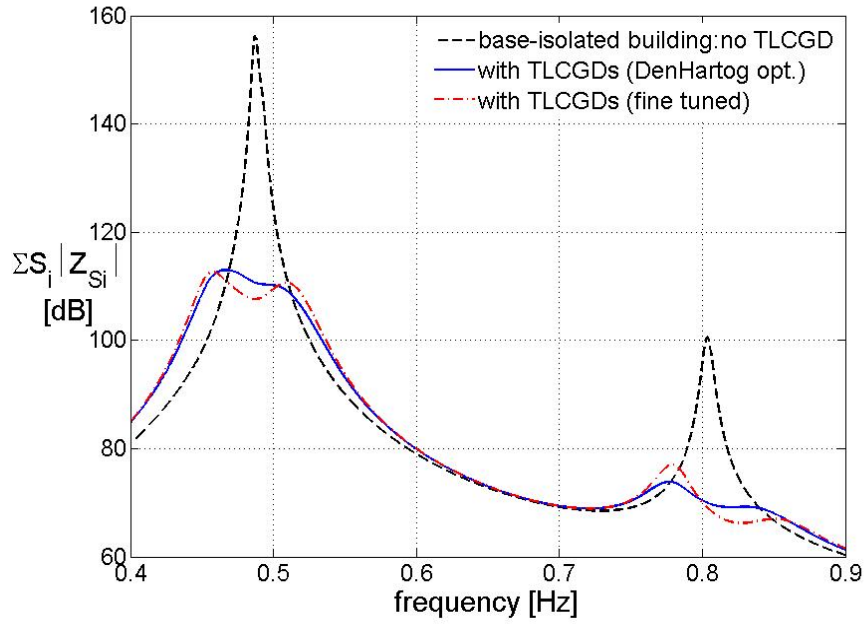


Fig. 4.37: Weighed sum of amplitude response function for the base-isolated building with three TLCGDs attached and without TLCGDs, $\alpha_{cr}=125^0$.

The response in terms of horizontal displacements of C_M of the base-isolated building excited by El Centro seismogram scaled to $0.32g$ at critical angle of incidence $\alpha_{cr} = 125^0$ is calculated by (4.92) and illustrated in Fig. 4.38.

$$v_M = q_1\phi_{11} + q_2\phi_{21} + q_3\phi_{31}, \quad w_M = q_1\phi_{12} + q_2\phi_{22} + q_3\phi_{32}. \quad (4.92)$$

In addition, the horizontal total acceleration of C_M of the base-isolated building excited by El Centro seismogram scaled to $0.32g$ is calculated by (4.93), and illustrated in Fig. 4.39.

$$a_{ty} = (\ddot{q}_1\phi_{11} + \ddot{q}_2\phi_{21} + \ddot{q}_3\phi_{31}) + a_g \cos \alpha, \quad a_{tz} = (\ddot{q}_1\phi_{12} + \ddot{q}_2\phi_{22} + \ddot{q}_3\phi_{32}) + a_g \sin \alpha \quad (4.93)$$

4. Novel Base Isolation System

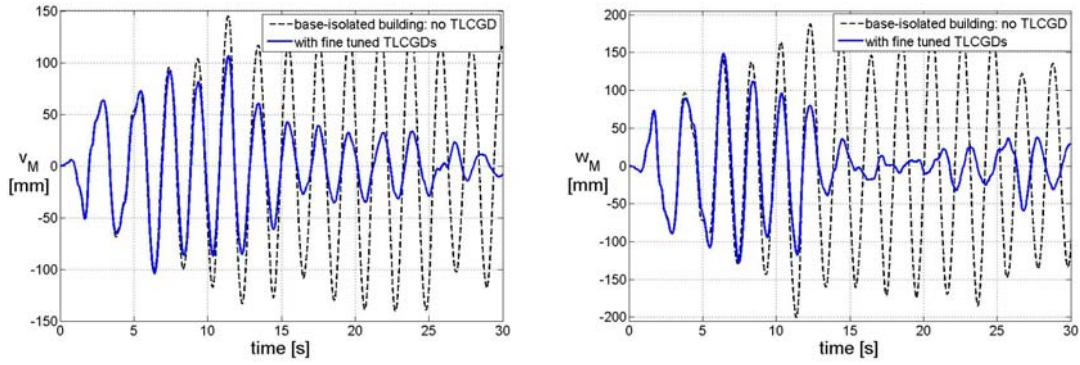


Fig. 4.38: Horizontal displacements of C_M of the base-isolated building forced by El Centro seismogram scaled to 0.32g.

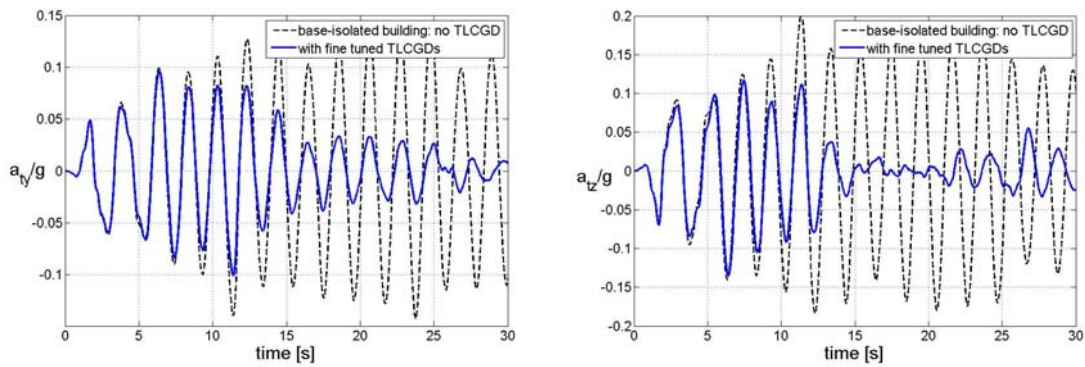


Fig. 4.39: Total horizontal acceleration of C_M of the base-isolated building forced by El Centro seismogram scaled to 0.32g.

It is quite evident from Fig. 4.38 and Fig. 4.39 that vibration response of the base-isolated building is effectively damped by the fine tuned TLCGDs. It is also noted that all TLCGDs need several vibration cycles before they start to mitigate the structural vibrations. In other words, early peaks in the response of the base-isolated building are hardly affected by passive damping. This is because of the fact that TLCGD is a passive type damping device and unable to damp the early peaks. However, if necessary, these early peaks can be reduced by the application of actively controlled (with gas-pressure injections) tuned liquid column-gas dampers (ATLCGDs), for details, see Soong^[4-27] and Hochrainer-Ziegler^[4-19] for a hybrid actively controlled, ATLCGD.

The resulting time response of the liquid strokes in each TLCGD is recorded in Fig. 4.40 to Fig. 4.42.

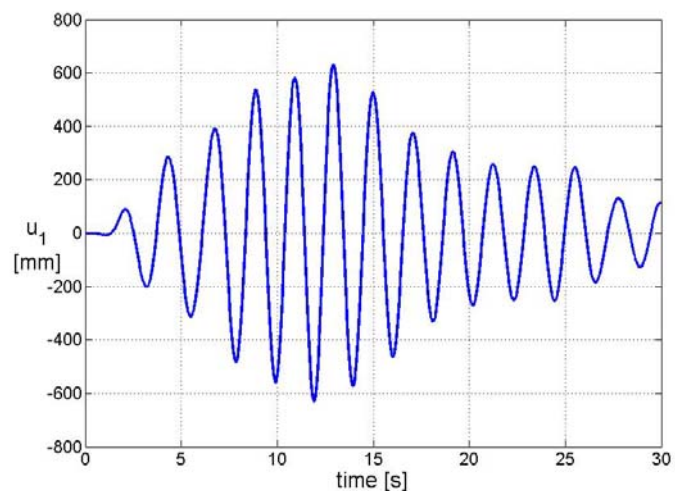


Fig. 4.40: Liquid stroke in TLCGD1 under El Centro seismogram scaled to 0.32g.

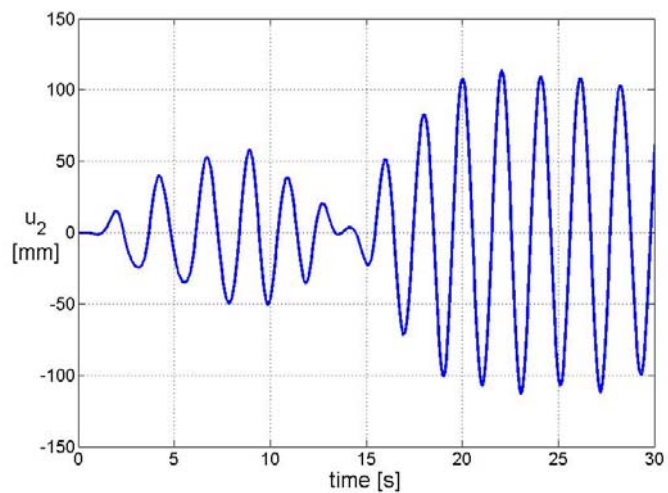


Fig. 4.41: Liquid stroke in TLCGD2 under El Centro seismogram scaled to 0.32g.

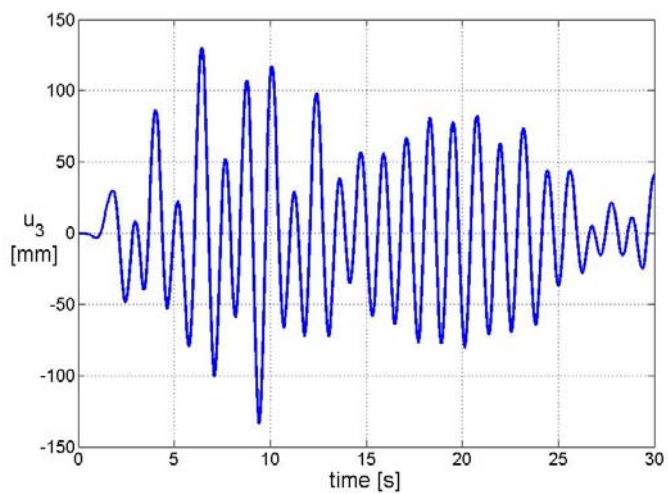


Fig. 4.42: Liquid stroke in TLCGD3 under El Centro seismogram scaled to 0.32g.

The resulting time response of the liquid strokes in TLCGD3 is rather small but reflects the beat phenomenon as already observed for modally isolated system. So the torsional tuned liquid column-gas damper (TTLCGD) properly tuned to the corresponding mode, see again Fu^[4-17] and Fu-Ziegler^[4-18], would render even better results. However, since the contribution of third mode to the overall response is rather small, the TTLCGD is not further discussed within this dissertation.

References

- [4-1] Bachmann H., Seismic upgrading of a fire-brigade building by base isolation in Basel, Switzerland, *Structural Engineering International*, 2010; **20/7**, 268-274.
- [4-2] Wang, Yen P., *Fundamentals of seismic base isolation*, National Center for Research on Earthquake Engineering, Taiwan, 2002.
- [4-3] Reitherman R., *Historic development in the evolution of earthquake engineering*, Consortium of Universities for Research in Earthquake Engineering (CUREE), California, USA, 1997.
- [4-4] Kelly J. M., *Implementation of base isolation in United States*, Proc. of 10th World Conf. on Earthquake Engineering (10 WCEE), Madrid, Spain, 1992, Balkema, Rotterdam; **11**, 6507-6517, ISBN 9054100710.
- [4-5] Flesch R., *Baudynamik Praxisgerecht. Vol. I: Berechnungsgrundlagen*, Bauverlag, Wiesbaden, 1993.
- [4-6] Symans M. D., *Seismic protective systems: seismic isolation*, National Institute of Building Sciences (NIBS), FEMA-451, <http://www.nibs.org/client/assets/files/bssc/Topic15-7-SeismicIsolation.pdf>, 2003.
- [4-7] Kelly J. M., *National Information Service for Earthquake Engineering (NISEE)*. Internet publication: <http://nisee.berkeley.edu/lessons/kelly.html>.
- [4-8] <http://wapedia.mobi/en/File:LRBtest.jpg>.
- [4-9] Buckle I. G., Mayes R. L., *Seismic isolation history: application and performance- a world review*, *Earthquake Spectra*, 1990; **6**, 161-201.
- [4-10] Kunde M. C., Jangid R.S., *Seismic behavior of isolated bridges: A-state-of-the-art review*, *Electronic Journal of Structural Engineering*, 2003; **3**, 140-170.
- [4-11] Ziegler F., Khalid B., *A novel base isolation system for asymmetric buildings in seismic active zones: damping supplied by tuned liquid column gas dampers*, In: *Advanced Dynamics and Model-Based Control of Structures and Machines*, Eds.: A. Belyaev, H. Irschik and M. Krommer, Springer-Verlag Wien-New York, in press 2010.

- [4-12] Parkus H., *Mechanik der festen Körper*, 2nd ed., Springer, Vienna, 1996.
- [4-13] Wahl A. M., *Mechanical Springs*, McGraw-Hill, New York, 1963.
- [4-14] Nicholas P. C., *Spring Design and Application*, McGraw-Hill, New York, 1961.
- [4-15] Ziegler F., *Mechanics of Solids and Fluids*, corr. reprint of 2nd ed., Springer, New York, 1998.
- [4-16] Khalid B., Ziegler F., A novel base isolation system for asymmetric buildings effectively damped by tuned liquid column-gas dampers, Proc. of 14th European Conf. on Earthquake Engineering, Ohrid, Macedonia, 2010; CD-ROM paper, 8pages.
- [4-17] Fu Chuan, Effective damping of vibrations of plan-asymmetric buildings, Dissertation (in English), Vienna University of Technology, Austria, 2008; <http://www.tuwien.ac.at/>.
- [4-18] Fu Chuan, Ziegler F., Vibration prone multi-purpose buildings and towers effectively damped by tuned liquid column gas dampers. *Asian J. Civil Engineering*, 2009; **10/1**, 21-56.
- [4-19] Hochrainer M.J., Ziegler F., Control of tall building vibrations by sealed tuned liquid column dampers, *Structural Control and Health Monitoring*, 2006; **6/13**, 980-1002.
- [4-20] DenHartog J.P., *Mechanical vibrations*. 4th ed. McGraw-Hill, New York, 1956.
- [4-21] Hochrainer M.J., Control of vibrations of civil engineering structures with special emphasis on tall buildings, Dissertation (in English), Vienna University of Technology, Vienna, Austria, 2001; <http://www.tuwien.ac.at/>.
- [4-22] MATLAB, User Guide, Control Toolbox. MathWorks Inc., Version 7.8, R2009.
- [4-23] Chopra, A. K., *Dynamics of Structures*, 2nd ed., Prentice Hall, New Jersey, 2004.
- [4-24] Hochrainer M.J., Adam C., Dynamics of shear frames with tuned liquid column dampers, *ZAMM*, 2000; **80/2**, S283-S284.
- [4-25] Ziegler F., Special design of tuned liquid column-gas dampers for the control of spatial structural vibrations, *Acta Mechanica*, 2008; **201**, 249-267.
- [4-26] Young W. C., *Roark's Formulas for Stress & Strain*, 6th ed., McGraw-Hill, Inc. Prentice Hall, Singapore, 1989.
- [4-27] Soong T.T., *Active structural control: theory and practice*, New York, Wiley, 1990.

5 Conclusions

In my dissertation, a state-of-the-art novel base isolation system, - a combination of durable spring-pendulum (SP) units with compatible sliding elements (without continuous energy dissipation) and low-cost tuned liquid column-gas dampers (TLCGDs), - is presented to overcome some of the disadvantages of the conventional ones, e.g., by avoiding any lifetime problems. In addition, the effectiveness of the tuned liquid column-gas damper (TLCGD), tuned and optimally placed with respect to the fundamental mode of vibration of a laboratory scaled structural model (space frame), is experimentally verified in general horizontal motion. Many useful conclusions were obtained within the dissertation, which may be considered as guidelines for practical applications of the novel base isolation system. The main contributions and conclusions are summarized:

- The novel base isolation system is functionally equivalent to a conventional one in extending structure's time period (i.e. acting as a low-pass-filter) but with the additional advantageous features such as temperature-insensitivity, durability and maintenance-free long life. The properly designed compatible sliding elements not only supply the necessary static friction against wind load but also do not cause any continuous energy dissipation (abrasive friction) during the relative horizontal movement under seismic excitation.
- With a selected natural mode of vibration of the isolated building considered (rendering the generalized two-degree-of-freedom (2-DOF) modally coupled TLCGD-main system), the modal tuning of the TLCGD is conveniently performed by taking advantage of the well-documented Den Hartog's optimization formulas for tuning mechanical dampers, TMD, by means of a simple transformation.
- The placement of the modally tuned TLCGDs becomes optimal with normal

distance to the modal centers of velocity maximum. Therefore, diagonally arranged TLCGD1 and TLCGD2 for the base-isolated asymmetric building is preferred because of their better performance than that of those placed parallel to the outer perimeter. However, portions of the piping system should be integrated in the structural carrying system, if at all possible.

- Numerical simulations approve the novel base isolation system as a replacement of classical elastomeric bearings with or without sliding elements, and illustrate the effectiveness of TLCGDs to mitigate the seismically forced vibrations of the base-isolated asymmetric buildings with fairly small mass ratio assigned.
- It is also noted that all TLCGDs need several vibration cycles before they start to mitigate the structural vibrations i.e., early peaks in the response of the base-isolated building are hardly affected by passive damping supplied by TLCGDs. However, if necessary, these early peaks can be reduced by the application of actively controlled (with gas-pressure injections) tuned liquid column-gas dampers (ATLCGDs).
- For a laboratory scaled light-weight structural model, the static and modal properties are reasonably changed after the installation of TLCGD because of the added dead fluid-mass and mass of the piping system, comparable to the mass of the structural model, and hence lower its natural frequencies. Therefore, modal properties are updated for the exact tuning of the TLCGD. However, in real buildings, the dead mass is rather negligible when compared to the mass of the structure.
- The laboratory experiments verify the tuning of TLCGD achieved by means of the gas-spring effect. It is also confirmed experimentally that “open TLCD” does not damp the vibrations of the structural model because the gas-spring effect vanishes, resulting in a detuned TLCD, and its effect is just that of the added dead mass. Therefore, only a TLCGD properly tuned with respect to frequency and less importance to damping of the fluid motion can serve the purpose effectively.

References

The alphabetically arranged list of references with respect to the first author is given below by using the style “[section number] page number”;

- Achs G., Anwendung von flüssigkeitstilgern bei schrägseilbrücken im freivorbauzustand unter windanregung, Master Thesis (in German), Vienna University of Technology, Vienna, Austria, 2005: [3]53.
- Bachmann H., Seismic upgrading of a fire-brigade building by base isolation in Basel, Switzerland, *Structural Engineering International*, 2010; **20/7**, 268-274: [1]2, [1]4, [4]66, [4]72, [4]83.
- Balendra T., Wang C. M., H. F, Effectiveness of tuned liquid column dampers for vibration control of towers, *Engineering Structures*, 1995; **17/9**, 668-675: [1]6.
- Buckle I. G., Mayes R. L., Seismic isolation history: application and performance- a world review, *Earthquake Spectra*, 1990; **6**, 161-201: [1]2, [4]69.
- Chopra A. K., *Dynamics of Structures*, 2nd ed., Prentice Hall, New Jersey, 2004: [2]17, [4]96, [4]98.
- Clough R.W., Penzien J., *Dynamics of Structures*, 2nd ed., McGraw-Hill, New York, 1993: [2]16, [3]46.
- Den Hartog J.P., *Mechanical Vibrations*, 4th ed., McGraw-Hill, New York, 1956: [1]6, [2]36, [3]60, [4]89.
- Dowrick D.J., Cousins W.J, Robinson W.H. & J. Barbor, Recent developments in seismic isolation in New Zealand, Proc. of 10th World Conf. on Earthquake Engineering (10 WCEE), Madrid, Spain, 1992, Balkema, Rotterdam; **4**, 2305-2310, ISBN 9054100648: [1]4.
- Flesch R., *Baudynamik Praxisgerecht. Vol. I: Berechnungsgrundlagen*, Bauverlag, Wiesbaden, 1993: [4]67.
- Fu Chuan, Effective damping of vibrations of plan-asymmetric buildings, Dissertation (in English), Vienna University of Technology, Austria, 2008; <http://www.tuwien.ac.at/>: [1]7, [2]13, [2]35, [3]48, [3]51, [4]89, [4]126, [4]132.
- Fu Chuan, Ziegler F. Vibration prone multi-purpose buildings and towers effectively damped by tuned liquid column gas dampers. *Asian J. Civil Engineering*, 2009; **10/1**, 21-56: [1]6, [2]13, [3]48, [3]50, [3]51, [3]57, [4]89, [4]108, [4]126, [4]132.
- Giuliani G.C., Design experience on seismically isolated buildings, *Nuclear Engineering and Design*, 1991; **127/3**, 349-366: [1]4.
- Hitchcock P. A., Kwok K. C. S., Watkins R. D., Samali B., Characteristics of liquid column vibration absorbers (LCVA)-I, *Engineering Structures*, 1997; **19/2**, 126-134: [1]7, [1]8.
- Hochrainer M.J., Adam C., Dynamics of shear frames with tuned liquid column dampers, *ZAMM*, 2000; **80/2**, S283-S284: [4]97, [4]100.

- Hochrainer M.J., Control of vibrations of civil engineering structures with special emphasis on tall buildings, Dissertation (in English), Vienna University of Technology, Vienna, Austria, 2001; <http://www.tuwien.ac.at/>: [1]7, [2]12, [2]13, [2]20, [2]25, [2]26, [3]60, [4]90, [4]104.
- Hochrainer M.J., Ziegler F., Control of tall building vibrations by sealed tuned liquid column dampers, *Structural Control and Health Monitoring*, 2006; **6/13**, 980-1002: [1]7, [2]13, [2]20, [2]25, [3]60, [4]89, [4]90, [4]96, [4]100, [4]131. <http://wapedia.mobi/en/File:LRBtest.jpg>: [4]69.
- Huo L.S., Li H. N., Sun L., Parameter study of TLCD control system excited by multi-dimensional ground motions, *Earthquake Engineering and Engineering Vibration*, 2001; **21/4**, 147-153: [1]7.
- Jolivet J., Richli M.H., Aseismic foundation system for nuclear power stations, Proc. of SMiRT-4, San Francisco, CA, 1977; Paper K.9/2: [1]4.
- Kelly J. M., Implementation of base isolation in United States, Proc. of 10th World Conf. on Earthquake Engineering (10 WCEE), Madrid, Spain, 1992, Balkema, Rotterdam; **11**, 6507-6517, ISBN 9054100710: [1]3, [4]66, [4]67, [4]68.
- Kelly J. M., National Information Service for Earthquake Engineering (NISEE). Internet publication: <http://nisee.berkeley.edu/lessons/kelly.html>: [4]69.
- Kelly J. M., Seismic base isolation: review and bibliography, *Soil Dynamics and Earthquake Engineering*, 1986; **5**, 202-216: [1]2.
- Khalid B., Ziegler F., A novel base isolation system for asymmetric buildings effectively damped by tuned liquid column-gas dampers. Proc. of 14th European Conference on Earthquake Engineering (14 ECEE), Ohrid, Macedonia, 2010; CD-ROM paper, 8 pages: [1]4, [4]73, [4]76.
- Kofler M., Eine experimentelle und numerische modelluntersuchung von ebenen rahmentragwerken mit U-rohrförmigen flüssigkeitsdämpfern, Master Thesis (in German), Vienna University of Technology, Vienna, Austria, 2000: [3]53.
- Kunde M. C., Jangid R.S., Seismic behavior of isolated bridges: A-state-of-the-art review, *Electronic Journal of Structural Engineering*, 2003; **3**, 140-170: [4]70.
- Lee L., A base isolation measure for aseismic building in China, Proc. of 8th World Conf. on Earthquake Engineering, San Francisco (8 WCEE), CA, 1984; **VI**, 791-798: [1]4.
- Lindner-Silvester T., Schneider W., The moving contact line with weak viscosity effects-an application and evaluation of Shikhmurzaev's model, *Acta Mechanica*, 2005; **176**, 245-258: [2]26, [3]60.
- MATLAB, User Guide, Control Toolbox. MathWorks Inc., Version 7.8, R2009: [2]17, [3]48, [4]95, [4]96, [4]129.
- Naeim F., Kelly J. M., Design of Seismic Isolated Structures, John Wiley & Sons, New York, 1999: [1]1, [1]4.
- Nicholas P. C., Spring Design and Application, McGraw-Hill, New York, 1961: [4]73.
- Parkus H., Mechanik der festen Körper, 2nd ed., Springer, Vienna. 1996, [4]73.
- Reiterer M., Damping of vibration-prone civil engineering structures with emphasis on bridges, Dissertation (in German), Vienna University of Technology, Austria, 2004, <http://www.tuwien.ac.at/>: [2]26.

- Reiterer M., Ziegler F., Control of pedestrian-induced vibrations of long-span bridges, *Structural Control and Health Monitoring*, 2006; **13/6**, 1003-1027: [1]7, [2]26.
- Reitherman R., Historic development in the evolution of earthquake engineering, Consortium of Universities for Research in Earthquake Engineering (CUREE), California, USA, 1997: [1]2, [1]4, [4]66.
- Sakai F., Takaeda S., Tamaki T., Tuned liquid column damper-new type device for suppression of building vibration. Proc. of Int. Conf. on High-rise Buildings, Nanjing, China, 1989; 926-931: [1]7.
- Soong T.T., Active structural control: theory and practice, New York, Wiley, 1990, [4]131.
- Symans M. D., Seismic protective systems: seismic isolation, National Institute of Building Sciences (NIBS), FEMA-451, <http://www.nibs.org/client/assets/files/bssc/Topic15-7-SeismicIsolation.pdf>, 2003: [4] 68.
- Wahl A. M., Mechanical Springs, McGraw-Hill, New York, 1963: [4]73.
- Wang, Yen P., Fundamentals of seismic base isolation, National Center for Research on Earthquake Engineering, Taiwan, 2002: [4]66.
- Ziegler F., Khalid B., A novel base isolation system for asymmetric buildings in seismic active zones: damping supplied by tuned liquid column.gas dampers, In: *Advanced Dynamics and Model-Based Control of Structures and Machines*, Eds.: A. Belyaev, H. Irschik and M. Krommer. Springer-Verlag Wien-New York, in press 2010: [4]70, [4]70, [4]71, [4]73.
- Ziegler F., *Mechanics of Solids and Fluids*, corr. reprint of 2nd ed., Springer, New York, 1998: [2]15, [2]16, [2]17, [2]20, [2]21, [2]22, [2]24, [2]25, [2]28, [3]47, [3]48, [3]62, [4]73, [4]80, [4]86, [4]87, [4]95, [4]100, [4]110, [4]116.
- Ziegler F., Special design of tuned liquid column gas dampers for the control of spatial structural vibrations, *Acta Mechanica*, 2008; **201**, 249-267: [1]7, [2]26, [3]60, [4]99, [4]106, [4]114.

Curriculum Vitae

Personal Information:

Name: Basit Khalid
Date of birth: 20-11-1978
Sex: Male
Nationality: Pakistan

Academic Profile:

Successfully completed 18-years of education with excellent grade (A+) throughout;

March, 1994: Matriculation (SSC) from Govt. Central Model School, Lower Mall Lahore, Pakistan.

1994-1996: F.Sc. (Pre-Engg, HSSC) from Govt. F.C College Lahore, Pakistan.

1997-2001: B.Sc. Civil Engineering from University of Engineering & Technology (UET) Lahore, Pakistan.

Bachelor thesis: Analysis and Design of Industrial Building.

2001-2003: M.S. N.E. from Pakistan Institute of Engineering & Applied Sciences (PIEAS), Islamabad, Pakistan.

Master thesis: Numerical Modeling of Compressible Flows.

2007-present: Ph.D. Candidate at the Institute of Building Construction and Technology at Department of Civil Engineering, Vienna University of Technology (TU-Wien), Austria.

Ph.D. thesis: Control of Seismically Forced Vibrations of Asymmetric Buildings by Means of a Novel Base Isolation System.

Professional Experience:

2003-present: Senior Engineer (S.E) in a public sector organization involved in the analysis and design of civil engineering structures.